



TECHNISCHE UNIVERSITÄT CHEMNITZ

Frequency domain methods for the analysis of time delay systems

von der Fakultät für Naturwissenschaften der Technischen Universität Chemnitz
genehmigte

Dissertation

zur Erlangung des akademischen Grades

doctor rerum naturalium

(Dr. rer. nat.)

vorgelegt von M.Sc. Andreas Otto

geboren am 18. April 1983 in Greiz

eingereicht am 18. April 2016

Gutachter:

Prof. Dr. Günter Radons

Prof. Dr. Karl Heinz Hoffmann

Tag der Verteidigung 6. Juli 2016:

Bibliografische Beschreibung

Andreas Otto

Frequency domain methods for the analysis of time delay systems

Dissertation (in englischer Sprache)

Technische Universität Chemnitz, Fakultät für Naturwissenschaften, Chemnitz, 2016

140 Seiten, 20 Abbildungen, 2 Tabellen, 213 Literaturzitate

Referat

In dieser Dissertation wird ein neues Verfahren zur Analyse von Systemen mit Totzeiten im Frequenzraum vorgestellt. Nach Linearisierung einer nichtlinearen retardierten Differentialgleichung (DDE) mit konstanter verteilter Totzeit um eine konstante oder periodische Referenzlösung kann die sogenannte Hill-Floquet Methode für die Analyse der resultierenden linearen DDE angewendet werden. Darüber hinaus werden Systeme mit schnell oder langsam variierender Totzeit, Systeme mit einer variablen Totzeit, resultierend aus einem Transport mit variabler Geschwindigkeit, und entsprechende räumlich ausgedehnte Systeme vorgestellt, welche ebenfalls mit der vorgestellten Methode analysiert werden können.

Die neu eingeführte Hill-Floquet Methode basiert auf der Hillschen unendlichen Determinante und ermöglicht die Transformation eines Systems mit periodischen Koeffizienten auf ein autonomes System mit konstanten Koeffizienten. Dadurch können zur Analyse periodischer Systeme auch eine Vielzahl existierender Methoden für autonome Systeme genutzt werden und die Berechnung der Monodromie-Matrix für die Lösung des Systems über eine Periode entfällt. In dieser Arbeit wird zur Analyse des autonomen Systems die Tschebyscheff-Kollokationsmethode verwendet. Im Speziellen wird bei diesem Verfahren der periodische Teil der Lösung in einer Fourierreihe entwickelt und das exponentielle Verhalten durch die Werte der Fourierkoeffizienten an den Tschebyscheff Knoten approximiert, wohingegen bei klassischen spektralen Verfahren die komplette Lösung in bestimmten Basisfunktionen entwickelt wird.

Im Anwendungsteil der Arbeit werden neue Ergebnisse für drei Beispielsysteme präsentiert, welche mit den vorgestellten Methoden analysiert wurden. Es wird gezeigt, dass Welleninstabilitäten schon bei Einkomponenten-Reaktionsdiffusionsgleichungen mit verteilter oder variabler Totzeit auftreten können. In einem zweiten Beispiel werden Schwingungen an Werkzeugmaschinen betrachtet, wobei speziell simultane Drehbearbeitungsprozesse und Prozesse mit Drehzahlvariationen genauer untersucht werden. Am Ende wird die Synchronisation in Netzwerken mit heterogenen Totzeiten in den Kopplungstermen untersucht, wobei die Zerlegung in Netzwerk-Eigenmoden für synchrone periodische Orbits hergeleitet wird und konkrete numerische Ergebnisse für ein Netzwerk aus Hodgkin-Huxley Neuronen gezeigt werden.

Schlagwörter

Nichtlineare Dynamik, Stabilität, Floquet Theorie, Retardierte Differentialgleichungen, Musterbildung, Mechanische Schwingungen, Rattern, Synchronisation

To my parents

Preface

The presented results were obtained during my work in the Complex Systems and Non-linear Dynamics group at Chemnitz University of Technology. Many people helped me in the preparation of this thesis. In particular, I would like to thank

- Günter Radons for giving me the opportunity and the financial support to work in his group, for his scientific supervision and especially for many fruitful discussions, where I could benefit from his broad knowledge and experience in the field of theoretical physics and engineering.
- Josef Kleckner for filling me with enthusiasm for the investigation of machine-tool vibrations, for introducing me into the topic and making me aware of many practical aspects of the behavior of metal cutting vibrations.
- David Müller, Jian Wang, Firas Khasawneh, Stefan Rauh, Martin Kolouch, Gabor Orosz, Daniel Bachrathy, Mamadou Diagne and Nikos Bekiaris-Liberis for many valuable discussions on collaborative work related to DDEs and their applications that helped me in writing this thesis.
- The consortia of the BMBF projects VispaB and ReffiZ. The discussions with the project members inspired me to study the stability of turning, milling and drilling processes with frequency domain methods in detail taking into account the effects of time-varying, state-dependent and distributed delays. The results and experience on these numerical investigations provide the basis for this thesis.
- All current, former and visiting members of our KSND group. Especially, I would like to thank Hong-liu Yang, Sven Schubert and Michael Bauer for helpful discussions and Angelique Gaida for their administrative support.

Finally, I would like to give special thanks to my family Isabell, Ricardo and Lisandro for their motivation, understanding and their support during my work on the preparation of this thesis.

Andreas Otto

Abstract

In this thesis a new frequency domain approach for the analysis of time delay systems is presented. After linearization of a nonlinear delay differential equation (DDE) with constant distributed delay around a constant or periodic reference solution the so-called Hill-Floquet method can be used for the analysis of the resulting linear DDE. In addition, systems with fast or slowly time-varying delays, systems with variable transport delays originating from a transport with variable velocity, and the corresponding spatially extended systems are presented, which can be also analyzed with the presented method.

The newly introduced Hill-Floquet method is based on the Hill's infinite determinant method and enables the transformation of a system with periodic coefficients to an autonomous system with constant coefficients. This makes the usage of a variety of existing methods for autonomous systems available for the analysis of periodic systems, which implies that the typical calculation of the monodromy matrix for the time evolution of the solution over the principle period is no longer required. In this thesis, the Chebyshev collocation method is used for the analysis of the autonomous systems. Specifically, in this case the periodic part of the solution is expanded in a Fourier series and the exponential behavior of the solution is approximated by the discrete values of the Fourier coefficients at the Chebyshev nodes, whereas in classical spectral or pseudo-spectral methods for the analysis of linear periodic DDEs the complete solution is expanded in terms of basis functions.

In the last part of this thesis, new results for three applications with time delay effects are presented, which were analyzed with the presented methods. On the one hand, the occurrence of diffusion-driven instabilities in reaction-diffusion systems with delay is investigated. It is shown that wave instabilities are possible already for single-species reaction diffusion systems with distributed or time-varying delay. On the other hand, the stability of metal cutting vibrations at machine tools is analyzed. In particular, parallel orthogonal turning processes with multiple discrete delays and turning processes with a time-varying delay due to a spindle speed variation are studied. Finally, the stability of the synchronized solution in networks with heterogeneous coupling delays is studied. In particular, the eigenmode expansion for synchronized periodic orbits is derived, which includes an extension of the classical master stability function to networks with heterogeneous coupling delays. Numerical results are shown for a network of Hodgkin-Huxley neurons with two delays in the coupling.

Keywords

Nonlinear Dynamics, Stability, Floquet theory, Delay Differential Equations, Pattern formation, Mechanical vibrations, Chatter, Synchronization

Contents

Acronyms and nomenclature	11
1. Introduction	13
2. System definition and equivalent systems	19
2.1. System definition and memory	19
2.2. Equivalent time delay systems	20
2.2.1. Variable transport delays	20
2.2.2. Equivalent DDEs with time- or state-dependent delay	23
2.3. Equivalent spatially extended systems	26
2.3.1. Equivalent first order hyperbolic PDEs	26
2.3.2. PDE representations in population dynamics	29
2.4. Approximations for systems with variable delay distribution	31
2.4.1. Fast time-varying delays	31
2.4.2. Slowly time-varying delays	34
2.5. Summary	36
3. Analysis of nonlinear time delay systems	39
3.1. Mathematical background	39
3.2. Numerical methods	40
3.3. Stability analysis	40
3.3.1. Lyapunov's direct method	41
3.3.2. Lyapunov's indirect linearization method	41
3.4. Summary	42
4. Analytical solution of linear time delay systems	43
4.1. Laplace transform	43
4.2. Method of steps	45
4.3. Inverse Laplace transform via residue theory	47
4.4. Eigenmode expansion for DDEs	49
4.5. Summary	51
5. Frequency domain approach	53
5.1. Autonomous systems	53
5.1.1. Characteristic equation	53
5.1.2. Linear chain trick	54
5.1.3. Lambert W approach	55
5.1.4. Numerical methods	55

5.2. Periodic systems	56
5.2.1. Hill's infinite determinant method	57
5.2.2. Numerical methods	58
5.3. D-subdivision method	59
5.3.1. Autonomous systems	59
5.3.2. Periodic systems	60
5.3.3. Aperiodic systems	61
5.3.4. Floquet exponents from D-subdivision	62
5.4. Summary	62
6. Hill-Floquet method	63
6.1. The Hill-Floquet transformation	63
6.2. Non-uniqueness of the Hill-Floquet transformation	67
6.3. Chebyshev expansion of the Hill-Floquet system	70
6.4. The alternative method	73
6.5. Discussion of the two separate expansions	77
6.6. Solution operator from the Hill-Floquet method	78
6.6.1. Fundamental matrix solution	78
6.6.2. Monodromy matrix	80
6.6.3. Lyapunov-Floquet transformation	80
6.7. Summary	81
7. Applications	83
7.1. Delayed reaction-diffusion systems	83
7.1.1. Stability analysis for homogeneous equilibria	84
7.1.2. Diffusion-driven instabilities	85
7.1.3. Turing-like traveling waves	87
7.1.4. Diffusion-driven instabilities in systems with time-varying delay . .	87
7.2. Metal cutting vibrations	89
7.2.1. Parallel turning	90
7.2.2. Stability lobes for parallel turning	92
7.2.3. Turning with spindle speed variation	94
7.2.4. Stability lobes for turning with spindle speed variation	96
7.3. Networks with heterogeneous coupling delays	97
7.3.1. Synchronization in heterogeneously delay-coupled networks	97
7.3.2. Representation with the adjacency lag operator	98
7.3.3. Decomposition into network eigenmodes	99
7.3.4. Synchronized delay-coupled Hodgkin-Huxley neurons	102
7.4. Summary	105
8. Concluding remarks	107
Bibliography	109

A. Appendix	125
A.1. Equivalent systems	125
A.1.1. Relation between delay kernels	125
A.1.2. Characteristic curves for PDE representation	126
A.2. Analytical methods for linear DDEs	127
A.2.1. Laplace transform of non-autonomous DDEs	127
A.2.2. Propagator of linear DDEs	128
A.2.3. Method of steps for DDEs with discrete delays	130
A.2.4. Biorthonormality condition for eigenmode expansion of DDEs . . .	131
List of Figures	133
List of Tables	134
Selbstständigkeitserklärung nach §6 Promotionsordnung	135
Curriculum vitae	137

Acronyms and nomenclature

Acronyms

ODE	Ordinary differential equation
DDE	Delay differential equation
PDE	Partial differential equation
FRF	Frequency response function
DOF	Degree of freedom
FFT	Fast Fourier transform
SSV	Spindle speed variation

Nomenclature

$\dot{\mathbf{v}}(t)$	Time derivative of an arbitrary vector $\mathbf{v}(t)$
$\bar{\mathbf{v}}(s)$	Laplace transform of an arbitrary vector $\mathbf{v}(t)$
$\hat{\mathbf{v}}(\omega)$	Fourier transform of an arbitrary vector $\mathbf{v}(t)$
δ_{ij}	Kronecker delta
$\delta(t)$	Dirac delta function
$H(t)$	Heaviside step function
T	Principal period
i	Imaginary unit
\mathbf{I}	Identity matrix
$\mathbf{0}$	Vector or matrix with all entries equal to zero
$\sigma(\mathbf{X})$	Eigenvalues of an arbitrary matrix \mathbf{X}
\circ	Composition
$*$	Convolution
\otimes	Kronecker product
Δ	Laplace operator
t, \tilde{t}	Internal clock, physical time
$\Phi(\tilde{t}), \Omega(\tilde{t})$	Time scale transformation and its derivative
$\mathbf{u}(t), \tilde{\mathbf{u}}(\tilde{t})$	Configuration of a system in the internal clock and the physical time
$\tau, \tilde{\tau}$	Time delay in the internal clock and the physical time
$\tau_{\max}, \tilde{\tau}_{\max}(\tilde{t})$	Upper bound of the delay distribution
$\mathbf{u}_t, \tilde{\mathbf{u}}_{\tilde{t}}$	State of a time delay system
$\mathbf{K}(\tau), \tilde{\mathbf{K}}(\tilde{t}, \tilde{\tau})$	Delay distribution in the internal clock and the physical time
$\mathbf{r}_u(t), \tilde{\mathbf{r}}_{\tilde{u}}(\tilde{t})$	Memory in the internal clock and the physical time

Acronyms and nomenclature

$a(t), \tilde{a}(\tilde{t})$	Retarded access map in the internal clock and the physical time
A_τ, τ_m	Amplitude and mean of a delay modulation
$\mathbf{v}(\tau, t), \mathbf{w}(\tilde{\tau}, t)$	Configuration of the equivalent PDE in the internal clock
$\tilde{\mathbf{v}}(\tau, \tilde{t}), \tilde{\mathbf{w}}(\tilde{\tau}, \tilde{t})$	Configuration of the equivalent PDE in the physical time
$K_{\text{var}}(t, \tau), K_{\text{av}}(\tau)$	Time-varying and time-averaged delay distribution
$\mathbf{r}_u^{\text{var}}(t), \mathbf{r}_u^{\text{av}}(t)$	Time-varying and time-averaged memory
$\mathbf{r}_u^{\text{froz}}(t, t')$	Frozen memory
$\mathbf{x}(t), \tilde{\mathbf{x}}(\tilde{t})$	Infinitesimal perturbations
$\mathbf{A}(t), \mathbf{B}(t)$	Coefficient matrices in the linearized delay system
s	Laplace variable, characteristic root or Floquet exponent
λ, ω	Real part and imaginary part of s (growth rate and frequency)
$\Psi(t), \bar{\Psi}(s)$	Initial function and its weighted Laplace transform
$\mathbf{T}(t, t'), \bar{\mathbf{T}}(s, s')$	Propagator of a DDE and its Laplace domain representation
$\mathbf{M}(t, t')$	Propagator of an ordinary differential equation
$\mathbf{d}_k^T, \mathbf{q}_k$	Left and right eigenvectors in the characteristic equation
$\mathbf{x}_k(t)$	Eigenmode of a linear system
$\mathbf{p}_k(t)$	Periodic part of the eigenmode of a periodic system
$\mathbf{F}_l(t), \mathbf{F}^i(t)$	Hill-Floquet and inverse Hill-Floquet transformation
$\mathbf{C}_\infty(s)$	Hill's infinite matrix
$\mathbf{A}_\infty, \mathbf{B}_\infty(\tau)$	Coefficient matrices in the Hill-Floquet representation
$\mathbf{x}_\infty(t)$	Configuration in the Hill-Floquet representation
$\mathbf{D}_F, \mathbf{D}_M$	Fourier and Chebyshev differentiation matrix
n, M	Number of higher harmonics, number of Chebyshev nodes
$\mathbf{z}_\infty(t), \mathbf{H}_\infty$	Configuration and coefficient matrix in the Chebyshev expanded Hill-Floquet system
D, k	Diffusion coefficient and wavenumber
$b, h(t)$	Chip width, chip thickness
Ω_0	Nominal spindle speed
γ	Angle between the tools in parallel turning
$\mathbf{G}(\omega)$	Matrix of oriented frequency response functions
$\mathbf{P}(\omega, \Omega)$	Force coefficient matrix
A_Ω, f_Ω	Amplitude and frequency of a spindle speed variation
ω_n, ζ	Frequency and damping ratio of a structural eigenmode
w	Dimensionless chip width
d	Number of nodes of a network
\mathbf{C}	Adjacency matrix
$\mathcal{S}(\tau), \mathcal{C}$	Time lag operator, adjacency lag operator
\mathbf{L}, \mathcal{L}	Eigenvalue matrix, diagonal operator of the adjacency lag operator
$\mathbf{U}(t), \mathbf{V}(t)$	Left and right eigenvector matrix of adjacency lag operator
\mathcal{U}, \mathcal{V}	Matrix operators associated to $\mathbf{U}(t)$ and $\mathbf{V}(t)$

1. Introduction

It is well-known that typically dynamical systems can be described by ordinary differential equations (ODEs). In this case the state of the system is characterized by the instantaneous configuration $\mathbf{u}(t)$ of the ODE. If the initial state $\mathbf{u}(0)$ of the system is known, the solution of the ODE can be predicted by an integration of the differential equation. Beyond the classical ODE systems, there are dynamical systems, where the effects of time delays τ_0 are relevant and retarded configurations $\mathbf{u}(t - \tau_0)$ of the system cannot be neglected for the description of the dynamics of the system. These systems are called time delay systems and can be described by delay differential equations (DDEs)

$$\dot{\mathbf{u}}(t) = \mathbf{f}(\mathbf{u}(t), \mathbf{u}(t - \tau_0)). \quad (1.1)$$

One of the main difference between DDEs and ODEs is given by the fact, that DDEs are infinite dimensional systems. In particular, the state of the DDE Eq. (1.1) at time t is given by the function $\mathbf{u}_t = \mathbf{u}(t - \tau)$, $0 \leq \tau \leq \tau_0$. In other words, for ODEs an initial value $\mathbf{u}(0)$ specifies a unique solution of the system, whereas for DDEs an initial function \mathbf{u}_0 is necessary for specifying a unique solution. A famous example for a time delay system is related to the production of blood cells, which is known as Mackey-Glass equation [1]. There exists a significant delay τ_0 between the initiation of cellular production and the release of mature cells into the blood. This means that the rate of change $\dot{u}(t)$ of the blood cells at time t depends not only on the instantaneous number of blood cells $u(t)$ but also on the retarded configuration $u(t - \tau_0)$. The time delay τ_0 specifies the time from the initiation of a cell production until its maturity. For small delays, the number of blood cells from the solution of the Mackey-Glass equation is constant. However, if the time delay τ_0 increases, large amplitude oscillations occur. Indeed, the number of blood cells of normal healthy adults can be kept nearly constant, whereas an abnormal periodic behavior of the number of blood cells and an increased cellular generation time has been observed in patients with chronic granulocytic leukemia ([1] and Refs. therein). A second famous example, where time delays play a crucial role for the system dynamics, are machine tool vibrations [2, 3]. Large undesired vibrations in machining are called chatter. The occurrence of chatter leads to poor surface finish, noise and increased tool wear. In machining the cutting force on the cutting tool depends on the chip thickness. As can be seen from the turning example in Fig. 1.1 the chip thickness is affected both by instantaneous and delayed displacements of the structure at the tool tip, $u(t)$ and $u(t - \tau_0)$. In this example, the time delay τ_0 is equivalent to the time for one revolution of the workpiece. Fluctuations of the cutting force due to fluctuations of the chip thickness lead to new variations of the tool tip displacements and again to chip thickness variations. This mechanism for self-excited vibrations is known as regenerative

1. Introduction

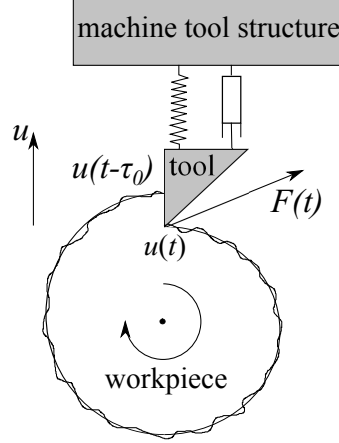


Figure 1.1.: Fluctuations of the cutting force $F(t)$ in turning occur not only due to the machine tool vibrations $u(t)$ at the present cut but also due to vibrations at the previous cut $u(t - \tau_0)$ left on the workpiece at some retarded time $t - \tau_0$.

effect. The regenerative effect has been identified as the main reason for chatter vibrations in metal cutting [4, 5].

In general, time delay systems can be found, for example, in climate dynamics [6, 7], life science [8, 9, 10], control theory [11, 12, 13] and network dynamics [14, 15]. A nice overview on time delay systems with models from mechanics, physics, engineering, biology, medicine and economy is given in [16]. In Eq. (1.1) only a constant delay $\tau = \tau_0$ is considered. However, it is also reasonable that the delay depends explicitly on time t or on the state \mathbf{u}_t of the system, which is known as a time-varying delay $\tau = \tau(t)$ or state-dependent delay $\tau = \tau(\mathbf{u}_t)$, respectively. For example, the Mackey-Glass equation with time-varying delay is studied numerically in [17]. Moreover, population models with time-dependent delay [18] or state-dependent delay [19, 20, 21] have been studied. In machining time-varying or state-dependent delays appear due to a continuous variation of the spindle speed [22, 23] or whenever the effect of vibrations on the angular position of the spindle is taken into account [24, 25, 26]. Other examples, for systems with time-varying and state-dependent delays can be found in variable [27, 28, 29] and adaptive [30] time-delayed feedback control or in the synchronization of complex networks with variable [31, 32, 33, 34] and state-dependent coupling delays [35, 36]. Apart from variable and state-dependent delays, systems with multiple delays or distributed delays are relevant in applications. In biology, distributed delays are often found in population models because, for example, the time to maturity will obviously not be the same for each individual of the population [37, 38, 39]. In metal cutting applications DDEs with multiple delays or distributed delays are used as models for milling processes with variable pitch [40] or variable helix tools [41, 42].

From the above-mentioned examples it can be seen that the stability analysis of time delay systems is important, for example, for understanding the control of biological systems [43]. In machining, there is a significant interest in the identification of stability

charts for machine tool vibrations because the so-called chatter stability lobes can be used either for increasing the productivity of manufacturing processes by an optimization of the cutting conditions [44] or for increasing the efficiency in the development of new machine tools [45, 46]. An overview on the stability analysis of time delay systems is presented in [47, 48]. There are two main concepts. The first approach is called Lyapunov's first or indirect linearization method and is based on the linearization of the nonlinear time delay system Eq. (1.1) around a reference solution or attractor

$$\dot{\mathbf{x}}(t) = \mathbf{A}(t)\mathbf{x}(t) + \mathbf{B}(t)\mathbf{x}(t - \tau_0). \quad (1.2)$$

In Eq. (1.2) the coefficient matrices $\mathbf{A}(t)$ and $\mathbf{B}(t)$ depend on the reference solution of the nonlinear system Eq. (1.1) and the configurations $\mathbf{x}(t)$ are small perturbations around the reference solution (see Sec. 3.3.2 for details). The reference solution is stable or unstable if the amplitude of the perturbations $\mathbf{x}(t)$ goes to zero or diverges, respectively. The advantage of the indirect method is the fact that precise results for the exponential behavior of the perturbations $\mathbf{x}(t)$ can be obtained from Eq. (1.2) for the specific reference solution. On the other hand, Eq. (1.2) holds only for infinitesimal perturbations, which means that the results are not robust and, in general, depend on the initial condition of the system. In 1892 Lyapunov suggests a second or direct method in his doctoral thesis [49], which is based on the concept of the so-called Lyapunov function. The system is stable if the Lyapunov function decreases to zero independent of the state of the system. Thus, the direct method can be used to guarantee the robust stability of a nonlinear system independent of a specific perturbation and solution. On the other hand, the direct method leads, in general, only to a conservative bound on the parameter regions where the system is stable. In this thesis, Lyapunov's indirect linearization method is considered, which means that the stability of linear DDEs similar to Eq. (1.2) is studied. For the autonomous case, i.e. for DDEs with constant coefficient matrices $\mathbf{A}(t) = \mathbf{A}_0$, $\mathbf{B}(t) = \mathbf{B}_0$, the frequency domain stability analysis of Eq. (1.2) is presented in [50, 51, 52, 53]. It is based on the Laplace transform of the DDE and the solution of the resulting characteristic equation. A nice overview on the methods for the stability analysis of autonomous DDEs can be found in [54].

Constant coefficient matrices in Eq. (1.2) occur only if the original system Eq. (1.1) is already linear or if an equilibrium of a nonlinear DDE Eq. (1.1) is analyzed. The focus of this thesis are non-autonomous DDEs and especially periodic DDEs. A linear DDE with periodic coefficients $\mathbf{A}(t) = \mathbf{A}(t + T)$ and $\mathbf{B}(t) = \mathbf{B}(t + T)$ occurs whenever a periodic solution $\mathbf{u}(t) = \mathbf{u}(t + T)$ of the nonlinear DDE Eq. (1.1) is analyzed. A specific example is chaos control with time-delayed feedback, where an unstable periodic orbit of a chaotic system with period τ_0 is stabilized by a control term proportional to $\mathbf{u}(t - \tau_0) - \mathbf{u}(t)$ [12, 13]. Other common examples are DDEs with periodic parametric excitation, where one or more parameters of the system are characterized by an explicit periodic variation. Such systems are often found in engineering, as for example in the stability analysis of machine tool vibrations [3, 55] or in act-and-wait control [56, 57, 58]. A paradigmatic example for systems with periodic parametric excitation is the delayed Mathieu equation [59, 60]. In addition to periodic coefficients, it is also possible that the time delay is periodically modulated [22, 23] or periodic solutions of DDEs with

1. Introduction

state-dependent delays are investigated [61]. In both cases, periodically varying delays $\tau(t) = \tau(t+T)$ appear in the linearized DDE Eq. (1.2), which are in the scope of this thesis as well. From a mathematical point of view the theory for DDEs with constant delays is well-developed [62, 63], whereas there are some fundamental difficulties in the analysis of systems with time-varying delays [64, 65] and state-dependent delays [66, 67]. The main part of Chapter 2 is dedicated to the reduction of the complexity of systems with variable and state-dependent delays by a transformation to systems with constant delays. In fact, it was already shown that some DDEs with a discrete periodically-varying delay are equivalent to DDEs with a constant delay similar to Eq. (1.2) [26, 68, 69, 70, 71, 72].

Most of the methods for the stability analysis of linear DDEs with periodic coefficients are based on the finite dimensional approximation of the state \mathbf{x}_t of the DDE and the construction of the monodromy matrix [3, 55, 73, 74]. In particular, the state is approximated by a finite number of basis functions and the monodromy matrix specifies the time evolution of the state vector over the principle period of the time delay system. Then, the stability can be obtained from the eigenvalues of the monodromy matrix. A more detailed description of these methods is given in Chapter 5. Alternatively to the time domain methods based on the construction of the monodromy matrix, frequency domain methods can be used for the stability analysis of periodic DDEs [2, 59]. The frequency domain approach is based on the Floquet decomposition for DDEs [75, 76] and the Fourier transformation of the periodic terms and is known as Hill's infinite determinant method [77, 78]. Note that the Hill's infinite determinant method is related to the central equation in solid state physics, which is used for the calculation of energy bands for electrons in periodic crystals [79, 80]¹. Frequency domain methods for the analysis of periodic DDEs are almost exclusively used for the calculation of stability charts of machine tool vibrations [2, 41, 81, 82]. In particular, specific root finding algorithms are used for the numerical solution of the transcendental characteristic equation that is associated with the Hill's infinite determinant. However, the numerical methods for finding the roots of the transcendental characteristic equation are not suitable for the explicit calculation of the dominant Floquet exponents because one cannot be sure that a dominant exponent is omitted by the numerical root finder. Nevertheless, there are two fundamental advantages of frequency domain methods. On the one hand, Fourier modes or, in general, complex exponentials are eigenfunctions of the differential operator, i.e. $\frac{d}{dt}e^{st} = se^{st}$. As a consequence, the structural behavior of the machine tool vibrations can be described by frequency response functions (FRFs), which specifies the amplitudes and the phases of a harmonic vibration at the tool tip in response to a harmonic excitation with a certain frequency² [83]. The concept of FRFs is not only limited to mechanical engineering. In fact, the FRFs in mechanical engineering are closely related to the impulse response in signal processing [84], the impedance in electrical engineering [85], the dynamic susceptibility or the linear response function in physics [86] and the transfer function in control theory [87]. On the other hand, the calculation of the monodromy matrix for the solu-

¹In solid state physics Floquet theory is commonly known as Bloch theory

²In many applications such a linear structural behavior is valid because, for example, the amplitude of the vibrations is very low compared to the size of the machine-tool structure

tion over one period is not necessary in the frequency domain approach, which can be an advantage to time domain methods, when the period of the excitation becomes very large.

Contribution of the present work

In this thesis a generalization of the frequency domain approach based on the Hill's infinite determinant method for the analysis of periodic DDEs with time-varying, state-dependent and distributed delay is presented. The main contribution is a new method that puts the frequency domain approach for periodic systems in a more general framework, which is called Hill-Floquet method. In general, the Hill-Floquet method can be used for a transformation of non-autonomous systems with periodic coefficients to higher dimensional autonomous systems with constant coefficients. This is a significant advance in comparison to the existing methods because it enables the use of a bulk of methods for the analysis of DDEs with periodic coefficients, which were initially designed for the analysis of autonomous DDEs. Thus, the Hill-Floquet method represents an alternative approach for the calculation of Floquet exponents and eigenvectors of periodic systems, which is not based on the approximation of the monodromy operator, and where no specific numerical method for the analysis of the Hill's infinite determinant is necessary.

The newly introduced Hill-Floquet method is described for DDEs with periodic coefficients and time-invariant distributed delays. However, an essential part of this thesis is devoted to equivalent representations of the system. For example, as mentioned above it is known that certain systems with a discrete time-varying delay can be transformed to systems with a constant delay [26, 68, 69, 70, 71, 72]. In this thesis, the application of such a nonlinear time scale transformation for DDEs with a time-varying or a state-dependent delay distribution is shown. Moreover, the equivalence of these systems to some first-order hyperbolic partial differential equations (PDEs) is presented, where the boundaries can be either constant or variable, associated to the constant or variable delay distribution, respectively. Nevertheless, it is also shown that not every DDE with a variable delay or a variable delay distribution can be transformed to a DDE with constant delay. Specifically, only variable delay distributions originating from a transport with a variable velocity over a constant distance can be described by a DDE with a time-invariant delay distribution and are in the scope of this thesis.

In addition, to the newly introduced Hill-Floquet method and the theoretical results on the equivalence of time delay systems some new results on the analytical solution of linear DDEs are presented. In particular, the Laplace transform is used to describe the solution of DDEs with distributed delays in terms of a time domain representation of the propagator of the system. An explicit representation of the propagator is derived with the method of steps and the inverse Laplace transform via residue theory. The spectral representation of the propagator for autonomous DDEs is used to derive the eigenmode decomposition for DDEs with distributed delay. The results on the analytical solution of linear DDEs fill some gaps in the existing literature, where the theory is only presented for scalar DDEs [88] or only for DDEs with discrete delays [89].

The presented theory is used for the derivation of new results in specific applications

1. Introduction

in the field of time delay systems. In particular, single species reaction-diffusion systems with a delay in the reaction term are studied. Whereas diffusion-driven or Turing-like instabilities are not possible for single species reaction-diffusion systems without delay or with a single delay in the reaction term [90], it is shown that an asymmetric delay distribution can lead to Turing-like waves in these systems. For parallel turning processes, where two tools are simultaneously cutting the same surface of the workpiece at different locations, a very efficient method for the construction of the stability lobe diagram is presented. It is shown that the radial angle between the cutting tools, which indeed affects the time delays in the system [91, 92], has no influence on the stability lobes as long as the structural coupling between the two tools can be neglected. For synchronization in networks with heterogeneous delay couplings a technique for the decomposition of the network dynamics into network eigenmodes is presented. This method is an extension of the so-called master stability function, which can be used for the analysis of synchronized solutions in networks with homogeneous delays [93], to networks with heterogeneous delays. Here, it is shown that heterogeneous delays in the coupling lead to larger parameter regions with unstable transversal network eigenmodes and desynchronized solutions.

Organization

In Chapter 2 the standard form of the considered systems is defined and their relation to equivalent time delay systems and equivalent spatially extended systems is given. The theoretical background and an overview on the methods for the analysis of nonlinear time delay systems is given in Chapter 3. The standard analytical techniques for the solution of linear time delay systems are shown in Chapter 4. In Chapter 5 the basic tools for the stability analysis of linear DDEs is presented. The new Hill-Floquet transformation for the transformation of a DDE with periodic coefficients to an autonomous DDE with constant coefficients is introduced in Chapter 6. In particular, in Sec. 6.3 the method is combined with a Chebyshev collocation method for the analysis of the resulting autonomous DDE. The application of the presented theory to specific time delay systems in engineering, physics and biology are presented in Chapter 7. In particular, the existence of diffusion-driven instabilities from equilibria of single species delayed reaction-diffusion systems is systematically analyzed in Sec. 7.1. The application of frequency domain methods for the stability analysis of metal cutting vibrations is presented in Sec. 7.2, and finally, the analysis of synchronized solutions in delay-coupled networks with heterogeneous coupling delays is studied in Sec. 7.3.

2. System definition and equivalent systems

In this chapter, in Sec. 2.1 the standard form for the considered dynamical systems is defined. In addition, a large part of this chapter is dedicated to systems, which are equivalent to the standard form, and therefore, fall within the scope of this thesis as well. In particular, these are DDEs with time-varying and state-dependent delay, which are presented in Sec. 2.2, and first-order hyperbolic PDEs with constant and moving boundaries, which are presented in Sec. 2.3. Moreover in Sec. 2.4 systems with fast and slowly variable delays are presented, which can be approximated with the standard form defined in Sec. 2.1.

2.1. System definition and memory

In this thesis non-autonomous dynamical systems with memory effects are studied. The theory for the analysis of linear DDEs in Chapter 4, Chapter 5 and Chapter 6 are presented for the standard form

$$\dot{\mathbf{u}}(t) = \mathbf{f}(t, \mathbf{u}(t), \mathbf{r}_{\mathbf{u}}(t)). \quad (2.1)$$

The N -dimensional vector $\mathbf{u}(t) \in \mathbb{R}^N$ is called the configuration of the system and the N_{τ} dimensional vector $\mathbf{r}_{\mathbf{u}}(t) \in \mathbb{R}^{N_{\tau}}$ is called the memory. The vector field $\mathbf{f} : \mathbb{R} \times \mathbb{R}^N \times \mathbb{R}^{N_{\tau}} \rightarrow \mathbb{R}^N$ can depend explicitly on the independent variable t , on the configuration $\mathbf{u}(t)$, and on the memory $\mathbf{r}_{\mathbf{u}}(t)$ of the system. The components of the memory vector are a linear combination of the retarded configurations $\mathbf{u}(t - \tau)$ of the system, and are defined by

$$\mathbf{r}_{\mathbf{u}}(t) = \int_0^{\tau_{\max}} \mathbf{K}(\tau) \mathbf{u}(t - \tau) d\tau. \quad (2.2)$$

The $N_{\tau} \times N$ dimensional matrix $\mathbf{K}(\tau)$ is a matrix of delay distributions because their elements contains distributions of the delay τ , where $\tau_{\max} \geq 0$ specifies an upper bound of the delay distributions. Thus, the system Eq. (2.1) with the memory Eq. (2.2) is a DDE with time-invariant distributed delay. For example, for a $N \times N$ diagonal matrix $\mathbf{K}(\tau) = K(\tau) \mathbf{I}$ with identical diagonal elements $K(\tau)$ the N dimensional memory vector is determined by the same delay distribution $K(\tau)$ for each component of the configuration and for a diagonal matrix $\mathbf{K}(\tau)$ with non-homogeneous diagonal elements different delay distributions for different components of the configuration $\mathbf{u}(t)$ can be specified. In the following the matrix $\mathbf{K}(\tau)$ is simply called delay distribution.

2. System definition and equivalent systems

As mentioned already in the introduction the instantaneous configuration $\mathbf{u}(t)$ is not sufficient for a unique determination of the solution of the time delay system Eq. (2.1). Instead, due to the influence of the memory $\mathbf{r}_{\mathbf{u}}(t)$ in Eq. (2.1) the state of the system is given by the vector function $\mathbf{u}_t = \mathbf{u}(t - \tau)$, which contains also retarded configurations $\mathbf{u}(t - \tau)$ of the system with $0 \leq \tau \leq \tau_{\max}$. A unique solution of Eq. (2.1) for $t > 0$ exists if the state at $t = 0$ is specified by a unique initial function \mathbf{u}_0 [62].

Note that DDEs with time-varying or state-dependent delay distributions and PDEs with constant and moving boundaries, which are presented in Sec. 2.2 and Sec. 2.3, respectively, are in the scope of this thesis as well. In particular, it turns out that in many applications the independent variable t of the standard form Eq. (2.1) is not necessarily equal to the physical time in the real-world. In fact, in engineering applications in Sec. 2.2.1 the independent variable t can specify a covered distance or as in the machine tool example in Sec. 7.2 an angle. In the biological examples in Sec. 2.3.2 the independent variable t can be often interpreted as the size or a specific amount of food. In this case in the physical time the system can be specified by a DDE with variable or state-dependent delay or by a PDE with constant or moving boundaries as it will be shown next in Sec. 2.2 and Sec. 2.3, respectively.

2.2. Equivalent time delay systems

In this section, time delay systems with a variable delay distribution are presented, which are related to the standard form Eq. (2.1) with constant delay via a nonlinear time scale transformation. The content of this Section is not necessarily required for the presented analysis in the remaining Chapters of this thesis. Nevertheless, it is necessary for the application of the presented theory to DDEs with time-dependent or state-dependent delay distribution. In particular, the presented theory is used in Sec. 7.2 for the analysis of machine tool vibrations in turning with a variable delay due to a spindle speed variation.

2.2.1. Variable transport delays

A nonlinear time scale transformation can be applied to the standard form Eq. (2.1), with the objective of changing the delay distribution $\mathbf{K}(\tau)$ of the memory $\mathbf{r}_{\mathbf{u}}(t)$ in Eq. (2.2). The nonlinear time scale transformation and its inverse are defined as

$$t = \Phi(\tilde{t}), \quad \text{and} \quad \tilde{t} = \Phi^{-1}(t). \quad (2.3)$$

Note that the time scale transformation $\Phi(\tilde{t})$ and its inverse may also depend on the configuration $\mathbf{u}(t)$ of the system. In particular, in some applications the inverse time scale transformation can be given by $\tilde{t} = \Phi_{\mathbf{u}}^{-1}(t, \mathbf{u}(t))$ [26, 94]. In this case the inverse transformation $\Phi^{-1}(t)$ consistent to Eq. (2.3) can be defined as $\Phi^{-1}(t) := \Phi_{\mathbf{u}}^{-1}(t, \mathbf{u}(t))$. Some additional remarks on state-dependent time scale transformations are given below. It is assumed that the time scale transformation $\Phi(\tilde{t})$ is differentiable and the derivative is strictly positive

$$\frac{dt}{d\tilde{t}} = \Omega(\tilde{t}) > 0. \quad (2.4)$$

2.2. Equivalent time delay systems

Thus, the inverse $\Phi^{-1}(t)$ is unique and a one-to-one mapping between the independent variables t and \tilde{t} is guaranteed.

In Sec. 2.2.2 an equivalent representation of the standard form Eq. (2.1) with the memory Eq. (2.2) in terms of the new variable \tilde{t} will be presented, where a time-varying delay distribution can appear. For this purpose, the instantaneous and the retarded configurations of the original system Eq. (2.1), $\mathbf{u}(t)$ and $\mathbf{u}(t - \tau)$, are expressed in terms of the new independent variable \tilde{t} as

$$\mathbf{u}(t) = \mathbf{u}(\Phi(\tilde{t})) = \tilde{\mathbf{u}}(\tilde{t}), \quad \mathbf{u}(t - \tau) = \mathbf{u}(\Phi(\tilde{t} - \tilde{\tau}(\tilde{t}))) = \tilde{\mathbf{u}}(\tilde{t} - \tilde{\tau}(\tilde{t})). \quad (2.5)$$

From Eq. (2.5) it follows that the condition between the original constant delay τ and the corresponding variable delay $\tilde{\tau}(\tilde{t})$ in the new representation can be given by

$$\Phi(\tilde{t} - \tilde{\tau}(\tilde{t})) = \Phi(\tilde{t}) - \tau \quad \leftrightarrow \quad \tau = \int_{\tilde{t} - \tilde{\tau}(\tilde{t})}^{\tilde{t}} \Omega(t') dt'. \quad (2.6)$$

The condition Eq. (2.6) can be interpreted as a transport with the variable velocity $\Omega(\tilde{t})$ over the constant distance τ . Time delays that are defined similar to Eq. (2.6) are called variable transport delays [72, 94] or threshold-type delays [9, 19, 20, 21]. A block diagram for a system with a distributed variable transport delay is given in Fig. 2.1a, where the delay is generated by a transport over a conveyor belt with the time-varying velocity $\Omega(\tilde{t})$. In this example, the independent variable t of the standard form Eq. (2.1) can be interpreted as a spatial variable and the new variable \tilde{t} can be interpreted as the physical time. More precisely, $t = \Phi(\tilde{t})$ specifies the absolute distance that has been covered by the conveyor belt over time \tilde{t} . The square-shaped particles on the left end of the conveyor belt are imprinted with the instantaneous configuration $\mathbf{u}(t)$ of the time delay system and the configuration of the particles does not change during the transport over the conveyor belt. This means that the configuration of the particles on the right hand side of the conveyor belt represents retarded configurations $\mathbf{u}(t - \tau)$ of the time delay system. Specifically, in the system Eq. (2.1) the instantaneous configuration $\mathbf{u}(t)$ is affected by the memory $\mathbf{r}_{\mathbf{u}}(t)$, which is, according to Eq. (2.2), a linear combination of the imprinted configurations of the particles on the conveyor belt. Such systems with a variable transport delay can be often found in engineering. For example, metal cutting vibrations [70], material flows in reactors [71], FIFO buffers in electronic circuits [29] or the fuel injection in automotive engineering [95, 96] can be described by DDEs with variable transport delays. Note that there is also a specific *Variable Transport Delay* block in MATLAB/Simulink for this type of delays [72]. In biology variable transport delays are typically known as threshold-type delays and appear, for example, in structured population models [9, 19, 20, 21, 66]. More details on variable transport delays in biological systems can be found in Sec. 2.3.2, where a PDE representation of the variable transport in Fig. 2.1a is discussed.

Variable transport delays $\tilde{\tau}(\tilde{t})$, which are implicitly defined by Eq. (2.6), are equal to the traveling time of the particles for a transport with the conveyor belt over the fixed

2. System definition and equivalent systems

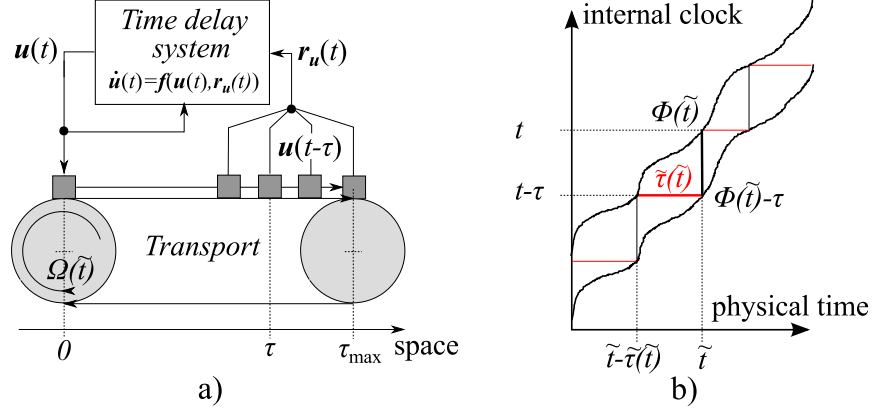


Figure 2.1.: a) A variable transport delay $\tilde{\tau}(\tilde{t})$ as defined in Eq. (2.6) appears when the delay is generated by a transport with the variable velocity $\Omega(\tilde{t})$ over a constant distance τ similar to the conveyor belt. b) Graphical interpretation of the relationship Eq. (2.6) between the constant distance τ and the variable traveling time $\tilde{\tau}(\tilde{t})$.

distance τ . The relationship between the variable traveling time $\tilde{\tau}(\tilde{t})$ and the constant distance τ is illustrated in Fig. 2.1b. The so-called internal clock t , which is the independent variable of the standard form Eq. (2.1), is mapped to the physical time \tilde{t} via the function $\Phi(\tilde{t})$. A constant shift τ of the function $\Phi(\tilde{t})$ in the vertical direction generates a variable horizontal shift in the physical time \tilde{t} . The varying horizontal distance between the two functions $\Phi(\tilde{t})$ and $\Phi(\tilde{t}) - \tau$ in Fig. 2.1b is equivalent to the variable transport delay $\tilde{\tau}(\tilde{t})$. Variable transport delays can be explicitly calculated by

$$\tilde{\tau}(\tilde{t}) = \tilde{t} - \Phi^{-1}(\Phi(\tilde{t}) - \tau). \quad (2.7)$$

In the literature only discrete variable transport delays were studied, which can be characterized by the delay distribution $\mathbf{K}(\tau) = \mathbf{K}_0\delta(\tau - \tau_0)$. However, distributed variable transport delays are also possible. Distributed variable transport delays appear, for example, in engineering for milling tools with non-uniform pitch or non-uniform helix angles [40, 41] or in population dynamics if precursor cells are released into the mature population at different maturity levels [20, 21]. For the representation of the system dynamics in terms of the physical time \tilde{t} in Sec. 2.2.2 a relationship between the memory \mathbf{r} of the standard form and the memory $\tilde{\mathbf{r}}$ in terms of the new variables must be derived. In general, for an arbitrary delay distribution the memory in the new variables can be written as

$$\tilde{\mathbf{r}}_{\tilde{\mathbf{u}}}(\tilde{t}) = \int_0^{\tilde{\tau}_{\max}(\tilde{t})} \tilde{\mathbf{K}}(\tilde{t}, \tilde{\tau}) \tilde{\mathbf{u}}(\tilde{t} - \tilde{\tau}) d\tilde{\tau} = \mathbf{r}_{\mathbf{u}}(t). \quad (2.8)$$

The maximum delay $\tilde{\tau}_{\max}(\tilde{t})$ in the physical time can be calculated from Eq. (2.7) with the corresponding constant maximum value $\tau = \tau_{\max}$ of the original delay distribution.

2.2. Equivalent time delay systems

The relationship between the time-invariant delay distribution $\mathbf{K}(\tau)$ of the original system and the time-varying distribution $\tilde{\mathbf{K}}(\tilde{t}, \tilde{\tau})$ of the tilded system can be identified as

$$\tilde{\mathbf{K}}(\tilde{t}, \tilde{\tau}) = \mathbf{K}(\Phi(\tilde{t}) - \Phi(\tilde{t} - \tilde{\tau})) \Omega(\tilde{t} - \tilde{\tau}). \quad (2.9)$$

A detailed derivation of the relationship Eq. (2.9) is given in Appendix A.1. Thus, the original delay distribution $\mathbf{K}(\tau)$ with a constant density in the fixed interval $[0, \tau_{\max}]$ is converted to a time-varying delay distribution $\tilde{\mathbf{K}}(\tilde{t}, \tilde{\tau})$ with a time-varying support $[0, \tilde{\tau}_{\max}(\tilde{t})]$.

For a homogeneous delay distribution $\mathbf{K}(\tau) = \mathbf{K}_0$, for example, the associated delay distribution in the transformed system can be determined by

$$\tilde{\mathbf{K}}(\tilde{t}, \tilde{\tau}) = \mathbf{K}_0 \Omega(\tilde{t} - \tilde{\tau}). \quad (2.10)$$

For a discrete delay τ_0 in the original system with $\mathbf{K}(\tau) = \mathbf{K}_0 \delta(\tau - \tau_0)$, the delay distribution $\tilde{\mathbf{K}}$ in the transformed system can be written as

$$\tilde{\mathbf{K}}(\tilde{t}, \tilde{\tau}) = \mathbf{K}_0 \delta(\Phi(\tilde{t}) - \Phi(\tilde{t} - \tilde{\tau}) - \tau_0) \Omega(\tilde{t} - \tilde{\tau}), \quad (2.11)$$

The argument of the delta distribution can be simplified by defining the function

$$g(\tilde{\tau}) := \Phi(\tilde{t}) - \Phi(\tilde{t} - \tilde{\tau}) - \tau_0, \text{ with } g'(\tilde{\tau}) = \Omega(\tilde{t} - \tilde{\tau}), \quad (2.12)$$

which leads to the expression $\tilde{\mathbf{K}}(\tilde{t}, \tilde{\tau}) = \mathbf{K}_0 \delta(g(\tilde{\tau})) g'(\tilde{\tau})$ for the delay distribution in Eq. (2.11). Since according to Eq. (2.4) the function $\Phi(\tilde{t})$ is strictly monotonic increasing the argument $g(\tilde{\tau})$ of the delta distribution has only one real root at $\tilde{\tau} = \tilde{\tau}_0(\tilde{t})$, where the root $\tilde{\tau} = \tilde{\tau}_0(\tilde{t})$ is defined by Eq. (2.7) with $\tau = \tau_0$. If the properties for a composition of the Dirac delta distribution are used the delay distribution Eq. (2.11) can be further simplified to

$$\tilde{\mathbf{K}}(\tilde{t}, \tilde{\tau}) = \mathbf{K}_0 \delta(\tilde{\tau} - \tilde{\tau}_0(\tilde{t})). \quad (2.13)$$

Eq. (2.13) coincides with the known result for the transformation of a constant discrete delay τ_0 to a variable discrete delay $\tilde{\tau}_0(\tilde{t})$ via a nonlinear time scale transformation Eq. (2.3) [23, 26, 94].

2.2.2. Equivalent DDEs with time- or state-dependent delay

With Eqs. (2.3), (2.4), (2.5), and (2.8) the original system Eq. (2.1) with a time-invariant delay distribution $\mathbf{K}(\tau)$ can be transformed into a system with a variable delay distribution

$$\tilde{\mathbf{u}}'(\tilde{t}) = \Omega(\tilde{t}) \mathbf{f}(\Phi(\tilde{t}), \tilde{\mathbf{u}}(\tilde{t}), \tilde{\mathbf{r}}_{\tilde{\mathbf{u}}}(\tilde{t})), \quad (2.14)$$

where the memory $\tilde{\mathbf{r}}_{\tilde{\mathbf{u}}}(\tilde{t})$ and the corresponding variable delay distribution $\tilde{\mathbf{K}}(\tilde{t}, \tilde{\tau})$ in the new variables are given by Eq. (2.8) and Eq. (2.9), respectively. The relationship between the DDE Eq. (2.14) with a time-varying delay distribution and the DDE Eq. (2.1) with a constant delay distribution is used in Sec. 7.2 for the analysis of machine tool chatter in turning, where a variable transport delay appears and the variable transport velocity

2. System definition and equivalent systems

$\Omega(\tilde{t})$ is equivalent to a variable spindle speed. The state of the transformed system Eq. (2.14) is defined by the vector function $\tilde{\mathbf{u}}_{\tilde{t}} = \tilde{\mathbf{u}}(\tilde{t} - \tilde{\tau})$ with $0 \leq \tilde{\tau} \leq \tilde{\tau}_{\max}(\tilde{t})$. Thus, the size $\tilde{\tau}_{\max}(\tilde{t})$ of the interval of the state space typically varies with time. Nevertheless, the following condition holds for the derivative of the maximum variable delay

$$\tilde{\tau}'_{\max}(\tilde{t}) = 1 - \frac{\Omega(\tilde{t})}{\Omega(\tilde{t} - \tilde{\tau}_{\max}(\tilde{t}))} < 1, \quad (2.15)$$

which means that a discussion as in [64, 65] about the causality of the time delay system is not necessary for DDEs with variable transport delays and a unique solution of Eq. (2.14) exists if the initial function $\tilde{\mathbf{u}}_0$ is specified in the interval $[-\tilde{\tau}_{\max}(0), 0]$. The DDE Eq. (2.1) with constant delay and the DDE Eq. (2.14) with variable delay are completely equivalent as long as the transformation $\Phi(\tilde{t})$ is bijective and differentiable, i.e. $\Phi(\tilde{t})$ is a diffeomorphism. If the transformation depends on the configuration of the DDE, i.e. $\Phi^{-1}(t) = \Phi_{\mathbf{u}}^{-1}(t, \mathbf{u}(t))$, state-dependent variable transport delays $\tilde{\tau}(\tilde{t}, \tilde{\mathbf{u}}_{\tilde{t}})$ appear. State-dependent variable transport delays can be found, for example, in machine tool vibrations [25, 26], in automotive engineering [95, 96] and in biology [9, 19, 20, 21, 66]. Obviously, for state-dependent variable transport delays it is not clear a priori if the condition Eq. (2.4) for a one-to-one mapping between the internal clock t and physical time \tilde{t} is fulfilled. However, the violation of the condition Eq. (2.4) typically corresponds to unphysical situations, where both the original representation Eq. (2.1) in terms of the internal clock and the new representation Eq. (2.14) in terms of the physical time are not meaningful [26, 94].

In general, the transformation from constant delay distributions to time-varying or state-dependent delay distributions is straightforward. However, the inverse problem is much more complex because not every variable delay fulfills condition Eq. (2.6) or not every delay distribution fulfills condition Eq. (2.9) for variable transport delays. Thus, for a system with a given variable delay $\tilde{\tau}_0(\tilde{t})$ or variable delay distribution $\tilde{\mathbf{K}}(\tilde{t}, \tilde{\tau})$ it is not clear if there exists a transformation to a system with a time-invariant delay τ_0 or time-invariant delay distribution $\mathbf{K}(\tau)$, respectively. For variable discrete delays $\tilde{\tau}_0(\tilde{t})$ the identification of variable transport delays is possible by studying the relationship Eq. (2.6) in more detail. The ongoing retarded access on delayed configurations in the two delay systems Eq. (2.1) and Eq. (2.14) with discrete delay distributions can be described by the iterated maps

$$t_{i+1} = a(t_i) := t_i - \tau_0, \quad -\infty < t_i < \infty, \quad (2.16a)$$

$$\tilde{t}_{i+1} = \tilde{a}(\tilde{t}_i) := \tilde{t}_i - \tilde{\tau}_0(\tilde{t}_i), \quad -\infty < \tilde{t}_i < \infty. \quad (2.16b)$$

The maps a and \tilde{a} are called retarded access maps. Using the map definitions in Eq. (2.16), the relationship Eq. (2.6) defines a topological conjugacy between the retarded access maps

$$\Phi \circ \tilde{a} = a \circ \Phi, \quad (2.17)$$

where \circ denotes function composition. This means, that properties, which are invariant under a topological conjugacy, must be the same for the two maps a and \tilde{a} . In other

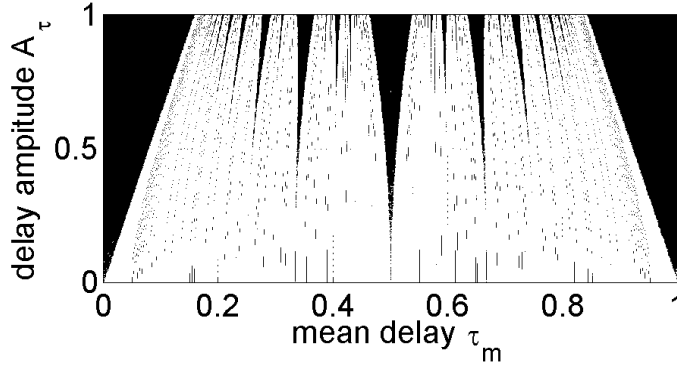


Figure 2.2.: Parameter regions for sinusoidal delays defined by the access map Eq. (2.18) ($T = 1$) that are equivalent to variable transport delays are fractal (white). The black regions correspond to the so-called Arnold tongues [99].

words the rotation number, the Lyapunov exponent or the invariant measure of the access map \tilde{a} of the system with variable delay $\tilde{\tau}_0(\tilde{t})$ can be used to check, whether the system is equivalent to a system with constant delay τ_0 or not. For the original system with constant delay the corresponding retarded access map Eq. (2.16a) is simply a linear shift map. For a sinusoidally varying delay, for example, the retarded access map is equivalent to the well-known circle map

$$\tilde{t}_{i+1} = \tilde{t}_i - \tau_m - \frac{A_\tau T}{2\pi} \sin\left(2\pi \frac{\tilde{t}_i}{T}\right), \quad (2.18)$$

where the parameters τ_m , A_τ and T specify the mean, the amplitude and the period of the delay variation. Circle maps similar to Eq. (2.18) and their topological conjugacy to the linear shift map Eq. (2.16a) were extensively studied in the literature [97, 98, 99]. As a result, in the parameter space of periodic continuous delays with $A_\tau < 1$ corresponding to the condition $\tilde{\tau}'(\tilde{t}) < 1$, the set of variable transport delays, i.e. variable delays, which are equivalent to constant delays, are a fractal [100].

For example, the type of the delay for sinusoidally varying delays Eq. (2.18) with $T = 1$ is illustrated in Fig. 2.2. The black regions in the τ_m - A_τ -plane are equivalent to the so-called Arnold tongues of the circle map. In these regions the Lyapunov exponent of the access map is negative and the circle map Eq. (2.18) is not topological conjugate to the linear shift map Eq. (2.16a). The delays corresponding to these parameters are called dissipative delays [100]. Only for parameters in the white regions in Fig. 2.2, the Lyapunov exponent of the corresponding circle map Eq. (2.18) is zero and is, therefore, equivalent to the Lyapunov exponent of the linear shift map Eq. (2.16a). This means that only these sinusoidal delays are variable transport delays. On closer inspection the white region is a fractal, which implies that it is not advisable to model variable transport delays by a parameter family in the physical time \tilde{t} because it depends extremely sensitive on the parameters of the time-varying delay whether it represents a variable transport delay or a dissipative delay. In fact, a description in terms of the internal clock t similar

2. System definition and equivalent systems

to Eq. (2.1) is recommended, where the discrete delay τ_0 in the memory is constant. More details on the dichotomy between variable transport delays with zero Lyapunov exponent of the access map \tilde{a} and dissipative delays with negative access map Lyapunov exponent can be found in [100].

2.3. Equivalent spatially extended systems

In this section, spatially extended systems are presented, which are related to the standard form Eq. (2.1) with constant delay via a transformation of variables. The content of this Section is not necessarily required for the presented analysis in the remaining chapters of this thesis, similar to the content in Sec. 2.2. Nevertheless, the presented transformations are useful in some biological and engineering applications.

2.3.1. Equivalent first order hyperbolic PDEs

In Sec. 2.2.2 it was shown, that DDEs with variable transport delays can be described in terms of the physical time \tilde{t} or the internal clock t with a time-varying or time-invariant delay distribution, respectively. In this subsection, it is shown that these time delay systems can be also described by hyperbolic PDEs. Specifically, these PDEs are related to different PDE descriptions of the transport in Fig. 2.1a. PDE models for time delay systems are often used in population dynamics [9, 19, 20, 21, 66] or in control theory [101, 102]. In these representations of the time delay system the delays τ or $\tilde{\tau}$ and the instantaneous time t or \tilde{t} are the space and the time variables of a hyperbolic PDE, respectively. Thus, in the PDEs the time and the delay variables are decoupled from each other. As a consequence, four equivalent PDE representations of the time delay system Eq. (2.1) are possible, where both, the time and the space variable of the PDE, can be specified either in terms of the internal clock or in terms of the physical time. In the following, a systematic overview on the four equivalent PDE representations is given. Later, in Sec. 2.3.2 more details on the biological interpretation of the PDE models are given.

The most obvious PDE representation of the time delay system follows from Eq. (2.1) with $\mathbf{v}(\tau, t) = \mathbf{u}(t - \tau)$. In a delay system the vector $\mathbf{u}(t)$ specifies the configuration of the particles at the left end of the conveyor belt in Fig. 2.1a and the configuration at the right hand side of the conveyor belt is specified by retarded configurations $\mathbf{u}(t - \tau)$ dependent on the transport distance τ . In contrast, in the PDE representation the vector $\mathbf{v}(\tau, t)$ specifies the configuration of the particles on the conveyor belt at the location τ at time t and no time-delayed arguments are necessary. The transport of the particles with the conveyor belt is given by the advection equation [54, 62, 94]

$$\frac{\partial}{\partial t} \mathbf{v}(\tau, t) + \frac{\partial}{\partial \tau} \mathbf{v}(\tau, t) = 0. \quad (2.19)$$

The PDE representation of the DDE Eq. (2.1) is completed by the boundary condition

$$\left. \frac{\partial \mathbf{v}(\tau, t)}{\partial \tau} \right|_{\tau=0} = -\mathbf{f}(t, \mathbf{v}(0, t), \mathbf{r}_v(t)), \quad (2.20)$$

2.3. Equivalent spatially extended systems

and the initial condition $\mathbf{v}(\tau, 0) = \mathbf{u}(-\tau)$ with $0 \leq \tau \leq \tau_{\max}$. As was already reported in [54], the boundary condition Eq. (2.20) for the PDE Eq. (2.19) is an interconnected boundary condition, that depends on the configuration $\mathbf{v}(\tau, t)$ of the PDE at the external boundaries at $\tau = 0$ and $\tau = \tau_{\max}$ as well as on interior points $0 \leq \tau < \tau_{\max}$. The dependence on the interior points is specified by the memory $\mathbf{r}_{\mathbf{v}}(t)$ as defined in Eq. (2.2) with the time-invariant delay distribution $\mathbf{K}(\tau)$. If Eq. (2.19) is interpreted as a transport mechanism similar to the conveyor belt in Fig. 2.1, both the location τ and the time t of the configuration $\mathbf{v}(\tau, t)$ of the system is specified in terms of a distance, because the internal clock t is a measure for the distance covered by the particles at the physical time \tilde{t} . A representation similar to the PDE Eq. (2.19), where both the time and the space variable of the PDE is measured in terms of the internal clock is only rarely used in applications. Instead, a second representation can be found much more often in applications. In the second representation the space variable of the PDE still describes the physical space τ along the conveyor belt, whereas the time is measured in terms of the physical time \tilde{t} . In this case the PDE can be written as

$$\frac{\partial}{\partial \tilde{t}} \tilde{\mathbf{v}}(\tau, \tilde{t}) + \Omega(\tilde{t}) \frac{\partial}{\partial \tau} \tilde{\mathbf{v}}(\tau, \tilde{t}) = 0. \quad (2.21)$$

Here, the relationship $\tilde{\mathbf{v}}(\tau, \tilde{t}) = \mathbf{u}(\Phi(\tilde{t}) - \tau)$ holds between the configurations of the PDE Eq. (2.21) and the DDE Eq. (2.1). The corresponding interconnected boundary condition can be specified as

$$\left. \frac{\partial \tilde{\mathbf{v}}(\tau, \tilde{t})}{\partial \tau} \right|_{\tau=0} = -\mathbf{f}(\Phi(\tilde{t}), \tilde{\mathbf{v}}(0, \tilde{t}), \mathbf{r}_{\tilde{\mathbf{v}}}(\Phi(\tilde{t}))). \quad (2.22)$$

The representation Eq. (2.21) is the natural representation of the transport in Fig. 2.1a, because the time and space variables \tilde{t} and τ of the PDE correspond to the physical interpretation of time and space of the transport. The third PDE representation is a description, where both the time \tilde{t} and the space variable $\tilde{\tau}$ of the PDE are time variables in the physical meaning of the transport. More precisely, the value $\tilde{\tau}$ is the traveling time for the particle transport on the conveyor belt over a distance τ , and therefore, can be used to specify a location in the PDE system. The resulting PDE can be described by

$$\frac{\partial}{\partial \tilde{t}} \tilde{\mathbf{w}}(\tilde{\tau}, \tilde{t}) + \frac{\partial}{\partial \tilde{\tau}} \tilde{\mathbf{w}}(\tilde{\tau}, \tilde{t}) = 0, \quad (2.23)$$

where the relationship $\tilde{\mathbf{w}}(\tilde{\tau}, \tilde{t}) = \tilde{\mathbf{u}}(\tilde{t} - \tilde{\tau})$ holds between the configurations of the PDE and the DDE with variable delay Eq. (2.14). The PDE Eq. (2.23) is the direct conversion of the DDE Eq. (2.14) into a spatially extended system. The corresponding boundary condition can be described by

$$\left. \frac{\partial \tilde{\mathbf{w}}(\tilde{\tau}, \tilde{t})}{\partial \tilde{\tau}} \right|_{\tilde{\tau}=0} = -\Omega(\tilde{t}) \mathbf{f}(\Phi(\tilde{t}), \tilde{\mathbf{w}}(0, \tilde{t}), \tilde{\mathbf{r}}_{\tilde{\mathbf{w}}}(\tilde{t})), \quad (2.24)$$

where the memory $\tilde{\mathbf{r}}$ is defined by Eq. (2.8) with the time-varying delay distribution Eq. (2.9). This implies that, in general, the boundary on the right hand side of the PDE

2. System definition and equivalent systems

varies with time. The last representation of the system is a PDE description in terms of the internal clock t on a temporal space $\tilde{\tau}$. This is completely contrary to the physical interpretation of the transport, because the time in the PDE is measured in terms of distance covered by conveyor belt and the space variable of the PDE is defined in terms of the traveling time $\tilde{\tau}$ of particles on the conveyor belt. The corresponding PDE can be given by

$$\frac{\partial}{\partial t} \mathbf{w}(\tilde{\tau}, t) + \frac{1}{\Omega(\Phi^{-1}(t))} \frac{\partial}{\partial \tilde{\tau}} \mathbf{w}(\tilde{\tau}, t) = 0. \quad (2.25)$$

The relationship between the configurations of the PDE and the configurations of the DDE Eq. (2.14) can be given by $\mathbf{w}(\tilde{\tau}, t) = \tilde{\mathbf{u}}(\Phi^{-1}(t) - \tilde{\tau})$. Similar to Eq. (2.23) the size of the state space of the PDE varies with time. The corresponding moving boundary condition can be characterized by

$$\left. \frac{\partial \mathbf{w}(\tilde{\tau}, t)}{\partial \tilde{\tau}} \right|_{\tilde{\tau}=0} = -\Omega(\Phi^{-1}(t)) \mathbf{f}(t, \mathbf{w}(0, t), \tilde{\mathbf{r}}_{\mathbf{w}}(\Phi^{-1}(t))). \quad (2.26)$$

The four hyperbolic PDE representations of the time delay system can be analyzed by the method of characteristics. In general, the solution of a hyperbolic PDE can be described by an ODE along the characteristic curves. The characteristic curves C_v , $C_{\tilde{v}}$, $C_{\tilde{w}}$ and C_w for the four PDE representations are derived in Appendix A.1.2 and can be given by the parametric curves

$$\begin{aligned} C_v &= \{(\tau, t) : \tau(s) = \tau(0) + s, \quad t(s) = t(0) + s\}, \\ C_{\tilde{v}} &= \{(\tau, \tilde{t}) : \tau(s) = \tau(0) + \Phi(s), \quad \tilde{t}(s) = \tilde{t}(0) + s\}, \\ C_{\tilde{w}} &= \{(\tilde{\tau}, \tilde{t}) : \tilde{\tau}(s) = \tilde{\tau}(0) + s, \quad \tilde{t}(s) = \tilde{t}(0) + s\}, \\ C_w &= \{(\tilde{\tau}, t) : \tilde{\tau}(s) = \tilde{\tau}(0) + \Phi^{-1}(s), \quad t(s) = t(0) + s\}. \end{aligned} \quad (2.27)$$

Some selected characteristic curves for each representation are illustrated in Fig. 2.3 by the black dashed curves. The configurations \mathbf{v} , $\tilde{\mathbf{v}}$, $\tilde{\mathbf{w}}$, and \mathbf{w} are constant along the characteristic curves due to a zero right hand side of the four PDEs. For Eq. (2.19) and Eq. (2.23) corresponding to Fig. 2.3a and Fig. 2.3d, where both the space and time variables of the PDE are consistently specified in terms of space or time variables of the transport, respectively, the velocity of the advection is constant. In contrast, for the PDEs with a mixed physical interpretation of the space and time variables of the PDE, i.e. Eq. (2.21) and Eq. (2.25) corresponding to Fig. 2.3c and Fig. 2.3b, respectively, the velocity of the transport varies. This result is manifested in the nonlinear behavior of the characteristic curves Eq. (2.27), i.e. the black dashed lines in Fig. 2.3. If the space variable of the PDE coincide with the physical interpretation of the space in the transport, the delay distribution $\mathbf{K}(\tau)$ is time-invariant and has a constant support, which means that the boundaries of the PDE are time-invariant. This is illustrated by the red solid curves in Fig. 2.3a and Fig. 2.3c for the exemplary delays τ_1 , τ_2 and τ_{\max} . Along these curves the delay distribution is constant. In contrast, in Eq. (2.23) and Eq. (2.25) corresponding to Fig. 2.3d and Fig. 2.3b, respectively, the delay distribution $\tilde{\mathbf{K}}(\tilde{t}, \tilde{\tau})$ varies with time. This is illustrated by the varying red solid curves specified by the time-varying delays $\tilde{\tau}_1(\tilde{t})$ and $\tilde{\tau}_2(\tilde{t})$, which are associated with the constant delays τ_1 and τ_2 .

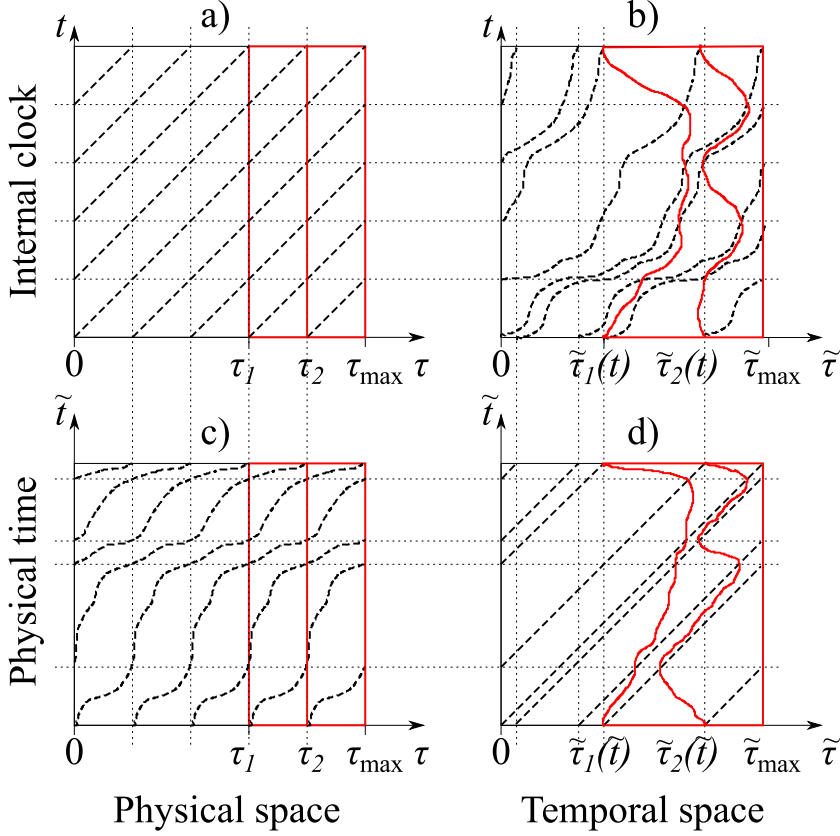


Figure 2.3.: Selected characteristic curves Eq. (2.27) (black, dashed) are presented for each of the four PDE representations in Sec. 2.3.1. Specific delays corresponding to a constant distance τ_1 and τ_2 and τ_{\max} are shown by red solid lines.

Along these curves the delay distributions are time-invariant $\tilde{\mathbf{K}}(\tilde{t}, \tilde{\tau}_1(\tilde{t})) = \mathbf{K}(\tau_1)$ and $\tilde{\mathbf{K}}(\tilde{t}, \tilde{\tau}_2(\tilde{t})) = \mathbf{K}(\tau_2)$. In general, a moving external boundary $\tilde{\tau}_{\max}(\tilde{t})$ appears in the PDE representations Eq. (2.23) and Eq. (2.25), where the space variable $\tilde{\tau}$ of the PDE is characterized by the traveling time of the transport. However, in the example the specific periodicity condition $\Phi^{-1}(t - \tau_{\max}) = \Phi^{-1}(t) - \tilde{\tau}_{\max}$ holds, and therefore, the external boundary $\tilde{\tau}_{\max}(\tilde{t}) = \tilde{\tau}_{\max}$ is always time-invariant in Fig. 2.3.

2.3.2. PDE representations in population dynamics

In this section the connection between the basic PDE models in Sec. 2.3.1 and PDEs with constant and moving boundaries as models for structured populations in biology is presented. A model, which is widely used for the description of structured populations, is the so-called McKendrick equation, Sharpe-Lotka-McKendrick equation or von Foerster

2. System definition and equivalent systems

equation [103, 104, 105]

$$\frac{\partial}{\partial t} \tilde{w}_p(\tilde{\tau}, \tilde{t}) + \frac{\partial}{\partial \tilde{\tau}} \tilde{w}_p(\tilde{\tau}, \tilde{t}) = -\mu \tilde{w}_p(\tilde{\tau}, \tilde{t}), \quad (2.28)$$

with the boundary condition

$$\tilde{w}_p(0, \tilde{t}) = \int_0^\infty \beta(\tilde{\tau}) \tilde{w}_p(\tilde{\tau}, \tilde{t}) d\tilde{\tau}. \quad (2.29)$$

In Eq. (2.28) $\tilde{w}_p(\tilde{\tau}, \tilde{t})$ specifies the number of individuals of a population at time \tilde{t} with age $\tilde{\tau}$, and μ is the mortality rate, which leads to an exponential decrease of the population for increasing age $\tilde{\tau}$. With the scaling $\tilde{w}_p(\tilde{\tau}, \tilde{t}) = e^{-\mu \tilde{t}} \tilde{\mathbf{w}}(\tilde{\tau}, \tilde{t})$ the PDE Eq. (2.28) simplifies to Eq. (2.23), i.e. the third PDE representation in Sec. 2.3.1. In the boundary condition Eq. (2.29), $\beta(\tilde{\tau})$ is the birth rate of the population. In many applications the population can be divided into the immature and the mature population and the age $\tilde{\tau} = \tilde{\tau}_0(\tilde{t})$ for maturity is defined by a threshold condition that is exactly equivalent to the condition Eq. (2.6) for a variable transport delay with the constant threshold $\tau = \tau_0$ [9, 19, 20, 21, 66]. In the biological context, the constant delay τ_0 is a constant amount of food or a constant size that must be reached for maturity and $\Omega(\tilde{t})$ is the velocity of maturation, which can also depend on the configuration $\tilde{\mathbf{u}}(\tilde{t})$ of the system. In the general case of a state-dependent velocity of maturation, the boundary between immature and mature population is state-dependent as well. It is assumed that the birth rate is zero $\beta(\tilde{\tau}) = 0$ for the immature population with $\tilde{\tau} \leq \tilde{\tau}_0(\tilde{t})$ and constant $\beta(\tilde{\tau}) = \beta_0$ for the mature population with $\tilde{\tau} > \tilde{\tau}_0(\tilde{t})$. Thus, in scaled variables the boundary condition Eq. (2.29) of the population model can be written as

$$\tilde{\mathbf{w}}(0, \tilde{t}) = \beta_0 \int_{\tilde{\tau}_0(\tilde{t})}^\infty \tilde{\mathbf{w}}(\tilde{\tau}, \tilde{t}) d\tilde{\tau}. \quad (2.30)$$

The time derivative of the boundary condition Eq. (2.30) yields

$$\frac{\partial}{\partial \tilde{t}} \tilde{\mathbf{w}}(0, \tilde{t}) = \beta_0 (1 - \tilde{\tau}'_0(\tilde{t})) \tilde{\mathbf{w}}(\tilde{\tau}_0(\tilde{t}), \tilde{t}), \quad (2.31)$$

where the PDE Eq. (2.23) has been used with $\tilde{\mathbf{w}}(\infty, \tilde{t}) = \tilde{\mathbf{w}}_p(\infty, \tilde{t}) = 0$. Eq. (2.31) is similar to the typical interconnected boundary condition Eq. (2.24) in the PDE representation of time delay systems. With the relationship $\tilde{\mathbf{w}}(\tilde{\tau}, \tilde{t}) = \tilde{\mathbf{u}}(\tilde{t} - \tilde{\tau})$ between the configurations of the PDE Eq. (2.23) and the configuration of the DDE Eq. (2.14) with variable delay, the corresponding time delay system can be given as

$$\tilde{\mathbf{u}}'(\tilde{t}) = \beta_0 (1 - \tilde{\tau}'_0(\tilde{t})) \tilde{\mathbf{u}}(\tilde{t} - \tilde{\tau}_0(\tilde{t})). \quad (2.32)$$

By using the relationship Eq. (2.15) for the time derivative $\tilde{\tau}'_0(\tilde{t})$ of the variable delay, the standard form Eq. (2.1) of the system with constant delay τ_0 reads

$$\dot{\mathbf{u}}(t) = \frac{\beta_0}{\Omega(\Phi^{-1}(t - \tau_0))} \mathbf{u}(t - \tau_0) = \mathbf{f}(t, \mathbf{r}_{\mathbf{u}}(t)), \quad (2.33)$$

2.4. Approximations for systems with variable delay distribution

where the delay distribution is given by $N \times N$ dimensional matrix $\mathbf{K}(\tau) = \mathbf{I}\delta(\tau - \tau_0)$.

This means that the McKendrick Eq. (2.28) with the specific boundary condition Eq. (2.30) is equivalent to the standard form Eq. (2.33) with constant delay (cf. [94]). Note that Eq. (2.33) is typically nonlinear because the relationship between the two time scales typically depends on the configuration of the system $\Phi^{-1}(t) = \Phi_{\mathbf{u}}^{-1}(t, \mathbf{u}(t))$. In this case, the representation Eq. (2.32) is also nonlinear, where the nonlinearity is hidden in the associated state-dependent delay $\tilde{\tau}_0(\tilde{t})$. From the standard form Eq. (2.33) the four equivalent PDE representations in Sec. 2.3.1 can be derived, where the time and the space variables of the PDE can be either described in terms of the internal clock or the physical time, respectively. In the literature, typically, the PDE representation Eq. (2.21) is used, where the time variable of the PDE is equivalent to the physical time \tilde{t} and the spatial variable of the PDE describes the level of maturity τ [9, 19, 20, 21, 66]. Whereas the four PDE representations in Sec. 2.3.1 are pure advection equations, where the right-hand side of the PDE is zero and the configuration remains constant along the characteristics Eq. (2.27), the examples in population dynamics are typically described by advection-reaction equations similar to Eq. (2.28), where the right hand side of the PDE is non-zero and the configuration changes along the characteristic curves. In particular, for the McKendrick equation Eq. (2.28) the solution along the characteristic curves can be described by (cf. Appendix A.1.2)

$$\tilde{\mathbf{w}}_p(\tilde{\tau}(0) + \tilde{t}, \tilde{t}) = e^{-\mu\tilde{t}} \tilde{\mathbf{w}}_p(\tilde{\tau}(0), 0). \quad (2.34)$$

Thus, in general, advection-reaction systems similar to Eq. (2.28) with constant or moving boundaries can be also described by time delay systems Eq. (2.1) with time-invariant delay distributions.

2.4. Approximations for systems with variable delay distribution

In addition to equivalent time delay systems in Sec. 2.2 and equivalent spatially extended systems in Sec. 2.3, the standard form Eq. (2.1) can be also used as an approximation of systems with a variable delay distribution. In particular, two approximations for systems with fast and slowly time-varying delay are presented in Sec. 2.4.1 and Sec. 2.4.2, respectively. In this thesis, approximations for systems with fast and slowly time-varying delays are used in Sec. 7.1 for the investigation of diffusion-driven instabilities in delayed reaction-diffusion systems.

2.4.1. Fast time-varying delays

Fast time-varying delays cannot be realized by variable transport delays because the maximum slope of a variable transport delay is bounded, i.e. the condition Eq. (2.15) must be fulfilled. In other words for decreasing periods of a variable transport delay, the amplitude of the delay variation vanishes. This can be also seen, for example, for sinusoidal delays as defined in Eq. (2.18). For sinusoidal variable transport delays it

2. System definition and equivalent systems

follows from Eq. (2.15) that an upper bound for the amplitude of the delay variation can be characterized by $A_\tau < 1$. This means that for small periods $T \rightarrow 0$ the term $\frac{A_\tau T}{2\pi}$ vanishes and according to Eq. (2.18) the delay approaches the constant mean delay $\tilde{\tau} \rightarrow \tau_m$. In fact, this is the main reason why a slow continuous spindle speed variation in metal cutting applications is more suitable than a fast variation because for fast spindle speed variations the effective amplitude of the delay variation is only marginal [23]. As a consequence, for a system with a fast time-varying delay typically no exact transformation to a system with a constant delay is possible via a nonlinear time scale transformation Eq. (2.3). Nevertheless, a system with a fast time-varying delay can be approximated by a system with a time-invariant delay distribution $\mathbf{K}(\tau)$ as it is demonstrated below.

For the sake of convenience, only systems with a periodic delay distribution $\mathbf{K}_{\text{var}}(t, \tau) = \mathbf{K}_{\text{var}}(t + T, \tau)$ and a small period T are considered, but the approximation is also possible for systems with aperiodic delay distributions. A system with fast time-varying distributed delay can be described by

$$\dot{\mathbf{u}}(t) = \mathbf{f}(t, \mathbf{u}(t), \mathbf{r}_{\mathbf{u}}^{\text{var}}(t)), \quad (2.35)$$

where the memory is defined by

$$\mathbf{r}_{\mathbf{u}}^{\text{var}}(t) = \int_0^{\tau_{\text{max}}} \mathbf{K}_{\text{var}}(t, \tau) \mathbf{u}(t - \tau) d\tau. \quad (2.36)$$

The exact solution of Eq. (2.35) over one period T can be formally determined by

$$\mathbf{u}(t + T) = \mathbf{u}(t) + \int_t^{t+T} \mathbf{f}(t', \mathbf{u}(t'), \mathbf{r}_{\mathbf{u}}^{\text{var}}(t')) dt'. \quad (2.37)$$

For fast time-varying delays, i.e. delays with a vanishing period T , Eq. (2.37) can be approximated by

$$\mathbf{u}(t + T) = \mathbf{u}(t) + \int_t^{t+T} \mathbf{f}(t, \mathbf{u}(t), \mathbf{r}_{\mathbf{u}}^{\text{var}}(t')) dt'. \quad (2.38)$$

In the approximation Eq. (2.38) it is assumed that the fluctuations of \mathbf{f} are much slower than the fluctuations of the memory $\mathbf{r}_{\mathbf{u}}^{\text{var}}(t)$ due to a fast time-varying delay distribution $\mathbf{K}_{\text{var}}(t, \tau)$. For small periods T Eq. (2.38) is similar to the Euler integration scheme with step size T and the derivative

$$\dot{\mathbf{u}}(t) = \frac{1}{T} \int_t^{t+T} \mathbf{f}(t, \mathbf{u}(t), \mathbf{r}_{\mathbf{u}}^{\text{var}}(t')) dt'. \quad (2.39)$$

Eq. (2.39) is the averaged system of Eq. (2.35), that is an adequate approximation of Eq. (2.35) in case of a fast time-varying delay distribution. Eq. (2.39) can be further simplified if \mathbf{f} depends only linearly on the memory $\mathbf{r}_{\mathbf{u}}^{\text{var}}(t)$, that is

$$\mathbf{f}(t, \mathbf{u}(t), \mathbf{r}_{\mathbf{u}}^{\text{var}}(t')) = \mathbf{f}_0(t, \mathbf{u}(t)) + \mathbf{f}_1(t, \mathbf{u}(t)) \mathbf{r}_{\mathbf{u}}^{\text{var}}(t'). \quad (2.40)$$

2.4. Approximations for systems with variable delay distribution

In this case the averaging over one period T takes place only in the delay distribution and the averaged system Eq. (2.39) can be written as

$$\dot{\mathbf{u}}(t) = \mathbf{f}_0(t, \mathbf{u}(t)) + \mathbf{f}_1(t, \mathbf{u}(t)) \mathbf{r}_u^{\text{av}}(t), \quad (2.41)$$

where the averaged memory $\mathbf{r}_u^{\text{av}}(t)$ and the averaged delay distribution $\mathbf{K}_{\text{av}}(\tau)$ are specified by

$$\mathbf{r}_u^{\text{av}}(t) = \int_0^{\tau_{\text{max}}} \mathbf{K}_{\text{av}}(\tau) \mathbf{u}(t - \tau) d\tau, \quad \text{and} \quad \mathbf{K}_{\text{av}}(\tau) = \frac{1}{T} \int_t^{t+T} \mathbf{K}_{\text{var}}(t', \tau) dt'. \quad (2.42)$$

For the illustration of the approximation of a system with a fast time-varying delay by a the averaged system the Hutchinson equation with a time-varying delay $\tau_0(t)$ is studied [106]

$$\dot{u}(t) = u(t)(1 - u(t - \tau_0(t))). \quad (2.43)$$

In Sec. 7.1 diffusion-driven instabilities of reaction-diffusion systems with delay are studied, where the Hutchinson equation with a variable delay is considered as an example for the reaction term. The time-varying delay $\tau_0(t)$ in Eq. (2.43) is specified by the variable discrete delay distribution $\mathbf{K}_{\text{var}}(t, \tau) = \delta(\tau - \tau_1)$ for $\text{mod}(t, T) \leq 0.5T$ and $\mathbf{K}_{\text{var}}(t, \tau) = \delta(\tau - \tau_2)$ otherwise, where the delay switches uniformly between the two values $\tau_1 = 1$ and $\tau_2 = 7$. In the Hutchinson equation Eq. (2.43) f depends only linearly on the memory r_u^{var} , which means that the averaged system can be given by Eq. (2.41) with the associated averaged delay distribution $K_{\text{av}}(\tau) = 0.5\delta(t - \tau_1) + 0.5\delta(t - \tau_2)$. In Fig. 2.4 the solution of the Hutchinson equation Eq. (2.43) is presented for a period $T = 2$ (red), $T = 1$ (blue) and for the corresponding system with the averaged delay distribution $K_{\text{av}}(\tau)$ (black, thick). It can be seen that the approximation with the distributed delay comparison system Eq. (2.41) is the better, the smaller the period of the delay variation is.

The concept behind the averaging of the delay distribution is similar to the classical method of averaging for ODEs [107] and functional differential equations [108, 109]. In these papers the fast time scale of the system was introduced due to a fast time-varying parameter of the system, whereas no fast time-varying delays were considered. The averaging method for time-varying delays was first shown for linear DDEs with time-varying discrete delays [110]. The stability analysis of nonlinear time delay systems with Lyapunov's indirect linearization method results always in the analysis of a linear DDE (cf. Sec. 3.3.2), which means that the approximation Eq. (2.41) with the averaged delay distribution Eq. (2.42) can be always used for the stability analysis of nonlinear DDEs with fast time-varying delay. In particular, the method was frequently used for the stability analysis of time-delay feedback control with variable delays [27, 28, 29] and the analysis of amplitude death in networks with time-varying coupling delays [33, 34]. However, whereas the stability of a specific solution of a nonlinear time delay system can be analyzed from the distributed delay comparison system Eq. (2.41), the solution of a system with a nonlinear dependence on the memory can be approximated, in general, only with the more general averaged system Eq. (2.39).

2. System definition and equivalent systems

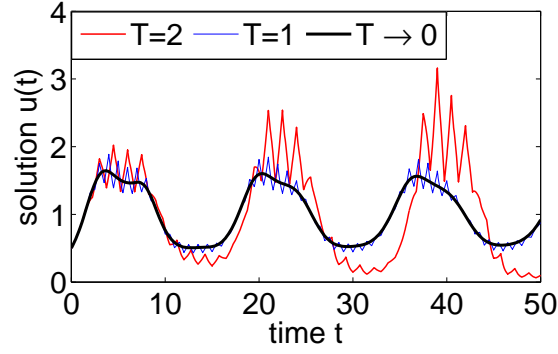


Figure 2.4.: The solution of the Hutchinson equation Eq. (2.43) is shown for a time-varying delay with period $T = 2$ (red), $T = 1$ (blue) and for the corresponding approximation with a time-invariant delay distribution (black). For decreasing period of the delay variation the solution converges to the solution of the distributed delay comparison system.

2.4.2. Slowly time-varying delays

In contrast to systems with fast time-varying delays which are approximated in Sec. 2.4.1, systems with a very slow variation of the delay distribution are also possible. For example, the continuous spindle speed variation in turning and milling can be approximated very well with a slowly time-varying delay because the frequency of the speed modulation is typically much lower than the frequency of the chatter vibrations [23, 111]. Indeed, from Sec. 2.2.1 it is known, that the delays in metal cutting are variable transport delays, and the systems can be transformed to systems with a constant delay distribution. Nevertheless, the approximation of a slowly time-varying variable transport delay by systems with a time-invariant delay distribution can help to get an understanding for the dynamics of machine tool vibrations in case of a SSV [23]. In addition, the approximation for slowly time-varying delay can be helpful for systems with a slowly time-varying dissipative delay, which cannot be transformed to systems with a time-invariant delay with a nonlinear time scale transformation Eq. (2.3) [100].

In general, time delay systems with a slowly time-varying delay can be described by Eq. (2.35) with the memory Eq. (2.36). Similar to the analysis in Sec. 2.4.1 for fast time-varying delays, the exact solution of the delay system can be determined by Eq. (2.37), where the period T of the delay modulation in the upper boundary of the integration can be replaced by a small but finite step size h . For a periodic delay with a large period T , the delay distribution can be assumed to be constant in the interval $[t, t+h]$ with $h \ll T$. In this case the exact solution of the delay system can be approximated by

$$\mathbf{u}(t+h) = \mathbf{u}(t) + \int_t^{t+h} \mathbf{f}(t', \mathbf{u}(t'), \mathbf{r}_{\mathbf{u}}^{\text{froz}}(t, t')) dt', \quad (2.44)$$

2.4. Approximations for systems with variable delay distribution

where the memory $\mathbf{r}_{\mathbf{u}}^{\text{froz}}(t, t')$ is defined by

$$\mathbf{r}_{\mathbf{u}}^{\text{froz}}(t, t') = \int_0^{\tau_{\max}} \mathbf{K}_{\text{var}}(t, \tau) \mathbf{u}(t' - \tau) d\tau. \quad (2.45)$$

In Eq. (2.44) with the frozen memory $\mathbf{r}_{\mathbf{u}}^{\text{froz}}(t, t')$ in Eq. (2.45) the variable delay distribution $\mathbf{K}_{\text{var}}(t, \tau)$ is assumed to be constant during the integration from time t to the next step $t + h$. Thus, the DDE Eq. (2.35) with a slowly varying delay distribution Eq. (2.36) can be approximated by a sequence of DDEs with time-invariant distributed delays

$$\dot{\mathbf{u}}(t) = \sum_{i=0}^{\infty} \mathbf{H}(t - t_i) \mathbf{H}(t_{i+1} - t) \mathbf{f}(t, \mathbf{u}(t), \mathbf{r}_{\mathbf{u}}^{\text{froz}}(t_i, t)), \quad (2.46)$$

where $t_i = ih$ are the discrete time steps, and $\mathbf{H}(x)$ is the Heaviside step function. Eq. (2.46) is called frozen time approximation and represents a relation between the dynamics of the system with a slowly time-varying delay distribution $\mathbf{K}_{\text{var}}(t, \tau)$ and the dynamics of the system with all adopted 'frozen' delay distributions $\mathbf{K}_{\text{var}}(t_i, \tau)$. A slow variation of the delay in Eq. (2.46) means there is only a small change of the delay distribution from step t_i to step t_{i+1} , that is $\mathbf{K}_{\text{var}}(t_{i+1}, \tau) - \mathbf{K}_{\text{var}}(t_i, \tau) \rightarrow 0$. As a consequence, the system remains in its steady state, whereas the dynamic properties of the steady state changes slightly from t_i to t_{i+1} . After a long time the continuous slight change of the dynamic properties of the steady state due to a slow change of the delay distribution becomes significant for the dynamic behavior of the system. Note that the frozen time approach for systems with a slowly time-varying delay is closely related to the adiabatic theorem [112]. More details on the frozen time approach for systems with slowly time-varying delays can be found in [23].

The frozen time approach was used for the explanation of the stability behavior in turning and milling with spindle speed variation (SSV), where a slowly time-varying discrete delay appears [111]. In this case, the frozen time approach can be used to develop a strategy for finding optimal parameters of the spindle speed variation [23]. In particular, the stability lobes for a milling process with constant discrete delay (constant spindle speed) and a slowly time varying delay due to a SSV are shown in Fig. 2.5. The results of the approximation Eq. (2.46) (black, thick) for this example are close to the exact numerical results (red, solid) and the experimental results (red, dashed) obtained from metal cutting experiments with SSV. In general, the stability lobes that separate stable from unstable behavior of the system with SSV (red) are an average of the lobes for the system with constant spindle speeds (blue). This is a consequence of the above-mentioned relationship to the adiabatic theorem. According to Eq. (2.46), for a slow SSV the exponential behavior of the vibrations of the non-autonomous system with time-varying delay is related to the exponential behavior of the steady state solution of the autonomous systems with the successive time-invariant frozen delay distribution $\mathbf{K}_{\text{var}}(t_i, \tau)$. As a result, the exponential behavior of the system with the a slowly time-varying delay distribution over one period of the delay variation can be approximated by the average of the characteristic exponents of the autonomous systems with all adopted frozen delays [23].

2. System definition and equivalent systems

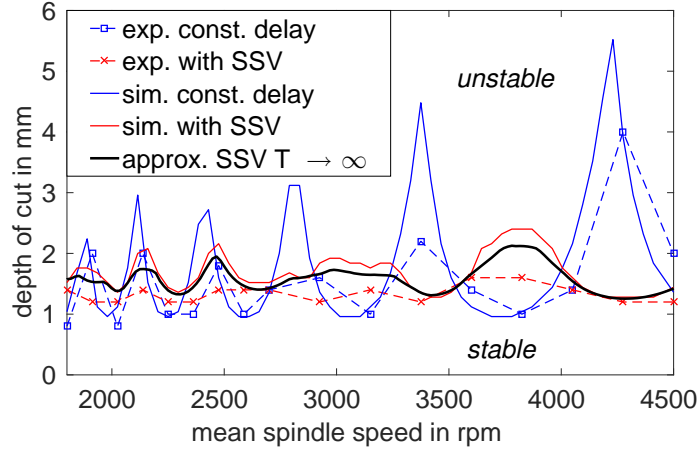


Figure 2.5.: The stability lobes of a milling process with constant spindle speed (blue) and with a slow SSV (red) with $T = 0.5s$ are shown. The experimental results (dashed) agree with the simulation results (solid), which can be approximated with Eq. (2.46) (black, thick).

2.5. Summary

In Sec. 2.1 the standard form of the systems under investigation was defined in Eq. (2.1) with the memory Eq. (2.2). In particular, the standard form is given by a DDE with a time-invariant delay distribution but it is not only a representation for systems with a constant delay distribution. In fact, in Sec. 2.2 the equivalence between the standard form Eq. (2.1) and other time delay systems was shown. It turns out that the transformation from DDEs with a constant delay to DDEs with a time-varying or state-dependent delay is possible. From the resulting conjugacy relation Eq. (2.17) between the retarded access maps \tilde{a} and a of the variable delay and the constant delay, it can be concluded that not all variable delays can be generated from a constant delay by a nonlinear time scale transformation. For example, only sinusoidal delays that corresponds to circle maps with irrational rotation numbers are conjugate to constant delays and are called variable transport delays, whereas delays with parameters in the region of Arnold tongues, i.e. delays corresponding to circle maps with rational rotation numbers, cannot be transformed to constant delays. In this thesis, the concept of variable transport delays was extended to distributed delays. The relationship between the delay distribution of a system with a time-invariant and a variable delay distribution is given in Eq. (2.9). Further results on variable transport delays can be found in [26, 94, 100].

In Sec. 2.3 the equivalence between the standard form Eq. (2.1) and spatially extended systems was derived. In particular, it has been shown that there are four different types of advection equations with interconnected boundaries that are equivalent to the original DDE Eq. (2.1) with time-invariant distributed delay. Moreover, it was shown that some advection-reaction equations which are often used as models for structured population dynamics are equivalent to the considered time delay system, which is defined in Sec. 2.1.

In addition to the concept of variable transport delays and the resulting equivalence between time delay systems with constant and variable delay distributions and hyperbolic PDEs with constant and moving boundaries, the standard form Eq. (2.1) can be used as an approximation of DDEs with a slowly and fast time-varying delay distribution as it was shown in Sec. 2.4. In particular, the concept of averaging for fast time-varying discrete delays was extended to systems with variable distributed delays. The relation between the original variable delay distribution and the time-averaged delay distribution in the distributed delay comparison system is given in Eq. (2.42). On the other hand, for slowly time-varying delays a possible approximation by a series of autonomous systems based on the adiabatic theorem was presented in Eq. (2.46). This method was successfully used in applications to explain the behavior of metal cutting processes with SSV [23, 111].

In summary, it was shown in this chapter that systems with a time-varying delay distribution, systems with a state-dependent delay distribution as well as first-order hyperbolic PDEs with constant and moving boundaries can be described by a DDE with a time-invariant delay distribution. The results are useful for applications, where typically variable delays appear. Specific examples with variable delays are presented in Chapter 7.1 and Chapter 7.2.

3. Analysis of nonlinear time delay systems

In this section, the mathematical theory and numerical methods for the analysis of time delay systems are briefly introduced. It gives a framework for the theory, which is presented in this thesis. Specifically, Lyapunov's indirect linearization method, which is presented in Sec. 3.3.2, is considered in this thesis and provides the basis for the presented methods in Chapter 4, Chapter 5 and Chapter 6.

3.1. Mathematical background

DDEs for the description of the dynamics of time delay systems belong to the class of functional differential equations. They are also known as retarded differential equations or retarded functional differential equations or differential equations with aftereffect. If the memory contains a delay distribution, the systems are called DDEs with distributed delay, delay-integro-differential equations or Volterra integral equations. The mathematical theory for autonomous DDEs with discrete delays is well developed [62], [63]. One of the main difference between DDEs and ODEs is their dimension. Whereas ODEs are finite dimensional systems, DDEs are infinite dimensional systems. The infinite dimension in a DDE shows up in the necessity of an initial function for the characterization of the initial state of the DDE, whereas the initial state of an ODE is specified by a finite dimensional initial condition. The existence and uniqueness of the solution of DDEs for a given initial function is shown in [62], [63]. There are well-established results on the smoothness, boundedness and numerical calculation of the solutions of DDEs [113, 114]. For delay-integro differential equations some results on the mathematical theory and the numerical solution can be found in [115, 116]. For periodic DDEs with a constant delay the classical Floquet theory for ODEs with periodic coefficients was generalized to DDEs [62, 75, 76]. In this case small solutions, which are solutions that decay faster than exponentially can exist [117]. For DDEs with a time-varying delay, problems with the definition of the state space, reachability of an arbitrary state and causality can appear [64, 65]. For DDEs with state-dependent delay the classical theory is not applicable. In this case, some questions related to the existence, uniqueness and smooth dependence on the initial data of the solution of DDEs with state-dependent delay are still open [66, 67]. Nevertheless, the systems with a state-dependent delay distribution, which are presented in Sec. 2.2, can be transformed to systems with a constant delay distribution, which means that the classical theory is applicable.

3.2. Numerical methods

One of the first papers on the numerical solution of DDEs are the presentations of the so-called method of steps for DDEs with constant and time-varying delay [118, 119]. The method of steps is characterized by a stepwise integration of the delay system and is presented in more detail in Sec. 4.2. Until now a vast number of methods for the numerical integration of DDEs has been proposed. A nice overview on the methods for the numerical solution of DDEs can be found in [114]. They are typically based on Runge-Kutta methods for a finite dimensional ODE approximation of the DDE. For example, a common solver for the numerical solution of DDEs is given in [113] and implemented in the MATLAB function *dde23*. In addition to the classical solvers, which are often restricted to DDEs with constant delays, there are numerical integrators for DDEs with time-varying and state-dependent delays. For examples, the MATLAB function *ddesd* [120] or the Fortran code *RADAR5* [121] can be used for the numerical calculation of the solution for DDEs with state-dependent delay. In engineering MATLAB/Simulink is often used for the numerical integration of time delay systems in the time domain, which provides only numerical solvers for ODEs. In this environment time delay systems can be implemented by using the so-called *Transport Delay*-block, where the history of the input values are stored in a buffer. As mentioned already in Sec. 2.2.1 there is also a *Variable Transport Delay*-block for systems with variable transport delays as defined in Eq. (2.6) [72].

In general, numerical solvers can be used to for an effective calculation of the asymptotic solution of time delay systems but the numerical integration of the DDE cannot be used to find unstable periodic solutions of nonlinear systems. In [122] a spectral element method for the numerical calculation of periodic solutions of nonlinear DDEs with a single constant delay from the solution of a boundary value problem is presented, which can be also used for the determination of unstable periodic orbits. Apart from the numerical calculation of the solution, often some additional information is necessary for a detailed analysis of the dynamic behavior, such as the stability and bifurcation of specific solutions. For this purpose, powerful software packages such as *DDE-Biftool* [123] and *Knut* [124] are designed. In particular, the packages can be used for the numerical calculation of equilibria and periodic orbits of nonlinear DDEs and for the numerical continuation of these solutions for parameter changes. In addition, the stability, bifurcations and much more properties of the solutions can be determined. The software package *DDE-Biftool* was used for the calculation of periodic solutions in a network of Hodgkin-Huxley neurons with heterogeneous coupling delays in Sec. 7.3, whereas for the stability analysis of the transversal eigenmodes of the network a separate stability analysis was performed.

3.3. Stability analysis

In this section two fundamental different methods for the stability analysis of nonlinear time delay systems are presented. Lyapunov's direct method, which is briefly described in Sec. 3.3.1, is suitable for the robust stability analysis of nonlinear DDEs, whereas

Lyapunov's indirect linearization method in Sec. 3.3.2 can be used to obtain a precise result on the stability behavior for specific solutions of nonlinear DDEs.

3.3.1. Lyapunov's direct method

The global stability of nonlinear ODEs can be analyzed by Lyapunov's direct method [49], where global means that the stability information is independent of the specific solution of the system. Lyapunov's approach is based on a scalar positive function, which is now known as Lyapunov function. It depends on the state \mathbf{u}_t of a nonlinear system and is a generalization of the energy concept to arbitrary systems. The system is stable if the time derivative of the Lyapunov function is negative for an arbitrary state of the system, i.e. the Lyapunov function decreases to zero.

There are two main approaches for the extension of Lyapunov's direct method to time delay systems. On the one hand, due to the infinite dimension of time delay systems, Lyapunov functionals instead of Lyapunov functions can be studied, which is known as Lyapunov-Krasovskii functional approach. On the other hand, classical Lyapunov functions can be constructed for time delay systems, which is known as Lyapunov-Razumikhin approach. More details on the robust stability analysis of DDEs based on Lyapunov's direct method can be found in [125, 126].

The direct method can be used to guarantee the global stability of a nonlinear system independent of the size of the perturbation or the specific initial condition. However, with the direct method typically only a conservative bound for the stability of the system can be obtained because the stability information is independent of the specific solution. A more precise and specific information on the stability can be obtained with Lyapunov's first linearization method, which is considered in this thesis and presented next.

3.3.2. Lyapunov's indirect linearization method

The stability for a specific reference solution $\mathbf{u}^*(t)$ of a nonlinear system can be obtained with Lyapunov's indirect linearization method. In particular, the reference solution is called locally stable if small perturbations $\mathbf{x}(t) = \mathbf{u}(t) - \mathbf{u}^*(t)$ around the reference solution are bounded forward in time. Here, local stability means that the system is stable around the solution $\mathbf{u}^*(t)$ for small perturbations $\mathbf{x}(t)$ but not necessarily stable with respect to large perturbations $\mathbf{x}(t)$. More precisely, in Lyapunov's indirect linearization method only infinitesimal small perturbations $\mathbf{x}(t)$ are considered, and therefore, the dynamics of the perturbations can be described by a linear system. Since the stability of a linear system does not depend on its specific solution, a precise information on the stability of the reference solution can be obtained. However, the reference solution $\mathbf{u}^*(t)$ may be unstable with respect to a finite perturbation $\mathbf{x}(t)$, which drives the system to another attractor with a different stability behavior.

The linearized dynamics corresponding to the standard form Eq. (2.1) can be derived

3. Analysis of nonlinear time delay systems

from the linear Taylor approximation for the solution $\mathbf{u}(t) = \mathbf{u}^*(t) + \mathbf{x}(t)$ as

$$\begin{aligned} \dot{\mathbf{u}}^*(t) + \dot{\mathbf{x}}(t) &= \mathbf{f}(t, \mathbf{u}^*(t) + \mathbf{x}(t), \mathbf{r}_{\mathbf{u}^* + \mathbf{x}}(t)) \\ &\approx \mathbf{f}(t, \mathbf{u}^*(t), \mathbf{r}_{\mathbf{u}^*}(t)) \\ &\quad + \mathbf{Df}_2(t, \mathbf{u}^*(t), \mathbf{r}_{\mathbf{u}^*}(t)) \mathbf{x}(t) + \mathbf{Df}_3(t, \mathbf{u}^*(t), \mathbf{r}_{\mathbf{u}^*}(t)) \mathbf{r}_{\mathbf{x}}(t), \end{aligned} \quad (3.1)$$

where \mathbf{Df}_2 and \mathbf{Df}_3 refer to the Jacobian matrices of the vector field \mathbf{f} with respect to the second and third argument. If the dynamics of the reference solution $\mathbf{u}^*(t)$ is subtracted from both sides of Eq. (3.1), a linear DDE for the dynamics of the perturbations $\mathbf{x}(t)$ is obtained

$$\dot{\mathbf{x}}(t) = \mathbf{A}(t)\mathbf{x}(t) + \mathbf{B}(t)\mathbf{r}_{\mathbf{x}}(t). \quad (3.2)$$

The $N \times N$ dimensional coefficient matrix $\mathbf{A}(t)$ and the $N \times N_r$ dimensional coefficient matrix $\mathbf{B}(t)$ are defined as

$$\mathbf{A}(t) = \mathbf{Df}_2(t, \mathbf{u}^*(t), \mathbf{r}_{\mathbf{u}^*}(t)), \quad \text{and} \quad \mathbf{B}(t) = \mathbf{Df}_3(t, \mathbf{u}^*(t), \mathbf{r}_{\mathbf{u}^*}(t)). \quad (3.3)$$

The methods for the stability analysis in this thesis are based on Lyapunov's linearization method. In particular, the methods, which are presented in Chapter 4, Chapter 5 and Chapter 6, focus on the analysis of the linearized dynamics Eq. (3.2). Specific examples for Lyapunov's indirect linearization method are presented in Chapter 7, where the local stability of equilibria and periodic solutions of some applications with time delays are analyzed.

3.4. Summary

A very brief overview on the theory for the analysis of time delay systems was given in Sec. 3.1. Since the considered time delay systems with state-dependent delay distributions in Sec. 2.2 are equivalent to DDEs with constant delay distributions, the classical mathematical theory, which is given in [62], [63], can be also applied to these systems. Specific numerical methods for the analysis of nonlinear DDEs were presented in Sec. 3.2. Especially, the software packages for the numerical bifurcation analysis are powerful tools for the investigation of the dynamics of nonlinear DDEs. Nevertheless, in some situations it is suitable to use a separate method for the stability analysis.

Two main concepts for the stability analysis of nonlinear DDEs are briefly introduced in Sec. 3.3. Whereas Lyapunov's direct method provides an information on the global stability behavior, and is, therefore, suitable for the robust stability analysis, it gives, in general, only a conservative bound on the stable parameter regions. In contrast, the results from Lyapunov's indirect linearization method are only valid for specific solutions of the nonlinear DDE but the linearization method can be used to obtain precise results on the parameter regions, where the specific solution is stable or unstable.

4. Analytical solution of linear time delay systems

In this section an overview on the standard analytical methods for the solution of linear DDEs is given. The existing analytical approaches for the analysis of linear DDEs are often presented only for discrete delays or scalar DDEs, whereas the extension to distributed delays and vector-valued DDEs is, in general, not straightforward. In this thesis the standard analytical techniques for time delay systems are extended for the application to vector-valued DDEs with distributed delay. The solution based on the Laplace transform of the DDE in Sec. 4.1 is closely related to the frequency domain approach in Chapter 6. Specifically, the eigenmode decomposition for linear autonomous DDEs, which is presented in Sec. 4.4, is used to provide a better understanding of the newly introduced Hill-Floquet method in Chapter 6.

4.1. Laplace transform

Formally, the Laplace transform can be used to solve the linear DDE Eq. (3.2). In this thesis, the Laplace transform and its inverse for a quantity \mathbf{v} is defined by

$$\bar{\mathbf{v}}(s) = \int_0^{\infty} \mathbf{v}(t) e^{-st} dt \quad , \quad \mathbf{v}(t) = \int_{(\Gamma)} \bar{\mathbf{v}}(s) e^{st} ds, \quad (4.1)$$

where the Bromwich integral is abbreviated by

$$\int_{(\Gamma)} ds \bar{\mathbf{v}}(s) e^{st} = \frac{1}{2\pi i} \lim_{T \rightarrow \infty} \int_{\gamma - iT}^{\gamma + iT} ds \bar{\mathbf{v}}(s) e^{st}. \quad (4.2)$$

In Eq. (4.2) the integration in the complex plane is done along a vertical contour $\text{Re}(s) = \gamma$ such that all singularities of $\bar{\mathbf{v}}(s)$ are to the left of this contour. The basic theory for the solution of autonomous DDEs with discrete delay via the Laplace transform is presented in [50]. The formal Laplace transform of the linear non-autonomous DDE Eq. (3.2) with distributed delay can be given by

$$s\bar{\mathbf{x}}(s) - \bar{\mathbf{A}}(s) * \bar{\mathbf{x}}(s) - \bar{\mathbf{B}}(s) * (\bar{\mathbf{K}}(s)\bar{\mathbf{x}}(s)) = \bar{\Psi}(0) + \bar{\Psi}(s), \quad (4.3)$$

where $*$ denotes convolution and $\bar{\mathbf{K}}(s)$ is the Laplace transform of the delay distribution $\mathbf{K}(\tau)$. A separate definition for the initial function is given by $\bar{\Psi}(t) = \mathbf{x}(t)\text{H}(-t)$, which

4. Analytical solution of linear time delay systems

means that $\Psi(t) = \mathbf{0}$ for $t > 0$ and $\Psi(t) = \mathbf{x}(t)$ for $t \leq 0$. Furthermore, the weighted Laplace transform $\bar{\Psi}(s)$ of the initial memory is defined by

$$\bar{\Psi}(s) = \int_0^{\infty} dt \mathbf{B}(t) \mathbf{r}_{\Psi}(t) e^{-st}. \quad (4.4)$$

Note that due to the definition of the function $\Psi(t)$ only retarded configurations $\mathbf{x}(t - \tau) = \Psi(t - \tau)$ in the region of the initial function with $t - \tau < 0$ contribute to the weighted Laplace transform of the memory in Eq. (4.4). A detailed derivation of the Laplace transform representation Eq. (4.3) of the linear DDE with distributed delay Eq. (3.2) can be found in Appendix A.2.1.

The structure of the Laplace transform Eq. (4.3) can be understood by defining the inverse of the propagator in the Laplace domain

$$\bar{\mathbf{T}}^{-1}(s, s') = \mathbf{I} s' \delta(s - s') - \bar{\mathbf{A}}(s - s') - \bar{\mathbf{B}}(s - s') \bar{\mathbf{K}}(s'), \quad (4.5)$$

which means that the Laplace transform of the linear DDE Eq. (3.2) can be written as

$$\int_{(\Gamma)} ds' \bar{\mathbf{T}}^{-1}(s, s') \bar{\mathbf{x}}(s') = \Psi(0) + \bar{\Psi}(s). \quad (4.6)$$

The left hand side of Eq. (4.6) can be interpreted as the application of the inverse propagator on the Laplace domain representation $\bar{\mathbf{x}}(s')$ of the solution and the right hand side of Eq. (4.7) is the Laplace domain representation of the initial data of the time delay system. In general, for the non-autonomous system with the inverse propagator Eq. (4.5) the inversion of the propagator in the Laplace domain is not straightforward. However, it is shown in detail in Appendix A.2.2 that the Laplace domain solution can be rearranged to

$$\bar{\mathbf{x}}(s'') = \int_{(\Gamma)} ds \bar{\mathbf{T}}(s'', s) (\Psi(0) + \bar{\Psi}(s)), \quad (4.7)$$

and therefore, it can be concluded that the application of the inverse Laplace transform to Eq. (4.7) leads to a formal solution of the DDE for $t \geq 0$ as

$$\mathbf{x}(t) = \mathbf{T}(t, 0) \Psi(0) + \int_0^{\tau_{\max}} d\theta \mathbf{T}(t, \theta) \mathbf{B}(\theta) \mathbf{r}_{\Psi}(\theta). \quad (4.8)$$

In Eq. (4.7) and Eq. (4.8) $\bar{\mathbf{T}}(s'', s)$ and $\mathbf{T}(t, t')$ are the Laplace domain and the time domain representations of the propagator, respectively. In general, the propagator is also known as Green's function or fundamental matrix solution.

Only for time-invariant coefficient matrices $\mathbf{A}(t) = \mathbf{A}_0$ and $\mathbf{B}(t) = \mathbf{B}_0$ an explicit definition of the Laplace domain representation $\bar{\mathbf{T}}(s'', s)$ of the propagator is given in this thesis as (see Appendix A.2.2)

$$\bar{\mathbf{T}}(s'', s) = (\mathbf{I} s - \mathbf{A}_0 - \mathbf{B}_0 \bar{\mathbf{K}}(s))^{-1} \delta(s'' - s). \quad (4.9)$$

The calculation of the propagator for the non-autonomous case is not straightforward and outside the scope of this thesis. After applying the inverse Laplace transform to Eq. (4.9), the time domain representation of the propagator Eq. (4.9) for the autonomous case can be formally given by (cf. Appendix A.2.2)

$$\mathbf{T}(t, t') = \int_{(\Gamma)} ds (\mathbf{I}s - \mathbf{A}_0 - \mathbf{B}_0 \bar{\mathbf{K}}(s))^{-1} e^{s(t-t')} H(t-t') = \mathbf{T}(t-t'). \quad (4.10)$$

From Eq. (4.10) it follows that for time-invariant coefficients the propagator is translation invariant $\mathbf{T}(t, t') = \mathbf{T}(t-t')$, which means that the propagator depends only on the step size $t-t'$ as one would expect for autonomous systems. An explicit expression for the propagator in the time domain can be derived by the method of steps [118, 119], that is the successive integration of the DDE. This is shown in Sec. 4.2. A second method is a series expansion of the propagator $\bar{\mathbf{T}}(s, s')$ in the Laplace domain and a step by step inverse Laplace transform of the series. This method is used in [50] and [89] to obtain the propagator for autonomous DDEs with multiple discrete delays. Alternatively, the inverse Laplace transform of the propagator can be performed with residue theory, which is shown in Sec. 4.3. The connection between the propagator and the eigenmodes of the time delay system is presented in [88] for a scalar autonomous DDE. The extension of the eigenmode expansion to vector-valued autonomous DDEs with distributed delay is presented in Sec. 4.4.

4.2. Method of steps

In this subsection the method of steps is used to derive an explicit expression for the propagator $\mathbf{T}(t, t')$ of the linearized time delay system Eq. (3.2). If τ_{\min} specifies a lower bound on the delay distribution $\mathbf{K}(\tau)$ in the memory $\mathbf{r}_{\Psi}(t)$ of the time delay system, for $t \in [0, \tau_{\min})$ the DDE Eq. (3.2) with distributed delay can be interpreted as a non-homogeneous ODE

$$\dot{\mathbf{x}}(t) = \mathbf{A}(t)\mathbf{x}(t) + \mathbf{B}(t)\mathbf{r}_{\Psi}(t). \quad (4.11)$$

The fundamental matrix solution $\mathbf{M}(t, t')$ for the homogeneous part of the ODE Eq. (4.11) satisfies

$$\dot{\mathbf{M}}(t, t') = \mathbf{A}(t)\mathbf{M}(t, t'), \quad \mathbf{M}(t', t') = \mathbf{I}, \quad (4.12)$$

and the variation of constants formula can be used to solve Eq. (4.11) in the first interval with $t \in [0, \tau_{\min})$ as

$$\mathbf{x}(t) = \mathbf{M}(t, 0)\Psi(0) + \int_0^t d\theta \mathbf{M}(t, \theta)\mathbf{B}(\theta)\mathbf{r}_{\Psi}(\theta). \quad (4.13)$$

Comparison of Eq. (4.13) and Eq. (4.8) in combination with $\mathbf{T}(t, \theta) = 0$ for $\theta \geq t$ reveals the equivalence $\mathbf{M}(t, t') = \mathbf{T}(t, t')$ in the first interval. The solution $\mathbf{x}(t)$ in the first interval can be assumed to be the new initial condition for the calculation of the

4. Analytical solution of linear time delay systems

solution in the second interval with $t > \tau_{\min}$. As a consequence the stepwise application of Eq. (4.13) can be used to construct the propagator $\mathbf{T}(t, t')$ of the time delay system. This method was originally proposed by Bellman in [118] for the numerical solution of time delay systems with constant delays and was later extended to the solution of DDEs with variable delays [119]. Nowadays, the method is commonly known as method of steps [114].

Here, for the sake of convenience an explicit expression for the propagator $\mathbf{T}(t, t')$, which can be obtained with the method of steps, is only given for systems with one discrete delay τ_0 , i.e. systems with a delay distribution $\mathbf{K}(\tau) = \mathbf{K}_0 \delta(\tau - \tau_0)$. In particular, the recursive application of Eq. (4.13) leads to an expression with the same structure as Eq. (4.8), where the propagator $\mathbf{T}(\theta_k, t')$ with $\theta_k \in [t' + k\tau_0, t' + (k+1)\tau_0)$ for the calculation of the solution in the k th interval can be identified as (see Appendix A.2.3)

$$\mathbf{T}(\theta_k, t') = \sum_{n=0}^k \left(\prod_{j=1}^n \int_{t' + (n-j)\tau_0}^{\theta_{k-j+1} - \tau_0} d\theta_{k-j} \mathbf{M}(\theta_{k-j+1}, \theta_{k-j} + \tau_0) \mathbf{B}_K(\theta_{k-j} + \tau_0) \right) \mathbf{M}(\theta_{k-n}, t'), \quad (4.14)$$

with $\mathbf{B}_K(t) = \mathbf{B}(t)\mathbf{K}_0$. From Eq. (4.14) one can see, that for $k < 0$ the propagator of the DDE $\mathbf{T}(\theta_k, t') = 0$, because in this case $\theta_k < t'$. In the first interval ($k = 0$) the propagator of the time delay system defined by Eq. (4.14) is equivalent to the propagator of the ODE part $\mathbf{T}(\theta_0, t') = \mathbf{M}(\theta_0, t')$, which is consistent with Eq. (4.13). If the coefficient matrices are time-invariant, i.e. $\mathbf{A}(t) = \mathbf{A}_0$ and $\mathbf{B}(t) = \mathbf{B}_0$, the propagator $\mathbf{M}(t, t')$ of the ODE part of the delay system can be specified by $\mathbf{M}(t, t') = e^{(t-t')\mathbf{A}_0}$. If, in addition, the coefficient matrices commute, i.e. $\mathbf{A}_0(\mathbf{B}_0\mathbf{K}_0) = (\mathbf{B}_0\mathbf{K}_0)\mathbf{A}_0$, the propagator $\mathbf{T}(\theta_k, t') = \mathbf{T}(\theta_k - t')$ of the time delay system can be simplified to

$$\mathbf{T}(\theta_k - t') = \sum_{n=0}^k e^{(\theta_k - t' - n\tau_0)\mathbf{A}_0} (\mathbf{B}_0\mathbf{K}_0)^n \prod_{j=1}^n \int_{t' + (n-j)\tau_0}^{\theta_{k-j+1} - \tau_0} d\theta_{k-j}. \quad (4.15)$$

With the substitution $\theta'_{k-j} = \theta_{k-j} - t' - (n-j)\tau_0$ for $1 \leq j \leq n$ the integrals in Eq. (4.15) can be simplified to

$$\mathbf{T}(\theta_k - t') = \sum_{n=0}^k e^{(\theta_k - t' - n\tau_0)\mathbf{A}_0} (\mathbf{B}_0\mathbf{K}_0)^n \int_0^{\theta_k - t' - n\tau_0} d\theta'_{k-1} \prod_{j=2}^n \int_0^{\theta'_{k-j+1}} d\theta'_{k-j}, \quad (4.16)$$

which leads to the following compact form of the propagator

$$\mathbf{T}(\theta_k - t') = \sum_{n=0}^k e^{(\theta_k - t' - n\tau_0)\mathbf{A}_0} (\mathbf{B}_0\mathbf{K}_0)^n \frac{(\theta_k - t' - n\tau_0)^n}{n!}. \quad (4.17)$$

In fact, the explicit expression for the propagator $\mathbf{T}(\theta_k - t')$ in Eq. (4.17) satisfies the above-mentioned translation invariance for autonomous systems. Results similar

4.3. Inverse Laplace transform via residue theory

to Eq. (4.17) for scalar autonomous systems can be found, for example, in [89, 127, 128] and were obtained either with the method of steps or by inverse Laplace transform.

In fact, Eq. (4.14) is the basis of the expressions for the construction of the monodromy matrix in one step via semidiscretization, which are given in the book [3]. Moreover, a systematic structure can be found in the equations for the propagator. In particular, Eq. (4.14) and Eq. (4.17) can be interpreted as a path integral, that is, the propagator is specified by an integration over all possible paths from the initial time t' to the finite time θ_k . The paths are composed of delay steps \mathbf{B}_K of length τ_0 or ODE steps \mathbf{M} of arbitrary length. With this interpretation it is possible to generate the propagators of time delay systems without the excessive calculations in Appendix A.2.3 simply by considering all possible paths from t' to θ_k . For example, for constant coefficient matrices all paths that contain exactly n delay steps are specified by the coefficient $(\mathbf{B}_0 \mathbf{K}_0)^n$ in the sum in Eq. (4.17). In this case, the corresponding ODE steps are of length $\theta_k - t' - n\tau_0$. The remaining term $(t - n\tau_0 - t')^n/n!$ is a measure for the number of combinations of the ODE steps with n delay steps between the initial time t' and the finite time θ_k .

The calculation of the propagator with Eq. (4.14) or Eq. (4.17) is suitable for the analysis of the short term behavior of the solution. However, the upper bound of the sum and the number of integrations in Eq. (4.14) increases with increasing k , which means that for the characterization of the asymptotic behavior of time delay systems with $k \rightarrow \infty$ the expressions in Eq. (4.14) and Eq. (4.17) are not suitable. In this case the spectral representation of the propagator is much more suitable, which can be derived from the inverse Laplace transform as shown in the next section.

4.3. Inverse Laplace transform via residue theory

In this section, the spectral representation of the propagator for the autonomous case with constant coefficient matrices \mathbf{A}_0 and \mathbf{B}_0 is derived by the inverse Laplace transform via residue theory. According to Eq. (4.10), the Laplace domain representation $\bar{\mathbf{T}}(s)$ of the propagator for the linearized DDE Eq. (3.2) with constant coefficients can be written as

$$\bar{\mathbf{T}}(s) = \int_0^\infty dt \mathbf{T}(t) e^{-st} = (\mathbf{I}s - \mathbf{A}_0 - \mathbf{B}_0 \bar{\mathbf{K}}(s))^{-1}. \quad (4.18)$$

The inverse Laplace transform of Eq. (4.18) can be performed via residue calculation, which has been shown in [89] for scalar DDEs with a discrete delay τ_0 . For the sake of convenience only first order poles s_k of the propagator $\bar{\mathbf{T}}(s)$ are assumed. In this case, the propagator in the Laplace domain can be given by [129]

$$\bar{\mathbf{T}}(s) = \sum_{k=0}^{\infty} \frac{1}{s - s_k} \mathbf{R}_k, \quad (4.19)$$

where the matrices \mathbf{R}_k are the residues. If the propagator is given by Eq. (4.19) the inverse Laplace transform is straightforward and the propagator in the time domain can

4. Analytical solution of linear time delay systems

be expressed as

$$\mathbf{T}(t - t') = \sum_{k=0}^{\infty} e^{s_k(t-t')} \mathbf{R}_k. \quad (4.20)$$

Eq. (4.20) is the spectral representation of the propagator $\mathbf{T}(t - t')$ in the time domain. The spectral representation is suitable for the characterization of the asymptotic behavior of the DDE because for $t \rightarrow \infty$ the sum in Eq. (4.20) is dominated only by one or two summands with the poles s_k with the largest real part. Hence, the calculation of the poles or characteristic exponents s_k is sufficient for the identification of the stability of the linearized system Eq. (3.2). In particular, the poles s_k of the propagator are the solutions of the characteristic equation

$$\det(\mathbf{I}s - \mathbf{A}_0 - \mathbf{B}_0 \bar{\mathbf{K}}(s)) = 0. \quad (4.21)$$

In general, Eq. (4.21) is a transcendental equation, and leads to a discrete set of infinitely many characteristic exponents s_k [62]. There are many numerical methods for the calculation of the characteristic exponents s_k of time delay systems [110]. For example, for a scalar system with discrete delay τ_0 , that is for $K(\tau) = \delta(\tau - \tau_0)$, the exponents s_k can be calculated with the Lambert W function [130, 131, 132]. A more detailed overview on different methods for the calculation of the characteristic exponents s_k of autonomous time delay systems is presented in Sec. 5.1.

With Eq. (4.8) the spectral representation Eq. (4.20) of the propagator can be also used for the calculation of the exact form of the perturbations $\mathbf{x}(t)$ for a given initial condition, i.e. the solution of the linearized system Eq. (3.2). For this purpose a method for the calculation of the residues \mathbf{R}_k is presented, which is an extension of the method presented in [129]. At first a spectral representation of the propagator $\bar{\mathbf{T}}(s)$ in the Laplace domain is defined as

$$\bar{\mathbf{T}}(s) = \sum_{l=1}^N \frac{\mathbf{q}_l(s) \mathbf{d}_l^T(s)}{\sigma_l(s)}, \quad (4.22)$$

where $\mathbf{d}_l(s)^T$, $\mathbf{q}_l(s)$ and $\sigma_l(s)$ are the left, the right eigenvectors and the inverse eigenvalues of the matrix $\bar{\mathbf{T}}(s)$ as a function of s . According to Eq. (4.18), these functions are defined by

$$(\mathbf{I}s - \mathbf{A}_0 - \mathbf{B}_0 \bar{\mathbf{K}}(s)) \mathbf{q}_l(s) = \sigma_l(s) \mathbf{q}_l(s), \quad (4.23a)$$

$$\mathbf{d}_l^T(s) (\mathbf{I}s - \mathbf{A}_0 - \mathbf{B}_0 \bar{\mathbf{K}}(s)) = \mathbf{d}_l^T(s) \sigma_l(s). \quad (4.23b)$$

Note that the left and the right eigenvectors of the matrix function $\bar{\mathbf{T}}(s)$ are biorthonormal, i.e. $\mathbf{d}_k^T(s) \mathbf{q}_l(s) = \delta_{kl}$. If Eq. (4.22) is substituted in Eq. (4.19) and multiplied with $(s - s_n)$ one obtains

$$\sum_{l=1}^N \frac{\mathbf{q}_l(s) \mathbf{d}_l^T(s)}{\sigma_l(s)} (s - s_n) = \sum_{k=0}^{\infty} \frac{s - s_n}{s - s_k} \mathbf{R}_k, \quad (4.24)$$

where s_n is one specific pole of the propagator with $\sigma_l(s_n) = 0$. If the limit $s \rightarrow s_n$ is taken, only one term in each of the two sum in Eq. (4.24) is non-zero. In particular,

4.4. Eigenmode expansion for DDEs

these are the terms, where the denominators $\sigma_l(s)$ and $s - s_k$ vanish. This means that Eq. (4.24) becomes

$$\mathbf{R}_n = \lim_{s \rightarrow s_n} \mathbf{q}_l(s) \mathbf{d}_l^T(s) \frac{s - s_n}{\sigma_l(s)}, \quad (4.25)$$

where l is defined by $\sigma_l(s_n) = 0$. Using L'Hopital's rule and denoting the left and the right eigenvectors at the poles as $\mathbf{d}_n^T = \mathbf{d}_l^T(s_n)$ and $\mathbf{q}_n = \mathbf{q}_l(s_n)$, Eq. (4.25) for the calculation of residues simplifies to

$$\mathbf{R}_n = \frac{\mathbf{q}_n \mathbf{d}_n^T}{\mathbf{d}_n^T \left(\mathbf{I} - \mathbf{B}_0 \bar{\mathbf{K}}'(s_n) \right) \mathbf{q}_n}, \quad (4.26)$$

where $\bar{\mathbf{K}}'(s_n)$ is the derivative of the Laplace transform of the delay distribution at the pole $s = s_n$. Substituting Eq. (4.26) in Eq. (4.20) for the case of a scalar DDE with a discrete delay, i.e. $\bar{K}(s) = e^{-s\tau_0}$, the spectral representation of the propagator in the time domain simplifies to

$$T(t - t') = \sum_{k=-\infty}^{\infty} \frac{e^{s_k(t-t')}}{1 + B_0 \tau_0 e^{-s_k \tau_0}}, \quad (4.27)$$

which coincide with the known results for the spectral representation of the propagator in [88, 89].

4.4. Eigenmode expansion for DDEs

The eigenmode expansion for a scalar DDE with a single discrete delay is presented by Amann et al. in [88]. In this paper, the eigenmodes and the dual eigenfunctions are defined and used to derive the spectral representation of the propagator $\mathbf{T}(t, t')$ in the time domain. Amann et al. do not provide a systematic approach for the construction of the dual eigenfunctions or the residues \mathbf{R}_n , which might be used to derive the dual eigenfunctions for vector-valued DDEs with distributed delay. However, in this thesis the spectral representation of the propagator in the time domain Eq. (4.20) was already derived in Sec. 4.3 from the Laplace transform of vector-valued DDEs with distributed delay, which was presented in Sec. 4.1. As a result, in this subsection the eigenmode expansion for vector-valued DDEs with distributed delay is derived from the spectral representation Eq. (4.20) of the propagator, which provides a systematic approach for the construction of the eigenmode expansion for time delay systems.

The solution of an autonomous DDE Eq. (4.8) in terms of the propagator can be rearranged to

$$\mathbf{x}(t) = \mathbf{T}(t) \left(\mathbf{\Psi}(0) + \int_0^{\tau_{\max}} d\tau \int_{-\tau}^0 d\theta' \mathbf{T}(-(\theta' + \tau)) \mathbf{B}_0 \mathbf{K}(\tau) \mathbf{\Psi}(\theta') \right), \quad (4.28)$$

4. Analytical solution of linear time delay systems

where Eq. (2.2) was substituted for $\mathbf{r}_\Psi(\theta)$ and the variable transformation $\theta = \theta' + \tau$ was made. If the spectral representation of the propagator Eq. (4.20) with the residues Eq. (4.26) is put into Eq. (4.28) the solution can be expressed as

$$\mathbf{x}(t) = \sum_{k=-\infty}^{\infty} e^{s_k t} \frac{\mathbf{q}_k \mathbf{d}_k^T}{N_k} \int_{-\tau_{\max}}^0 d\theta \left(\mathbf{I} \delta(\theta + 0) + \mathbf{B}_0 \int_0^{\tau_{\max}} d\tau \mathbf{K}(\tau) e^{-s_k(\theta+\tau)} \mathbf{H}(\theta + \tau) \right) \Psi(\theta), \quad (4.29)$$

where the notation $\delta(t + 0) = \lim_{\epsilon \rightarrow 0} \delta(t + \epsilon)$ is used and the normalization constant N_k is equal to the denominator of the residues in Eq. (4.26)

$$N_k = \mathbf{d}_k^T \left(\mathbf{I} - \mathbf{B}_0 \bar{\mathbf{K}}'(s_k) \right) \mathbf{q}_k. \quad (4.30)$$

Eq. (4.29) can be decomposed by defining the k th eigenmode of the DDE

$$\mathbf{x}_k(t) = \mathbf{q}_k e^{s_k t} \in \mathbb{R}^N, \quad (4.31)$$

and the corresponding dual eigenfunction

$$\mathbf{y}_k^T(t) = \frac{\mathbf{d}_k^T}{N_k} \left(\mathbf{I} \delta(t + 0) + \mathbf{B}_0 \int_0^{\tau_{\max}} d\tau \mathbf{K}(\tau) e^{-s_k(t+\tau)} \mathbf{H}(t + \tau) \right). \quad (4.32)$$

With these definitions the solution of the DDE can be given by a superposition of the infinitely many eigenmodes

$$\mathbf{x}(t) = \sum_{k=-\infty}^{\infty} \mathbf{x}_k(t) c_k = \sum_{k=-\infty}^{\infty} \mathbf{q}_k e^{s_k t} c_k, \quad (4.33)$$

where the time-invariant coefficients c_k are determined by the dual eigenfunctions as

$$c_k = \int_{-\tau_{\max}}^0 d\theta \mathbf{y}_k^T(\theta) \Psi(\theta). \quad (4.34)$$

This means that the characteristic exponents s_k together with the right eigenvectors \mathbf{q}_k specify an infinite set of fundamental solutions $\mathbf{x}_k(t)$ of the DDE Eq. (3.2) with constant coefficients. They are called eigenmodes because the right eigenvectors \mathbf{q}_k specify time-invariant eigendirections in the N dimensional space for the configurations \mathbf{x} of the DDE, and the time evolution along these fixed eigendirections is specified by the scalar term $e^{s_k t}$. This means that the dynamics becomes decoupled if a superposition of the eigenmodes Eq. (4.31) are put in the linearized DDE Eq. (3.2). In other words, the eigenmodes $\mathbf{x}_k(t)$ and the dual eigenfunctions $\mathbf{y}_k^T(t)$ form a biorthonormal system in the interval of the initial function of the DDE, that is

$$\int_{-\tau_{\max}}^0 d\theta \mathbf{y}_j^T(\theta) \mathbf{x}_k(\theta) = \delta_{jk}. \quad (4.35)$$

The proof of Eq. (4.35) is given in Appendix A.2.4. The eigenmodes $\mathbf{x}_k(t)$ are linearly independent functions, and the superposition of the infinitely many eigenmodes can be used to specify the state of the DDE similar to Eq. (4.33)¹. In Sec. 5.1.1 the eigenmodes Eq. (4.31) are used to derive the characteristic equation Eq. (4.21) of an autonomous DDE with distributed delay and in Sec. 6 the derivation of the eigenmodes for periodic DDEs with distributed delays with the Hill-Floquet method is presented.

4.5. Summary

The fundamental analytical approaches for the solution of linear DDEs were presented in this Chapter. In particular, in Sec. 4.1 the Laplace transform of the linearized DDE was used for the formal definition of the propagator of DDEs with distributed delay and for the representation of the solution Eq. (4.8) in terms of the propagator of the time delay system. Eq. (4.8) is the basic representation for solutions of non-autonomous linear DDEs with distributed delay and can be used to construct the solution operator for such systems. This fills some open gaps in the existing literature, where typically only systems with one or multiple discrete delays or only scalar systems are considered [50, 88, 89].

In general, there are different methods for the determination of an explicit expression of the propagator for time delay systems. The first approach is based on the method of steps, which was used in Sec. 4.2 to derive a new expression for the propagator of non-autonomous DDEs with one discrete delay in terms of multiple nested integrals in Eq. (4.14). The analytical solution of the nested integrals is, in general, only possible for the case of constant commuting coefficient matrices resulting in Eq. (4.17), which is closely related to the known result for scalar systems. In Sec. 4.2 it was also shown, that the propagator for time delay systems can be interpreted as a path integral, where the paths are composed of all possible combinations of ODE steps and delay steps between the starting and the end time. This interpretation is very useful for the direct determination of the propagator by summing up all paths directly, where no extensive calculations are necessary.

A second method for obtaining a time domain representation of the propagator for time delay system is the direct application of the inverse Laplace transform, which is useful for autonomous DDEs. In particular, in Sec. 4.3 the inverse Laplace transform of linear DDEs with constant coefficients and distributed delay via residue theory is used to calculate the spectral representation Eq. (4.20) of the propagator in the time domain. Whereas, the time domain representation of the propagator Eq. (4.14) from the method of steps is suitable for the characterization of the short term behavior of the solution of linear DDEs, the spectral representation Eq. (4.20) is suitable for the characterization of the long term behavior of the solution because for large times $t \rightarrow \infty$ only one summand dominates the propagator.

The different summands in the spectral representation of the propagator Eq. (4.20) can be interpreted as eigenmodes of the time delay system. In Sec. 4.4, the eigenmode ex-

¹Note that according to the assumptions in Sec. 4.3 only the generic case of non-degenerate poles s_k is discussed in detail here.

4. Analytical solution of linear time delay systems

pansion for autonomous vector-valued DDEs with distributed delay was presented. This is an extension to the results in [88]. In addition, the Laplace transform of the DDE and the inverse Laplace transform of the spectral representation of the propagator provides a systematical way for the derivation of the eigenmode decomposition of autonomous DDEs with distributed delay.

The results in Chapter 4 show the limits of the analytical approaches for the solution of time delay systems. In general, either the numerical solution of nested integrals in Eq. (4.14) or the determination of the characteristic roots in Eq. (4.20) is necessary for the calculation of the solution of linear DDEs. This emphasizes the necessity for numerical or semi-analytical methods for the analysis of non-autonomous DDEs with distributed delay. For the analysis in this thesis, especially the asymptotic behavior of the solution of time delay systems is relevant. Thus, the remaining theory for the analysis of linear DDEs, which is presented in Chapter 5 and Chapter 6, is focused on the determination of the most dominant characteristic roots of the time delay system for the autonomous as well as the non-autonomous case.

5. Frequency domain approach

In this chapter frequency domain methods for the analysis of linear time delay systems Eq. (3.2) with the memory Eq. (2.2) are presented. In Sec. 5.1 some detailed remarks on the calculation of the characteristic roots of autonomous DDEs with distributed delay based on the characteristic Eq. (4.21) are given. In Sec. 5.2 the theory is extended to DDEs with periodic coefficients, which leads to an infinite dimensional characteristic equation, the so-called Hill's infinite determinant. This method is mainly used for the calculation of the stability chart in a parameter space based on the D-subdivision method, which is presented in Sec. 5.3.

5.1. Autonomous systems

The characteristic Eq. (4.21) for autonomous DDEs with distributed delay was already derived in Sec. 4.3 for the calculation of the poles of the Laplace domain representation $\bar{\mathbf{T}}(s)$ of the propagator. It is the basis for the frequency domain approach for the stability analysis of autonomous time delay systems, which is presented in this Section. Note that especially the numerical methods for the calculation of the characteristic roots for linear autonomous systems, which are presented in Sec. 5.1.4 can be combined with the Hill-Floquet transformation for the analysis of linear DDEs with periodic coefficients, which is introduced in Chapter 6.

5.1.1. Characteristic equation

The autonomous case is characterized by constant coefficient matrices $\mathbf{A}(t) = \mathbf{A}_0$ and $\mathbf{B}(t) = \mathbf{B}_0$ in the linearized system Eq. (3.2). In this case the dynamics of the perturbations can be given by

$$\dot{\mathbf{x}}(t) = \mathbf{A}_0 \mathbf{x}(t) + \mathbf{B}_0 \int_0^{\tau_{\max}} \mathbf{K}(\tau) \mathbf{x}(t - \tau) d\tau. \quad (5.1)$$

From the eigenmode decomposition in Sec. 4.4 it is known, that the dynamics can be decoupled by expanding the solution in eigenmodes of the form $\mathbf{x}_k(t) = \mathbf{q}_k e^{s_k t}$. Putting this ansatz $\mathbf{x}(t) = \mathbf{x}_k(t)$ in Eq. (5.1) results in the characteristic equation

$$s_k \mathbf{q}_k = (\mathbf{A}_0 + \mathbf{B}_0 \bar{\mathbf{K}}(s_k)) \mathbf{q}_k. \quad (5.2)$$

The typically complex eigenvalues $s_k = \lambda_k + i\omega_k$ of Eq. (5.2) are called characteristic exponents and are the poles of the Laplace domain representation $\bar{\mathbf{T}}(s)$ of the propagator as defined in Eq. (4.18). They are also known as characteristic roots because they

5. Frequency domain approach

are equivalent to the roots of the characteristic Eq. (4.21), which was given already in Sec. 4.3. The real part λ_k and the imaginary part ω_k of the characteristic exponents specify the exponential behavior and the frequency of the eigenmode $\mathbf{x}_k(t)$. The real and the imaginary part of the characteristic Eq. (4.21) can be split into two scalar equations. For fixed coefficient matrices \mathbf{A}_0 , \mathbf{B}_0 and a fixed delay distribution $\mathbf{K}(\tau)$ there are two unknowns λ_k and ω_k , which means that the problem is well-defined and the solution of the characteristic Eq. (4.21) yields the discrete spectrum s_k of the DDE [54, 62]. In the following it is assumed that the characteristic exponents s_k are ordered according to their real part with $\lambda_k > \lambda_{k+1}$ and $k \geq 0$, that is, s_0 is the root with the maximum real part. The largest real part λ_0 determines the stability of the DDE. For $\lambda_0 > 0$ the system is unstable with exponentially diverging solutions and for $\lambda_0 < 0$ the system is stable because the amplitude of all eigenmodes $\mathbf{x}_k(t)$ converges exponentially to zero.

In general, the characteristic Eq. (4.21) of a DDE with distributed delay is a transcendental equation and has infinitely many roots s_k . This can be seen easily for a discrete delay distribution $\mathbf{K}(\tau) = \mathbf{K}_0 \delta(\tau - \tau_0)$. In this case the characteristic equation becomes

$$\det(\mathbf{I}s - \mathbf{A}_0 - \mathbf{B}_0 \mathbf{K}_0 e^{-s\tau_0}) = 0. \quad (5.3)$$

Other examples for typical delay distributions $\mathbf{K}(\tau)$, which result in a transcendental equation can be found in [110]. The infinite number of characteristic exponents s_k is due to the infinite dimension of a DDE. It can be proven, that the spectrum of autonomous DDEs is discrete and that there are always only a finite number of characteristic exponents s_k with positive real part $\lambda_k > 0$ [62].

5.1.2. Linear chain trick

There exist specific delay distributions, where only a finite number of characteristic exponents appears. These delay distributions are given by the gamma distribution

$$\mathbf{K}(\tau) = \mathbf{K}_0 \frac{\beta^j \tau^{j-1} e^{-\beta\tau}}{(j-1)!}, \quad \tau \geq 0, \quad (5.4)$$

where $j \in \mathbb{N}^+$ and $\beta \in \mathbb{R}^+$ are arbitrary shape and rate parameters. The Laplace transform of the gamma distribution Eq. (5.4) is given by [10]

$$\bar{\mathbf{K}}(s) = \mathbf{K}_0 \frac{\beta^j}{(s + \beta)^j}, \quad (5.5)$$

which results in the characteristic equation

$$\det((\mathbf{I}s - \mathbf{A}_0)(s + \beta)^j - \mathbf{B}_0 \mathbf{K}_0 \beta^j) = 0. \quad (5.6)$$

Eq. (5.6) is a polynomial with only a finite number of characteristic roots s_k . Hence, a DDE with a delay distribution equal to the gamma distribution Eq. (5.4) is only finite dimensional, which means that such a DDE is equivalent to an ODE system. The transformation of a DDE with a gamma distribution Eq. (5.4) to an ODE is known as linear chain trick and is often used in models for population dynamics [10, 38]. In this thesis the form of the delay distribution is not restricted to the gamma distribution and the generic case of a transcendental characteristic equation is studied.

5.1.3. Lambert W approach

In addition, to the linear chain trick, where an analytical solution of the polynomial characteristic Eq. (5.6) is possible, a semi-analytical solution of the characteristic Eq. (5.2) can be obtained for the specific case of an autonomous DDE with a discrete delay $\mathbf{K}(\tau) = \mathbf{K}_0\delta(t - \tau_0)$ and commuting coefficient matrices, i.e. $\mathbf{A}_0(\mathbf{B}_0\mathbf{K}_0) = (\mathbf{B}_0\mathbf{K}_0)\mathbf{A}_0$. In this case the characteristic equation Eq. (5.2) can be written as

$$(\mathbf{I}s - \mathbf{A}_0) \tau_0 e^{(\mathbf{I}s - \mathbf{A}_0)\tau_0} \mathbf{q}_j = \mathbf{B}_0\mathbf{K}_0\tau_0 e^{-\mathbf{A}_0\tau_0} \mathbf{q}_j, \quad (5.7)$$

where \mathbf{q}_j denotes the j th eigenvector of the coefficient matrices \mathbf{A}_0 and $\mathbf{B}_0\mathbf{K}_0$. Eq. (5.7) has a structure similar to the equation $W(z)e^{W(z)} = z$, where the function $W(z)$ is called Lambert W function and has infinitely many branches [131]. As a consequence, for commuting coefficient matrices \mathbf{A}_0 and $\mathbf{B}_0\mathbf{K}_0$ the characteristic exponents $s_{j,l}$ can be calculated directly by

$$s_{j,l} = \sigma_j(\mathbf{A}_0) + \frac{1}{\tau_0} W_l(\sigma_j(\mathbf{B}_0\mathbf{K}_0\tau_0 e^{-\mathbf{A}_0\tau_0})), \quad (5.8)$$

where $\sigma_j(\mathbf{X})$ denotes the j th eigenvalue of an arbitrary matrix \mathbf{X} corresponding to the j th eigenvector \mathbf{q}_j , and W_l denotes the l th branch of the Lambert W function [130].

The advantage of the Lambert W approach relies in the fact, that the Lambert W-function defines a clear relationship between the infinitely many characteristic exponents of the system, and therefore, is suitable for the control of the infinite dimensional delay system with a finite number of parameters. If the coefficient matrices do not commute, in general, a calculation of the characteristic exponents s_k with the Lambert W function is no longer possible [54, 130, 133]. In this case the characteristic exponents must be calculated numerically.

5.1.4. Numerical methods

The calculation of the roots of the characteristic equation for linear autonomous DDEs is a standard technique in the analysis of time delay systems, which is described for example in [52, 53]. In particular, the software package *TRACE-DDE* is a numerical tool for the calculation of the characteristic exponents based on the solution of the characteristic Eq. (4.21) [134]. Furthermore, there are many more numerical methods for the solution of the characteristic equation of autonomous DDEs, which is, in general, the solution of a nonlinear eigenvalue problem. A nice overview can be found in [54]. Many of these methods can be interpreted as a polynomial approximation of the exponential term $e^{-s\tau_0}$ in the characteristic Eq. (5.3) or a polynomial approximation of the Laplace transform of the delay distribution $\bar{\mathbf{K}}(s)$ in the characteristic Eq. (4.21) for the general case of a continuous delay distribution. In practice, this polynomial approximation is often obtained by a finite approximation of the state of the DDE Eq. (3.2) \mathbf{x}_t by a finite dimensional vector instead of a function. In general, the finite dimensional approximation of the state \mathbf{x}_t , i.e. the function $\mathbf{x}(t + \theta)$ of the DDE in one delay interval $\theta \in [-\tau_{\max}, 0]$, can be described by an expansion in terms of a finite number of basis functions. The resulting

5. Frequency domain approach

finite dimensional representation of the solution operator or the finite dimensional approximation of the infinitesimal generator of the DDE in terms of the basis functions can be used to approximate the most dominant characteristic exponents s_k of the DDE.

The classification of these methods can be done similar to the related methods for the analysis of partial differential equations (PDEs) [135]. On the one hand, there are finite difference methods, where one basis function determines the solution in a small subinterval, i.e. the basis functions are local functions. Classical examples for finite difference methods are the Semidiscretization [3, 136], the Full-Discretization method [137] or the Continuous Time Approximation [138]. On the other hand, there are spectral methods, where the basis functions are global functions with non-zero values in the whole delay interval. Spectral methods based on Chebyshev polynomials, Legendre polynomials or a mixed Fourier basis can be found in [73, 139, 140, 141]. In addition, there are spectral element methods, which combine the advantages of the finite difference and the spectral approach and use extended high-order polynomials in several subintervals of the delay interval for the basis functions [74, 142]. In the context of time delay systems, these methods are also known as time finite element approach [143]. Another classification is possible according to the method for the minimization of the residual function, that is, the minimization of the error between the finite dimensional approximation and the original infinite dimensional system by using different test functions [135]. Some examples for a different minimization of the residual function are known as Galerkin or spectral-tau method [73, 140, 141], where the test functions are equivalent to the basis functions, spectral least squares method [140] and pseudospectral or collocation methods [73, 139], where the test functions are Dirac delta functions. Specifically, the Chebyshev collocation method is presented in more detail in Sec. 6.3, where the method is combined with the Hill-Floquet transformation for the calculation of the Floquet exponents of linear DDEs with periodic coefficients.

5.2. Periodic systems

The periodic case is characterized by T -periodic coefficient matrices $\mathbf{A}(t + T) = \mathbf{A}(t)$ and $\mathbf{B}(t + T) = \mathbf{B}(t)$. Such a situation occurs, for example, if the stability of periodic solutions of the standard form Eq. (2.1) are analyzed. In particular, in Sec. 7.3 the stability of periodic solutions of a Hodgkin-Huxley neuronal network with heterogeneous coupling delays is studied. Other examples are DDEs with periodic parametric excitation, which often occur in engineering and are characterized by a periodic variation of one or more parameters of the system. An application of a periodic parametric excitation is studied in Sec. 7.2, where the stability of mechanical vibrations in a turning process with a periodically varying spindle speed is investigated. In Sec. 5.2.1 the extension of the characteristic equation to periodic systems is presented, which is known as Hill's infinite determinant method. In Sec. 5.2.2 some remarks on alternative numerical methods for the calculation of the characteristic roots for periodic DDEs are given.

5.2.1. Hill's infinite determinant method

Dynamical systems with periodic coefficients can be analyzed with Floquet theory, which states that the eigenmodes of a periodic system can be written as [75, 76]

$$\mathbf{x}_k(t) = \mathbf{p}_k(t)e^{s_k t}, \quad \mathbf{p}_k(t+T) = \mathbf{p}_k(t), \quad (5.9)$$

where $\mathbf{p}_k(t)$ is a T -periodic coefficient and s_k is the characteristic exponent or Floquet exponent. Putting the ansatz (5.9) into the linearized DDE Eq. (3.2) yields

$$\dot{\mathbf{p}}_k(t) + s_k \mathbf{p}_k(t) = \mathbf{A}(t)\mathbf{p}_k(t) + \mathbf{B}(t) \int_0^{\tau_{\max}} \mathbf{K}(\tau)e^{-s_k \tau} \mathbf{p}_k(t-\tau) d\tau. \quad (5.10)$$

The Fourier transform is used to put Eq. (5.10) in the frequency domain. In this thesis the Fourier transform of an arbitrary vector $\mathbf{v}(t)$ and its inverse are defined by

$$\hat{\mathbf{v}}(\omega) = \int_{-\infty}^{\infty} \mathbf{v}(t)e^{-i\omega t} dt, \quad \mathbf{v}(t) = \frac{1}{2\pi} \int_{-\infty}^{\infty} \hat{\mathbf{v}}(\omega)e^{i\omega t} d\omega. \quad (5.11)$$

The frequency domain representation of the linear periodic DDE Eq. (5.10) can be written as

$$(s_k + i\omega)\hat{\mathbf{p}}_k(\omega) = \int_{-\infty}^{\infty} \left(\hat{\mathbf{A}}(\omega - \omega') + \hat{\mathbf{B}}(\omega - \omega')\bar{\mathbf{K}}(s_k + i\omega') \right) \hat{\mathbf{p}}_k(\omega') d\omega'. \quad (5.12)$$

Since the vector $\mathbf{p}_k(t)$ and the matrices $\mathbf{A}(t)$ and $\mathbf{B}(t)$ are T -periodic functions, their Fourier transforms are discrete with peaks at multiples of the basic frequency $\Omega = 2\pi/T$

$$\hat{\mathbf{p}}_k(\omega) = \sum_{l=-\infty}^{\infty} \hat{\mathbf{p}}_{k,l} \delta(\omega - l\Omega), \quad \hat{\mathbf{A}}(\omega) = \sum_{l=-\infty}^{\infty} \hat{\mathbf{A}}_l \delta(\omega - l\Omega), \quad \hat{\mathbf{B}}(\omega) = \sum_{l=-\infty}^{\infty} \hat{\mathbf{B}}_l \delta(\omega - l\Omega). \quad (5.13)$$

If Eq. (5.13) is put in Eq. (5.12) and the harmonics are balanced, an infinite dimensional characteristic equation can be obtained as

$$\det \mathbf{C}_{\infty}(s) = 0. \quad (5.14)$$

The infinite dimensional matrix \mathbf{C}_{∞} is composed of the $N \times N$ dimensional matrix blocks

$$\{\mathbf{C}_{\infty}(s)\}_{kl} = \mathbf{I}(s + ik\Omega)\delta_{kl} - \hat{\mathbf{A}}_{k-l} - \hat{\mathbf{B}}_{k-l}\bar{\mathbf{K}}(s + il\Omega), \quad (5.15)$$

with $k, l = -\infty, \dots, \infty$. The matrix \mathbf{C}_{∞} is called Hill's infinite matrix and the determinant in Eq. (5.14) is called Hill's infinite determinant.

The Hill's infinite determinant method was initially presented in the original work of Hill in 1886 for the analysis of the periodic lunar motion [77]. One year later, a generalized form of this method for the stability analysis of mechanical vibrations was presented

5. Frequency domain approach

in [78]. Apart from the dimension of the matrix $\mathbf{C}_\infty(s)$, the characteristic Eq. (5.14) for systems with periodic coefficients has the same structure as the characteristic Eq. (4.21) for systems with constant coefficients. It is a transcendental equation and the typically complex-valued roots $s_k = \lambda_k + i\omega_k$ of Eq. (5.14) are the characteristic exponents or Floquet exponents. Similar to the characteristic roots of Eq. (4.21), the Floquet exponents s_k are ordered according to their real part with $\lambda_k > \lambda_{k+1}$ and $k > 0$. Thus, the real part λ_0 of the dominant Floquet exponent determines the stability of the DDE. For $\lambda_0 > 0$ the linearized system Eq. (3.2) is unstable with exponentially diverging solutions and for $\lambda_0 < 0$ the system is stable and all solutions converge to zero. The convergence of the Hill's infinite determinant Eq. (5.14) for the delay-free case, i.e for $\mathbf{B}(t) = \mathbf{0}$, is studied in [144, 145, 146, 147, 148]. For DDEs some results on the convergence of the Hill's infinite determinant can be found in [149]. For the delay-free case, that is, where Eq. (3.2) reduces to an ODE, the Floquet exponents s_k are simply the eigenvalues of the matrix¹

$$\mathbf{A}_\infty = \begin{pmatrix} \ddots & \vdots & \vdots & \vdots & \ddots \\ \cdots & \hat{\mathbf{A}}_0 - \mathbf{I}i\Omega & \hat{\mathbf{A}}_{-1} & \hat{\mathbf{A}}_{-2} & \cdots \\ \cdots & \hat{\mathbf{A}}_1 & \hat{\mathbf{A}}_0 & \hat{\mathbf{A}}_{-1} & \cdots \\ \cdots & \hat{\mathbf{A}}_2 & \hat{\mathbf{A}}_1 & \hat{\mathbf{A}}_0 + \mathbf{I}i\Omega & \cdots \\ \ddots & \vdots & \vdots & \vdots & \ddots \end{pmatrix}. \quad (5.16)$$

The method is used, for example, for the analysis of vibrations in engineering [150, 151], for the analysis of periodic solutions in spatially extended systems [152, 153], or for the calculation of energy bands for electrons in periodic crystals [79, 80]². However, in general, for the DDE case a nonlinear eigenvalue problem appears and the calculation of the Floquet exponents s_k from the infinite dimensional characteristic Eq. (5.14) is not straightforward. A generalization of the Hill's infinite determinant method is shown later in Chapter 6 by the introduction of the Hill-Floquet transformation, which can be used for the calculation of Floquet exponents s_k of time delay systems.

5.2.2. Numerical methods

Since the Hill's infinite determinant method as presented in Sec. 5.2.1 is not suitable for the calculation of Floquet exponents for time delay systems, the analysis of DDEs with periodic coefficients is often performed in the time domain. In fact, the finite difference methods, the spectral methods and the spectral element methods, which are presented for the autonomous case in Sec. 5.1.4, can be also used for the calculation of the Floquet exponents for DDEs with periodic coefficients. An overview on these methods is given in [55]. For periodic systems the above-mentioned time domain methods require the construction of the solution over one period. In particular, the finite dimensional approximation of the solution operator of the system over the principle period in terms

¹In practice, the numerical implementation of the Hill's infinite determinant method is typically applied by truncating the bi-infinite Hill matrix.

²In solid state physics Floquet theory is commonly known as Bloch theory

of the basis functions is called monodromy matrix. The eigenvalues of the monodromy matrix are approximations of the dominant Floquet multipliers $e^{s_k T}$ and the system is stable if the modulus of all Floquet multipliers is smaller than one.

In addition to these methods, there is the method of characteristic matrices [154, 155]. In this approach the retarded configuration in the formal solution of the system over the principle period is expressed in terms of the unknown Floquet multiplier $e^{s_k T}$, which describes the time evolution of one eigenmode over the principle period T . The resulting algebraic equation can be interpreted as the characteristic equation of the periodic system. Note that the method requires the numerical approximation of the monodromy matrix or alternatively the calculation of the propagator for a system with periodic coefficients, which is, in general, not trivial as discussed in Chapter 4.

Whereas, the Hill's infinite determinant method as presented in Sec. 5.2.1 is not suitable for the calculation of Floquet exponents, the method can be used for the calculation of stability charts in parameter space. In general, this technique is known as D-subdivision method and is presented next.

5.3. D-subdivision method

In many applications the computation of a stability chart in the parameter space, which separates stable from unstable behavior is useful. For this purpose the real part of the characteristic exponents is set to zero $\lambda_k = 0$, which means that at least one characteristic root crosses the imaginary axis. In this case, only one free parameter ω_k is left in the characteristic Eq. (5.14). As a result, in a parameter space with at least one additional free parameter of the system the solution of the characteristic Eq. (5.14) with $s_k = i\omega_k$ results in hyperplanes that separate different domains with a different number of characteristic exponents s_k with positive real part $\lambda_k > 0$. The dimension of the hyperplanes is equal to the dimension of the parameter space minus one because the characteristic Eq. (5.14) are practically two scalar equations, one for the real part and one for the imaginary part of the determinant, and one free parameter is given by the frequency ω_k of the eigenmode. In other words, for one free parameter, there are points where the characteristic exponents $s_k = i\omega_k$ cross the imaginary axis. For two parameters, the hyperplanes that separate the parameter regions with a different number of unstable eigenmodes are curves in the parameter space and so on. This method is called D-subdivision and the curves in the parameter space are called D-curves [47, 52]. The D-curves that separate the domains of stable and unstable behavior are the ones with $\lambda_0 = 0$, i.e. the solution where the largest real part of the characteristic exponents becomes zero. An example for a stability chart with the D-curves is presented in Fig. 7.1, where the D-curves for equilibria of single species delayed reaction-diffusion systems were calculated.

5.3.1. Autonomous systems

An example of the analytical calculation of the D-curves and the stability chart of an autonomous DDE with distributed delay from the characteristic equation is shown for single species delayed reaction-diffusion systems in Sec. 7.1. Already for the autonomous

5. Frequency domain approach

case, the analytic construction of the stability chart from the characteristic Eq. (4.21) becomes very complex if the dimension of the systems increases [156]. As a consequence, the D-curves in Fig. 7.7a for the non-trivial equilibrium of the Hodgkin-Huxley neuronal network with heterogeneous delay couplings in Sec. 7.3 are calculated numerically. A very efficient numerical method for the calculation of the stability chart with the D-subdivision method for metal cutting vibrations is presented in the parallel turning example in Sec. 7.2.2.

Another elegant way for the calculation of stability charts for autonomous DDEs, which is also applicable for DDEs with multiple delays is called Cluster Treatment of the Characteristic Roots [157, 158]. It makes use of the Rekasius substitution for the exponential term in the characteristic equation, $e^{-s\tau_0} = \frac{1-sT_0}{1+sT_0}$, which holds for purely imaginary characteristic roots $s = i\omega$. As a result, the transcendental characteristic equation of a DDE for the calculation of the D-curves can be transformed to a polynomial characteristic equation with a finite number of solutions. Nevertheless, the infinite dimensional nature of the time delay system is preserved because an infinite number of delays τ_0 is associated to one critical parameter $T_0(\tau_0)$ associated with the D-curves. The advantage of this method is that standard methods for ODEs can be used for the calculation of the D-curves from the polynomial characteristic equation and a clear relationship between the infinitely many critical delays τ_0 corresponding to one T_0 is defined. However, this method can be only used for the identification of the D-curves with $s = i\omega$, where the characteristic roots cross the imaginary axis, but no information on the exponential behavior of the solution for arbitrary parameters of the system is available.

5.3.2. Periodic systems

For time delay systems with periodic coefficients the Hill's infinite determinant method Eq. (5.14) can be used for the calculation of the D-curves. A semi-analytic way for the construction of the D-curves is possible for some specific examples with harmonically varying coefficients [59, 81]. This method is typically also used in solid state physics for the calculation of energy bands in a sinusoidal potential [79, 80]. In general, a numerical algorithm is necessary for finding the roots of the system of two nonlinear equations for the real and the imaginary part of Eq. (5.14) in a high dimensional parameter space. Specific examples, where the D-curves are calculated numerically from the Hill's infinite matrix, can be found in [41, 42, 82, 159, 160]. Some of the numerical methods are based on the calculation of the eigenvalues of the Hill's infinite matrix [159], the Nyquist stability criterion [82] or the application of a multi-dimensional bisection method [42]. In particular, the multi-dimensional bisection method is a general method for the calculation of the roots of an arbitrary system of nonlinear equations in a multi-dimensional parameter space [161]. In general, the above mentioned numerical methods based on the Hill's infinite determinant method must be carefully adapted for the specific problem.

For the numerical solution of the infinite dimensional characteristic Eq. (5.14) a truncated version of the matrix \mathbf{C}_∞ with a finite number n of higher harmonics must be used. The number of harmonics should be chosen in such a way, that the interval $[-n\Omega, n\Omega]$ covers all dominant internal frequencies of the systems. For example, in metal cutting

applications these internal frequencies are the dominant eigenfrequencies of the machine-tool structure. Due to the structure of the matrix \mathbf{C}_∞ defined in (5.15), the following condition holds for $n \rightarrow \infty$

$$\det \mathbf{C}_\infty(s) = \det \mathbf{C}_\infty(s + i\Omega). \quad (5.17)$$

Moreover, due to the existence of complex conjugate characteristic exponents only positive imaginary parts of the exponents $\omega \geq 0$ must be taken into account. Both conditions can be used to reduce the considered space for a numerical frequency sweep to the interval $\omega \in I_\omega := [0, \Omega/2)$. Thus, the most effective and accurate solution can be obtained by choosing a large number of harmonics n and only a small interval I_ω for the sweep for the frequencies ω . However, for small excitation frequencies Ω the number of harmonics n for the interval $[-n\Omega, n\Omega]$ that covers all dominant internal frequencies becomes very large. In this case a second strategy is suitable, where the number of higher harmonics n is reduced but solutions of Eq. (5.14) are searched in larger intervals of ω around the internal frequencies of the system. This is the common strategy that is proposed in [2] for the calculation of the stability lobes in metal cutting.

5.3.3. Aperiodic systems

The Hill's infinite determinant method can be extended to systems with quasiperiodic coefficient matrices by balancing the Fourier coefficients of all emerging frequency peaks. This method was used for the stability analysis of the Mathieu equation, where the parametric excitation is composed of two periodic terms with irrational frequency ratio [162]. A quite similar approach was used for the stability analysis of milling with continuous spindle speed variation, where the nominal spindle rotation period and the speed variation period can become irrational [22].

In contrast to quasiperiodic coefficient matrices, in the case of chaotic dynamics of the nonlinear DDE Eq. (2.1) the Fourier transform is no longer discrete but rather continuous [99]. Since a chaotic signal can be interpreted as a periodic signal with an infinite period, an approximation of the Lyapunov exponents³ for chaotic signals is possible by assuming periodic coefficient matrices with a very large period. In this case a discrete spectrum appears and the known method for periodic systems presented in Sec. 5.2 can be used. In fact, the same approximation is done during the calculation of the Lyapunov exponents of chaotic systems with the standard method in the time domain [163], because the chaotic solution is calculated only in a finite time interval. For large periods the number of harmonics and therefore the size of the truncated matrix \mathbf{C}_∞ can become very large for obtaining accurate results. In this case one strategy is the fragmentation of the (infinitely) large period into smaller subintervals. For the evolution of the perturbations in the smaller subintervals a solution operator based on the Hill-Floquet method can be obtained (see Sec. 6.6). Then, the Lyapunov exponents can be calculated from the sequential application of the solution operator with the known QR-algorithm [163]. In

³Lyapunov exponents specify the relaxation rates of perturbations of a chaotic attractor. For a periodic solution they are equivalent to the real part of the Floquet exponents.

5. Frequency domain approach

the following frequency domain methods are only studied for time-invariant or periodic systems, because in this scenarios frequency domain methods are suitable.

5.3.4. Floquet exponents from D-subdivision

In principle, the numerical methods for the calculation of the D-curves can be also used to calculate the characteristic exponents $s_k = \lambda_k + i\omega_k$ if the real part λ_k is chosen as an additional parameter of the system. If all other parameters of the system are fixed there are two free variables, the real λ_k and the imaginary part ω_k of the characteristic exponents, and two equations, the real and the imaginary part of Eq. (5.14). Thus, a vanishing Hill's infinite determinant yields the discrete set of characteristic exponents of the DDE in the complex plane. However, for DDEs there are, in general, infinitely many characteristic exponents and it is difficult to find them from the numerical solution of Eq. (5.14). Moreover, the parameter range for the real part λ_0 of the most unstable eigenmode is not clear a priori. As a consequence, it is not clear if the most dominant exponents, i.e. the exponents with the largest real part are found from the numerical solution of the system of nonlinear equations Eq. (5.14). In Chapter 6, the Hill-Floquet method is introduced which can be used for a reliable and accurate calculation of the most dominant characteristic exponents of periodic time delay systems.

5.4. Summary

Different methods for the stability analysis of linear DDEs were presented in this chapter. On the one hand, there are time domain methods. For systems with periodic coefficients the time domain methods typically require the calculation of the solution operator over one period of the system and the stability is obtained from the eigenvalues of the solution operator. On the other hand, there are frequency domain methods based on the characteristic equation. The Hill's infinite determinant method represents a generalization of the frequency domain approach to periodic systems with an infinite dimensional characteristic Eq. (5.14). Frequency domain methods are very efficient for the calculation of stability charts because the stability can be obtained directly from the solution of an eigenvalue problem. However, at the moment no frequency domain method for the calculation of the Floquet multipliers of periodic DDEs can be found in the literature. A method, which fills this gap, is introduced in the next Chapter 6.

6. Hill-Floquet method

The calculation of Floquet exponents from Hill's infinite determinant Eq. (5.14) for systems with periodic coefficients is not suitable as discussed in Chapter 5. In fact, no strategy for the calculation of Floquet exponents from Hill's infinite determinant for time delay systems can be found in the literature. Here, a new method based on Hill's infinite determinant method is presented for the solution of this problem. It is called Hill-Floquet method because Hill's infinite determinant method and the Floquet decomposition of the solution is used to transform a finite dimensional time-periodic system to an infinite dimensional time-invariant system. As a result, after a truncation to a finite number of higher harmonics n , the standard methods for the analysis of autonomous DDEs can be used for the calculation of the Floquet exponents.

6.1. The Hill-Floquet transformation

The substitution of the Floquet ansatz Eq. (5.9) into the eigenmode decomposition Eq. (4.33) for linear DDEs with distributed delay yields

$$\mathbf{x}(t) = \sum_{k=-\infty}^{\infty} \mathbf{x}_k(t) c_k = \sum_{k=-\infty}^{\infty} \mathbf{p}_k(t) e^{s_k t} c_k. \quad (6.1)$$

The Hill's method, i.e. the Fourier expansion of the periodic part $\mathbf{p}_k(t)$ of the eigenmodes $\mathbf{x}_k(t)$, can be written as a matrix-vector product

$$\mathbf{p}_k(t) = \mathbf{F}^i(t) \mathbf{q}_{\infty,k}, \quad (6.2)$$

where the $N \times \infty$ -dimensional matrix $\mathbf{F}^i(t)$ is related to the inverse Fourier transform

$$\mathbf{F}^i(t) = (\dots, \mathbf{I} e^{-i\Omega t}, \mathbf{I}, \mathbf{I} e^{i\Omega t}, \dots). \quad (6.3)$$

The infinity dimensional vector $\mathbf{q}_{\infty,k}$ contains the infinitely many N -dimensional Fourier coefficients $\hat{\mathbf{p}}_{k,l}$ with $l = -\infty, \dots, \infty$ from Eq. (5.13) for the periodic part $\mathbf{p}_k(t)$ of the k th eigenmode of the periodic DDE

$$\mathbf{q}_{\infty,k} = (\dots, \hat{\mathbf{p}}_{k,-1}, \hat{\mathbf{p}}_{k,0}, \hat{\mathbf{p}}_{k,1}, \dots)^T. \quad (6.4)$$

Putting Eq. (6.2) in Eq. (6.1) leads to

$$\mathbf{x}(t) = \mathbf{F}^i(t) \mathbf{x}_{\infty}(t), \quad (6.5)$$

6. Hill-Floquet method

where the infinite dimensional configuration $\mathbf{x}_\infty(t)$ can be specified by

$$\mathbf{x}_\infty(t) = \sum_k \mathbf{x}_{\infty,k}(t) c_k = \sum_k \mathbf{q}_{\infty,k} e^{s_k t} c_k \in \mathbb{R}^\infty. \quad (6.6)$$

Whereas the Floquet decomposition Eq. (6.1) for a periodic DDE has the same dimension N compared to the eigenmode decomposition Eq. (4.33) of an autonomous DDE, for the periodic DDE the corresponding N -dimensional coefficient vector is time-dependent $\mathbf{p}_k(t)$, and therefore, the Floquet decomposition Eq. (6.1) is qualitatively different to the eigenmode decomposition Eq. (4.33). In contrast, Eq. (6.6) with the infinitely many time-invariant Fourier coefficients $\mathbf{q}_{\infty,k}$ of the periodic part $\mathbf{p}_k(t)$ has the same structure than the eigenmode expansion Eq. (4.33) of an autonomous DDE with infinite dimension. This means that the vector $\mathbf{x}_\infty(t)$ is the configuration of an infinite dimensional autonomous DDE, which is equivalent to the original N -dimensional periodic DDE Eq. (3.2). The infinite dimensional representation $\mathbf{x}_\infty(t)$ of the configuration $\mathbf{x}(t)$ is called Hill-Floquet representation and Eq. (6.5) specifies the transformation between the Hill-Floquet representation and the original representation of the configuration. In the following, the infinite dimensional autonomous DDE corresponding to the Hill-Floquet representation $\mathbf{x}_\infty(t)$ is derived.

If Eq. (6.5) is substituted in the linearized DDE Eq. (3.2), the time delay system is given in terms of the Hill-Floquet representation $\mathbf{x}_\infty(t)$ of the configuration as

$$\dot{\mathbf{F}}^i(t) \mathbf{x}_\infty(t) + \mathbf{F}^i(t) \dot{\mathbf{x}}_\infty(t) = \mathbf{A}(t) \mathbf{F}^i(t) \mathbf{x}_\infty(t) + \int_0^{\tau_{\max}} d\tau \mathbf{B}(t) \mathbf{K}(\tau) \mathbf{F}^i(t-\tau) \mathbf{x}_\infty(t-\tau). \quad (6.7)$$

From Fourier analysis it is known that the time derivative and the time shift of the matrix $\mathbf{F}^i(t)$ can be expressed as

$$\dot{\mathbf{F}}^i(t) = \mathbf{F}^i(t) \mathbf{D}_F, \quad \mathbf{F}^i(t-\tau) = \mathbf{F}^i(t) \mathbf{S}_F(\tau), \quad (6.8)$$

where the matrices \mathbf{D}_F and $\mathbf{S}_F(\tau)$ are block diagonal matrices that contain the matrix blocks $\mathbf{I} i l \Omega$ and $\mathbf{I} e^{-i l \Omega \tau}$ with $l = -\infty, \dots, \infty$ on their main diagonal, respectively. Moreover, from the convolution theorem the following relationship can be derived

$$\mathbf{A}(t) \mathbf{F}^i(t) = \mathbf{F}^i(t) \mathbf{A}_F, \quad \mathbf{B}(t) \mathbf{K}(\tau) \mathbf{F}^i(t) = \mathbf{F}^i(t) \mathbf{B}_F(\tau), \quad (6.9)$$

where the matrices \mathbf{A}_F and $\mathbf{B}_F(\tau)$ are called the Hill-Floquet representation of the

coefficient matrices $\mathbf{A}(t)$ and $\mathbf{B}(t)\mathbf{K}(\tau)$, and are specified by

$$\mathbf{A}_F = \begin{pmatrix} \ddots & \vdots & \vdots & \vdots & \ddots \\ \cdots & \hat{\mathbf{A}}_0 & \hat{\mathbf{A}}_{-1} & \hat{\mathbf{A}}_{-2} & \cdots \\ \cdots & \hat{\mathbf{A}}_1 & \hat{\mathbf{A}}_0 & \hat{\mathbf{A}}_{-1} & \cdots \\ \cdots & \hat{\mathbf{A}}_2 & \hat{\mathbf{A}}_1 & \hat{\mathbf{A}}_0 & \cdots \\ \ddots & \vdots & \vdots & \vdots & \ddots \end{pmatrix}, \quad \text{and} \quad (6.10)$$

$$\mathbf{B}_F(\tau) = \begin{pmatrix} \ddots & \vdots & \vdots & \vdots & \ddots \\ \cdots & \hat{\mathbf{B}}_0\mathbf{K}(\tau) & \hat{\mathbf{B}}_{-1}\mathbf{K}(\tau) & \hat{\mathbf{B}}_{-2}\mathbf{K}(\tau) & \cdots \\ \cdots & \hat{\mathbf{B}}_1\mathbf{K}(\tau) & \hat{\mathbf{B}}_0\mathbf{K}(\tau) & \hat{\mathbf{B}}_{-1}\mathbf{K}(\tau) & \cdots \\ \cdots & \hat{\mathbf{B}}_2\mathbf{K}(\tau) & \hat{\mathbf{B}}_1\mathbf{K}(\tau) & \hat{\mathbf{B}}_0\mathbf{K}(\tau) & \cdots \\ \ddots & \vdots & \vdots & \vdots & \ddots \end{pmatrix},$$

where $\hat{\mathbf{A}}_k$ and $\hat{\mathbf{B}}_k$ are the Fourier coefficients of the periodic matrices $\mathbf{A}(t)$ and $\mathbf{B}(t)$ from Eq. (5.13), respectively. If Eq. (6.8) and Eq. (6.9) are substituted in Eq. (6.7) the linearized DDE Eq. (3.2) can be written as

$$\mathbf{F}^i(t) \left(\dot{\mathbf{x}}_\infty(t) - (\mathbf{A}_F - \mathbf{D}_F) \mathbf{x}_\infty(t) - \int_0^{\tau_{\max}} d\tau \mathbf{B}_F(\tau) \mathbf{S}_F(\tau) \mathbf{x}_\infty(t - \tau) \right) = \mathbf{0}. \quad (6.11)$$

In Eq. (6.11) the periodic part of the configuration and the periodic part of the coefficients remains only in the term $\mathbf{F}^i(t)$ related to the inverse Fourier transform. By balancing the Fourier coefficients in Eq. (6.11), the infinite dimensional autonomous DDE corresponding to the eigenmode expansion Eq. (6.6) can be obtained as

$$\dot{\mathbf{x}}_\infty(t) = \mathbf{A}_\infty \mathbf{x}_\infty(t) + \int_0^{\tau_{\max}} d\tau \mathbf{B}_\infty(\tau) \mathbf{x}_\infty(t - \tau), \quad (6.12)$$

where the time-invariant coefficient matrices are defined by $\mathbf{A}_\infty = \mathbf{A}_F - \mathbf{D}_F$ equivalent to Eq. (5.16) and $\mathbf{B}_\infty(\tau) = \mathbf{B}_F(\tau) \mathbf{S}_F(\tau)$. The infinite dimensional autonomous DDE Eq. (6.12) contains the complete information of the original DDE Eq. (3.2) with periodic coefficients. In the rest of this thesis, Eq. (6.12) will be called Hill-Floquet representation of the original DDE Eq. (3.2) or simply Hill-Floquet representation. The configuration $\mathbf{x}(t)$ of the original system $\mathbf{x}(t)$ can be obtained from the solution of the Hill-Floquet representation $\mathbf{x}_\infty(t)$ by applying the inverse Hill-Floquet transformation Eq. (6.5).

The difference between the original representation Eq. (3.2) with periodic coefficients and the higher dimensional Hill-Floquet representation Eq. (6.12) with constant coefficients is, that the Hill-Floquet representation describes the periodic part $\mathbf{p}_k(t)$ of the eigenmodes in terms of its time-invariant Fourier coefficients \mathbf{q}_k according to Eq. (6.6). As a consequence, the time evolution of the Hill-Floquet representation $\mathbf{x}_\infty(t)$ with the Fourier expanded periodic part of the eigenmodes can be described by the autonomous

6. Hill-Floquet method

DDE Eq. (6.12). In other words, in Eq. (6.12) the periodic part of the solution of the original linearized system Eq. (3.2) is expanded in a Fourier series, but the exponential behavior of the eigenmodes $e^{s_k t}$ is still described in the time domain by an autonomous DDE. In other words, the Hill-Floquet transformation is equivalent to a separate Fourier transform of the periodic part $\mathbf{p}_k(t)$ of the eigenmodes $\mathbf{x}_k(t)$, whereas the exponential behavior of the solution remains unchanged. Please note that this is not equivalent to the Fourier transform to the original linearized DDE Eq. (3.2) because in this case the exponential part of the solution is not separated from the dynamics. In fact, in general the Hill-Floquet transformation can be obtained as described in this section. At first, the original configuration $\mathbf{x}(t)$ is expressed in terms of its Hill-Floquet transformation $\mathbf{x}_\infty(t)$ via Eq. (6.5). Secondly, the properties of the Fourier transform, given in Eq. (6.8) and Eq. (6.9), are used to obtain a relationship equal to Eq. (6.11). Then, the Hill-Floquet transformation can be obtained by balancing the Fourier coefficients in Eq. (6.11), which results in the infinite dimensional Hill-Floquet representation Eq. (6.12).

If one eigenmode $\mathbf{x}_{\infty,k}(t) = \mathbf{q}_{\infty,k} e^{s_k t}$ is substituted into the Hill-Floquet representation Eq. (6.12) the following eigenvalue equation is obtained

$$s_k \mathbf{q}_{\infty,k} = (\mathbf{A}_\infty + \bar{\mathbf{B}}_\infty(s_k)) \mathbf{q}_{\infty,k}, \quad (6.13)$$

where $\bar{\mathbf{B}}_\infty(s_k)$ is the Laplace transform of the matrix $\mathbf{B}_\infty(\tau)$. In particular, Eq. (6.13) is the eigenvalue problem corresponding to the characteristic Eq. (5.14) with the infinite Hill matrix \mathbf{C}_∞ defined in Eq. (5.15). Thus, the Hill-Floquet representation Eq. (6.12) is an infinite dimensional DDE with distributed delay and time-invariant coefficients matrices with a characteristic equation similar to Hill's infinite determinant Eq. (5.14).

If no delay appears, i.e. $\mathbf{B}(t) = \mathbf{0}$, the eigenvalue equation for the non-autonomous ODE simplifies to

$$s_k \mathbf{q}_{\infty,k} = \mathbf{A}_\infty \mathbf{q}_{\infty,k}, \quad (6.14)$$

with the characteristic equation

$$\det(\mathbf{I}s_k - \mathbf{A}_\infty) = 0. \quad (6.15)$$

Note that the characteristic equation Eq. (6.15) of the delay-free Hill-Floquet representation is also known as central equation in solid state physics [79]. In this application, t is a location on a lattice, the principal period T and frequency Ω are the lattice constant and the reciprocal lattice constant, respectively, the eigenvalues s_k are related to the energy eigenvalues, the eigenvector \mathbf{q}_k contains the Fourier coefficients of the wavefunction, and the matrix \mathbf{A}_∞ contains the Fourier coefficients of a periodic potential.

Eq. (6.12) with the nonlinear eigenvalue problem Eq. (6.13) is a bi-infinite dimensional system. On the one hand, the system is infinite dimensional due to the delay term and on the other hand the coefficient matrices are infinite dimensional. Even, the Hill-Floquet representation for the delay-free case with the linear eigenvalue problem Eq. (6.14) is infinite dimensional due to the infinite dimension of the coefficient matrix \mathbf{A}_∞ . In practice, a finite dimensional approximation of the coefficient matrices in the Hill-Floquet representation Eq. (6.12) is considered. If n higher harmonics are used for the Fourier

expansion \mathbf{q}_k of the periodic part $\mathbf{p}_k(t)$ of the eigenmodes, the coefficient matrices \mathbf{A}_∞ and $\mathbf{B}_\infty(\tau)$ in the truncated system are $N(2n+1) \times N(2n+1)$ dimensional. A similar truncation is already described in Sec. 5.3 for the calculation of stability charts from the Hill's infinite determinant. A rough estimate for the number of eigenmodes, which are necessary for an accurate description of the original dynamics can be obtained by following the argumentation in Sec. 5.3, that is either the interval $[-n\Omega, n\Omega]$ covers all dominant eigenfrequencies of the system or only the Fourier coefficients around the dominant eigenfrequencies of the system are considered. Moreover it is shown in the following section that the redundant nature of the Hill-Floquet representation can be used to check the accuracy of a finite dimensional approximation of Eq. (6.12).

6.2. Non-uniqueness of the Hill-Floquet transformation

The Hill-Floquet transformation is not bijective. This can be seen already in the discrepancy of the dimension of the original representation Eq. (3.2) and the Hill-Floquet representation Eq. (6.12). In fact, the inverse Hill-Floquet transformation Eq. (6.5) that transforms the configuration $\mathbf{x}_\infty(t)$ from the Hill-Floquet representation to the configuration $\mathbf{x}(t)$ in the original representation is surjective. In other words, there are various possibilities for the vector $\mathbf{x}_\infty(t)$ specifying one and the same configuration $\mathbf{x}(t)$ via the transformation given by Eq. (6.5). This can be understood by considering one eigenmode $\mathbf{x}_k(t)$ of the original system. Due to the non-uniqueness of the Floquet exponents, there are infinitely many different possibilities for the Floquet decomposition of this eigenmode

$$\mathbf{x}_k(t) = \mathbf{p}_k(t)e^{s_k t} = \mathbf{p}_{k,l}(t)e^{s_{k,l} t}, \quad (6.16)$$

where the corresponding Floquet exponents and eigenvectors are defined as $s_{k,l} = s_k + il\Omega$ and $\mathbf{p}_{k,l}(t) = \mathbf{p}_k(t)e^{-il\Omega t}$ with $l \in \mathbb{Z}$, respectively. In particular, an additional coefficient in the periodic part can be compensated by a shift in the imaginary part of the Floquet exponents. Note that, indeed, the Floquet exponents are not unique but the Floquet multipliers $e^{s_{k,l}T}$ corresponding to the Floquet exponents with fixed k but varying l are unique

$$e^{s_{k,l}T} = e^{(s_k + il\Omega)T} = e^{s_k T}. \quad (6.17)$$

In Eq. (6.17) $s_k = s_{k,0}$ are called the N reference Floquet exponents with an imaginary part ω_k in the reference interval $\omega_k \in [-\Omega/2, \Omega/2)$. All redundant exponents corresponding to the k th Floquet multiplier have the same real part λ_k but their imaginary part is shifted by a multiple of the basic frequency Ω . In solid state physics, where the period T is equal to the lattice constant of a one dimensional lattice, and Ω is the reciprocal lattice constant, the reference interval $[-\Omega/2, \Omega/2)$ is the first Brillouin zone [79, 80].

In the original system the direction of the eigenvectors $\mathbf{p}_{k,l}(t)$ does not depend on l . In contrast, this property does no longer hold for the eigenvectors $\mathbf{q}_{\infty,k,l}$ with fixed k but varying l in the Hill-Floquet representation corresponding to different representations $\mathbf{p}_{k,l}(t)$ of the periodic part $\mathbf{p}_k(t)$. In fact, if $\mathbf{q}_{\infty,k} = \text{col}(\dots, \hat{\mathbf{p}}_{k,-n}, \dots, \hat{\mathbf{p}}_{k,n}, \dots)$ is an eigenvector in the Hill-Floquet representation associated with a reference Floquet exponent s_k , then also the vector $\mathbf{q}_{\infty,k,l} = \text{col}(\dots, \hat{\mathbf{p}}_{k,-n+l}, \dots, \hat{\mathbf{p}}_{k,n+l}, \dots)$, where the entries

6. Hill-Floquet method

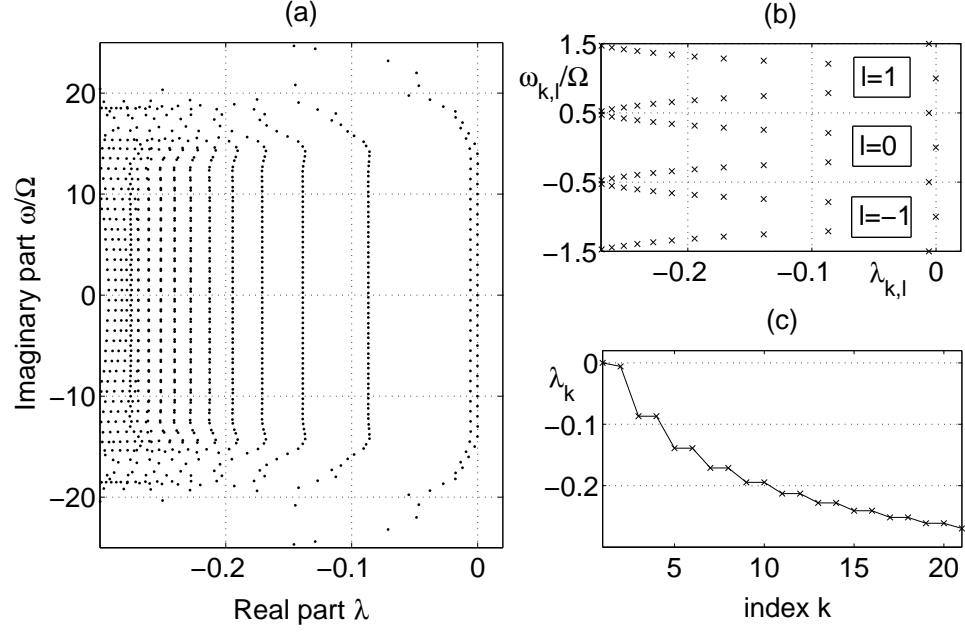


Figure 6.1.: a) Floquet exponents $\lambda_{k,l}$ for a limit cycle of the DDE Eq. (6.19) calculated from a truncated version of the Hill-Floquet system Eq. (6.12). b) Reference Floquet exponents in the first Brillouin zone ($l = 0$) and redundant exponents in the neighboring Brillouin zones ($l = \pm 1$). c) Real part λ_k of the reference Floquet exponents (Lyapunov spectrum).

are shifted by l positions, is an eigenvector of the system associated with the Floquet exponent $s_{k,l}$. This relationship can be derived from the characteristic Eq. (6.13) and the specific structure of the matrices \mathbf{A}_∞ and $\mathbf{B}_\infty(\tau)$ and follows from the fact that the vector $\mathbf{q}_{\infty,k,l}$ contains the Fourier coefficients of the periodic function $\mathbf{p}_{k,l}(t)$. A similar relation holds for the left eigenvectors $\mathbf{d}_{\infty,k,l}^T$ defined by the eigenvalue equation

$$s_{k,l} \mathbf{d}_{\infty,k,l}^T = \mathbf{d}_{\infty,k,l}^T (\mathbf{A}_\infty + \bar{\mathbf{B}}_\infty(s_k)), \quad (6.18)$$

which are also shifted versions of some reference left eigenvectors $\mathbf{d}_{\infty,k}^T = \mathbf{d}_{\infty,k,0}^T$. Since, the eigenvectors $\mathbf{q}_{\infty,k,l}$ corresponding to one reference Floquet exponent with fixed k but varying l does not point to the same direction, the redundant Floquet exponents $s_{k,l}$ and eigenvectors $\mathbf{q}_{\infty,k,l}$ appear as separate eigenvalues and eigenvectors in the Hill-Floquet representation. This means, that the eigenvalue problem Eq. (6.13) of the Hill-Floquet representation reveals infinitely many reference Floquet exponents s_k in the first Brillouin zone because of the transcendental structure of the equation, and in addition, infinitely many redundant Floquet exponents $s_{k,l}$, $-\infty < l < \infty$ associated with one and the same reference Floquet exponent s_k .

If a finite number n of higher harmonics are taken into account, an $N(2n+1)$ dimensional approximation of the Hill-Floquet system can be obtained, which means that, in

6.2. Non-uniqueness of the Hill-Floquet transformation

practice, not infinitely many redundant exponents can be calculated. In fact, most of the numerical methods for the calculation of the Floquet exponents can be interpreted as a polynomial approximation of the Laplace transform of the coefficient matrix $\bar{\mathbf{B}}_\infty(s_k)$, which results only in a finite number of reference Floquet exponents s_k . For the illustration of the two finite dimensional approximations of the bi-infinite dimensional system Eq. (6.12), the characteristic exponents for a periodic solution of a nonlinear DDE Eq. (2.1) were calculated numerically from the truncated Hill-Floquet representation Eq. (6.12) with n harmonics by using the Chebyshev collocation method, which is presented in Sec. 6.3. In particular, the Mackey-Glass equation was used for the calculation [1]

$$\dot{u}(t) = \frac{\alpha u(t - \tau_0)}{1 + u(t - \tau_0)^\gamma} - \beta u(t). \quad (6.19)$$

The parameters $\alpha = 0.2$, $\beta = 0.1$ and $\gamma = 10$ were taken from [164]. For the discrete delay $\tau_0 = 12$ the attractor of Eq. (6.19) is a limit cycle, and the corresponding Floquet exponents for $n = 50$ higher harmonics are shown in Fig. 6.1. In Fig. 6.1a it can be seen that there are bands of Floquet exponents with the same real part generated by the redundant exponents. In particular, the redundant Floquet exponents with large positive or large negative imaginary parts ($|l| > 15$) are disturbed by finite size effects of the matrix truncation. Nevertheless, as can be seen in Fig. 6.1b, the redundant exponents around the first Brillouin zone, i.e. around the interval $[-\Omega/2, \Omega/2)$, are nearly perfect copies of the reference Floquet exponents s_k shifted parallel to the imaginary axis by multiples of the frequency Ω . The real part of the reference exponents, i.e. the Lyapunov spectrum for the limit cycle, is shown in Fig. 6.1c.

The redundant Floquet exponents can be used to check whether the number n of higher harmonics is large enough for an accurate approximation of the periodic part $\mathbf{p}_k(t)$ of the eigenmodes. A band of Floquet exponents $s_{k,l}$ similar to the bands in Fig. 6.1a with redundant exponents with the same real part means that the corresponding eigenvectors $\mathbf{q}_{k,l}$, which are shifted versions of each other, are not disturbed by the matrix truncation. In this case, the entries of the vectors $\mathbf{q}_{k,l}$ at the boundaries, i.e. the Fourier coefficients $\hat{\mathbf{p}}_{k,-n}$ and $\hat{\mathbf{p}}_{k,n}$ for the n th harmonics, are approximately zero. Thus, if there are more than one Floquet exponents with the same real part λ_k around the first Brillouin zone, the number n of higher harmonics is large enough for an accurate approximation of the corresponding reference Floquet exponent s_k .

As a consequence of the redundant nature of the Hill-Floquet representation, there are also $(2n+1)$ linear independent possibilities for the presentation of a specific configuration $\mathbf{x}(t)$ of the original system

$$\mathbf{x}_\infty(t) = \mathbf{F}_l(t)\mathbf{x}(t), \quad -n \leq l \leq n. \quad (6.20)$$

Eq. (6.20) can be used, for example, to specify the initial function $\mathbf{x}_\infty(t)$ of the Hill-Floquet representation Eq. (6.12), which is equivalent to a specific initial function $\mathbf{x}(t)$ of the original non-autonomous linear DDE Eq. (3.2) with $t \leq 0$. For example, the matrices $\mathbf{F}_l(t)$ can be given by

$$\mathbf{F}_l(t) = \left(\dots, \mathbf{0}, \mathbf{I}e^{-il\Omega t}, \mathbf{0}, \dots \right)^T, \quad (6.21)$$

6. Hill-Floquet method

which means that the l th block of the matrix $\mathbf{F}_l(t)$ is the inverse of the l th block of the matrix $\mathbf{F}^i(t)$ in Eq. (6.3), and all the other blocks are zero. Alternatively, any scaled linear combination of the matrices $\mathbf{F}_l(t)$ can be used for a transformation of the configuration $\mathbf{x}(t)$ from the original representation to the Hill-Floquet representation $\mathbf{x}_\infty(t)$. For example, an alternative transformation can be given by

$$\mathbf{x}_\infty(t) = \frac{1}{2n+1} \sum_{l=-n}^n \mathbf{F}_l(t) \mathbf{x}(t). \quad (6.22)$$

Note that the inverse Hill-Floquet transformation Eq. (6.5) of Eq. (6.20) does always yield the original vector $\mathbf{x}(t)$, whereas the opposite is not true, i.e.

$$\mathbf{F}^i(t) \mathbf{F}_l(t) = \mathbf{I}, \quad \text{but} \quad \mathbf{F}_l(t) \mathbf{F}^i(t) \neq \mathbf{I}. \quad (6.23)$$

Eq. (6.23) is a direct consequence of the redundant nature of the Hill-Floquet representation. In other words, different matrices $\mathbf{F}_l(t)$ can be used to obtain a Hill-Floquet representation $\mathbf{x}_\infty(t)$ of the configuration $\mathbf{x}(t)$. After applying the inverse Hill-Floquet transformation $\mathbf{F}^i(t)$ always the same configuration $\mathbf{x}(t)$ in the original representation will be obtained. On the other hand, if the inverse Hill-Floquet transformation $\mathbf{F}^i(t)$ is applied at first on the configuration $\mathbf{x}_\infty(t)$ in the Hill-Floquet representation, some information on the specific structure of the Fourier coefficients is lost and the information can, in general, not be recovered by a multiplication with a matrix $\mathbf{F}_l(t)$ from Eq. (6.20). Nevertheless, since the Hill-Floquet representation contains the redundant eigenvalues and eigenvectors, the specific structure of the Fourier coefficients in the configuration $\mathbf{x}_\infty(t)$ is not important for the dynamics in the original system. As a consequence, an arbitrary matrix $\mathbf{F}_l(t)$ can be used, for example, for specifying the initial condition in the Hill-Floquet representation.

6.3. Chebyshev expansion of the Hill-Floquet system

In general, an arbitrary method can be used for the analysis of the autonomous Hill-Floquet representation Eq. (6.12). There are many established methods for the calculation of the characteristic exponents s_k and the corresponding eigenvectors \mathbf{q}_k for autonomous DDEs. Some of them are listed in Sec. 5.1. In this thesis, a very efficient collocation method is presented for the analysis of the Hill-Floquet representation Eq. (6.12), which can be used for an arbitrary DDE with time-invariant coefficients [54, 165]. In this section, the method is also used to demonstrate some properties of the Hill-Floquet representation and to get more insight into the Hill-Floquet method.

Collocation methods for the analysis of time delay systems can be interpreted as an approximation of a DDE by a higher dimensional ODE. In particular, the vector $\mathbf{z}_\infty(t)$ is used to approximate the state of the Hill-Floquet representation Eq. (6.12) by the storing the configuration $\mathbf{x}_\infty(t - \tau)$ at the discrete nodes τ_j , $j = 1, \dots, M$ with $\tau_1 = 0$, $\tau_{j+1} > \tau_j$ and $\tau_M = \tau_{\max}$ as

$$\mathbf{z}_\infty(t) = (\mathbf{x}_\infty(t - \tau_1), \dots, \mathbf{x}_\infty(t - \tau_M))^T \quad (6.24)$$

6.3. Chebyshev expansion of the Hill-Floquet system

Specifically, the $N(2n + 1)M$ dimensional vector $\mathbf{z}_\infty(t)$ contains the $2n + 1$ Fourier coefficients of dimension N at M different collocation points. With Eq. (6.24) the past configurations $\mathbf{x}_\infty(t - \tau)$ of the autonomous DDE Eq. (6.12) can be expressed in terms of the present configuration $\mathbf{z}_\infty(t)$ of the higher dimensional system. With a discrete $M - 1 \times M$ -dimensional differentiation matrix \mathbf{D}_M that depends on the choice of the collocation points and the specific differentiation scheme the autonomous DDE Eq. (6.12) can be approximated by the autonomous ODE

$$\dot{\mathbf{z}}_\infty(t) = \mathbf{H}_\infty \mathbf{z}_\infty(t) = \begin{pmatrix} \mathbf{A}_\infty & \int_{\tau_1}^{\tau_2} \mathbf{B}_\infty(\tau) d\tau & \cdots & \int_{\tau_{M-1}}^{\tau_M} \mathbf{B}_\infty(\tau) d\tau \\ & \mathbf{D}_M \otimes \mathbf{I}_{N(2n+1)} & & \end{pmatrix} \mathbf{z}_\infty(t). \quad (6.25)$$

The matrix blocks in the first row of the coefficient matrix in Eq. 6.25 are $N(2n + 1) \times N(2n + 1)$ dimensional, whereas the Kronecker product $\mathbf{D}_M \otimes \mathbf{I}_{N(2n+1)}$ in the second row results in a $(M - 1)N(2n + 1) \times MN(2n + 1)$ dimensional matrix block. A suitable choice for the collocation points are the Chebyshev nodes with the Chebyshev spectral differentiation matrix \mathbf{D}_M [166]. In this case the dominant characteristic exponent s_k of the autonomous DDE Eq. (6.12) can be approximated very accurately by the eigenvalues of the matrix \mathbf{H}_∞ [54]. Note that Eq. (6.25) can be interpreted as a discretization of the PDE representation Eq. (2.19) of the DDE. The first block row of dimension $N(2n + 1) \times N(2n + 1)M$ corresponds to the boundary condition equivalent to Eq. (6.12) and the last block row of dimension $N(2n + 1)(M - 1) \times N(2n + 1)M$ corresponds to the PDE Eq. (2.19).

In Fig. 6.2 the convergence of the Hill-Floquet method for the Floquet exponents of the limit cycle of the Mackey-Glass Eq. (6.19) is shown. The parameters are equal to Fig. 6.1, that is, the discrete delay $\tau_0 = 12$ is used and the other parameters are taken from [164]. The convergence of the real part λ_0 of the most dominant Floquet exponent for increasing n is shown in Fig. 6.2a. It can be seen that the real part converges exponentially with an increasing number of higher harmonics n , whereas an increasing number of the Chebyshev nodes from $M = 5$ (red crosses) to $M = 10$ (black solid) does not increase the accuracy. In fact, the results for $M = 5$ are better than for $M = 10$. In Fig. 6.2b the convergence of the real part of the other Floquet exponents is shown. A reference spectrum was calculated for $n = 200$ and $M = 20$ (black solid). For $n = 20$ and $M = 10$ (blue solid) roughly ten exponents are converged to the reference spectrum. Letting n constant and increasing the number of Chebyshev nodes to $M = 20$ (blue circles) does not change the number of converged exponents. However, for an increasing number of higher harmonics to $n = 40$ with $M = 10$ (red solid) nearly twenty exponents are converged to the reference spectrum. Again a further duplication of the number of Chebyshev nodes to $M = 20$ (red circles) does not change the spectrum significantly. This means that, in general, a further increase of the quality of the approximation of the eigenmodes $\mathbf{x}_k(t)$ and the Floquet exponents s_k is only possible by increasing the number of higher harmonics n , which increases the accuracy of the approximation of the periodic part $\mathbf{p}_k(t)$ of the eigenmodes. This is analyzed in more detail below in Fig. 6.3, where one can see that, indeed, the approximation of the Floquet exponents and eigenmodes

6. Hill-Floquet method

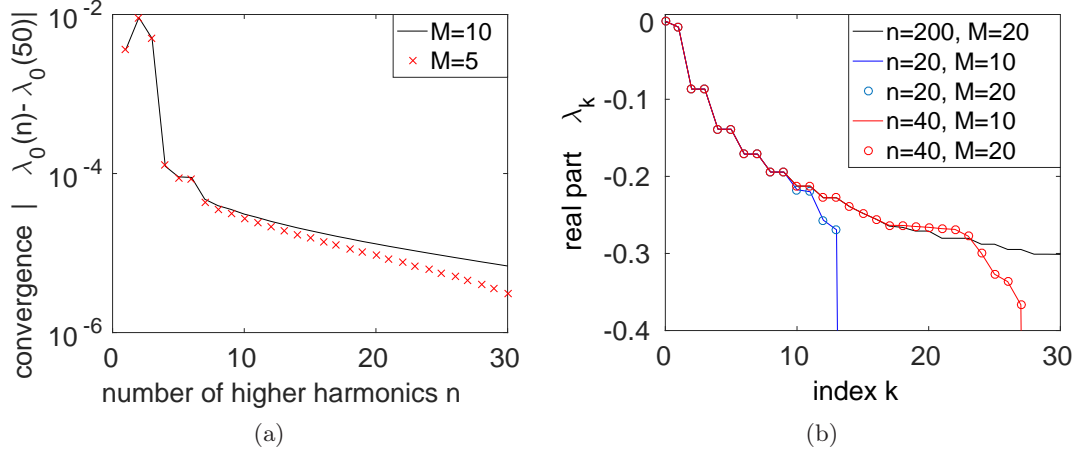


Figure 6.2.: a) Spectral convergence of the maximum Lyapunov exponent λ_0 of a periodic DDE for increasing number of higher harmonics n . The convergence does not significantly depend on the number of Chebyshev nodes M . b) The convergence of the other exponents λ_k with $k > 0$ can be increased by increasing the number of higher harmonics n , whereas increasing M has no significant influence.

of the DDE is limited by the accuracy of the Fourier expansion for the periodic part of the eigenmodes. As a result, a small number of Chebyshev nodes ($5 \leq M \leq 10$) is sufficient for the accurate approximation of the Floquet exponents s_k .

Another important point in Fig. 6.2b is the fact, that the maximum number of converged reference exponents for the Mackey-Glass equation, which is a scalar DDE ($N = 1$), is not limited to the number M of Chebyshev nodes. For example, for the red solid curve with $n = 40$ and $M = 10$ more than ten exponents are converged to the reference spectrum. From the theory in Sec. 6.2 one might deduce that the number M of Chebyshev nodes is a limit for the maximum number of the converged reference Floquet exponents s_k of the infinite dimensional DDE, and, in addition, $2n + 1$ redundant exponents with the same real part λ_k with $k = 1, \dots, M$ appear. However, in practice, in finite dimensional approximations of infinite dimensional systems, the eigenfunctions with the lowest frequencies are approximated best by the finite dimensional approximation. Indeed, in the Hill-Floquet representation the frequency components of the periodic part $\mathbf{p}_{k,l}(t)$ of the redundant eigenmodes corresponding to one reference Floquet exponent is shifted to higher values for increasing l as shown in Sec. 6.2. As a consequence, there are some reference eigenvectors $\mathbf{q}_{\infty,k}$ and corresponding eigenvalues s_k with $k > M$, which are well-approximated by the Fourier expansion, whereas some redundant eigenvectors $\mathbf{q}_{\infty,k,l}$ and exponents $s_{k,l}$ with $k < M$ but $l \gg 0$ cannot be well-approximated by the truncated Fourier series. Thus, with the Hill-Floquet method the finite number of converged exponents is not limited by the number of Chebyshev nodes M .

The eigenvectors $\mathbf{q}_{\infty,k}$ in Eq. (6.13) determine the periodic part of the eigenmode

$\mathbf{p}_k(t)$ via the relationship Eq. (6.2). The eigenmodes $\mathbf{x}_{\infty,k}(t)$ are typically complex. In nonlinear dynamics, the real parts $\text{Re}(\mathbf{x}_{\infty,k}(t))$ of the eigenmodes are equivalent to the covariant Lyapunov vectors of the dynamical system [167, 168]. The exponential part of the eigenmodes is determined by the Floquet exponents. The periodic part $\mathbf{p}_k(t)$ can be calculated from the eigenvectors \mathbf{h}_k of the matrix \mathbf{H}_∞

$$\mathbf{h}_{\infty,k} = \text{col}(\mathbf{q}_{\infty,k}, \mathbf{q}_{\infty,k}e^{-s_k\tau_2}, \dots, \mathbf{q}_{\infty,k}e^{-s_k\tau_M}). \quad (6.26)$$

The structure of the eigenvectors $\mathbf{h}_{\infty,k}$ in Eq. (6.26) follows immediately from Eq. (6.6) and the definition of $\mathbf{z}_\infty(t)$ in Eq. (6.24). The periodic part of the eigenmodes $\mathbf{p}_k(t)$ in the original representation can be calculated from the eigenvector $\mathbf{h}_{\infty,k}$ as

$$\mathbf{p}_{k,j}(t) = \mathbf{F}^i(t)\mathbf{h}_{\infty,k,j}e^{s_k\tau_j} = \mathbf{p}_k(t), \quad j = 1, \dots, M, \quad (6.27)$$

where $\mathbf{h}_{\infty,k,j} = \mathbf{q}_{\infty,k}e^{-s_k\tau_j}$ is related to the Fourier coefficients, which are stored at the j th Chebyshev node. Thus, in the matrix \mathbf{H}_∞ not only a redundancy due to the non-uniqueness of the Floquet exponent $s_{k,l}$ appears, but also an additional redundancy due to the Chebyshev expansion appears. In particular, the eigenvector $\mathbf{h}_{\infty,k}$ contains the k th eigenvector $\mathbf{q}_{\infty,k}$ of the Hill-Floquet representation at M different Chebyshev nodes $t - \tau_j$, $j = 1, \dots, M$. The redundant information can be used to verify the accuracy of the Chebyshev collocation method for the Hill-Floquet representation Eq. (6.12).

In Fig. 6.3 the periodic part $\mathbf{p}_{k,j}(t)$ of the eigenmodes for the Mackey-Glass equation with the same parameters as in Fig. 6.2 is shown for two different numbers of higher harmonics, $n = 20$ (blue) and $n = 40$ (red). It is assumed that for $n = 40$ the considered reference eigenvectors $\mathbf{q}_{\infty,9}$ and $\mathbf{q}_{\infty,10}$ are very close to the exact eigenvectors because for $n = 40$ higher harmonics the Floquet exponents s_9 and s_{10} are converged to the reference spectrum in Fig. 6.2b. The deviations in the periodic part of the eigenmodes in Fig. 6.3a for $k = 9$ are moderate but increase significantly for $k = 10$ in Fig. 6.3b. As a consequence, the eigenvalues s_k with $k \geq 10$ in Fig. 6.2b are not well-approximated by the Hill-Floquet method with $n = 20$ higher harmonics. In contrast, the deviations between the periodic part $\mathbf{p}_{k,j}(t)$, calculated at two different Chebyshev nodes $j = 1$ and $j = M$ for $k = 9$ and $k = 10$, are by orders of magnitude smaller as can be seen in Fig. 6.3c and Fig. 6.3d, respectively. This means that the exponential part of the eigenmodes is approximated very well for $M = 10$, whereas the approximation of the periodic part of the eigenmodes by a truncated Fourier series with n harmonics limits the accuracy of the finite dimensional approximation of the bi-infinite dimensional system Eq. (6.12).

6.4. The alternative method

An alternative possibility for obtaining an autonomous ODE from a periodic DDE is, at first, the approximation of the original N dimensional periodic DDE Eq. (3.2) by an NM dimensional periodic ODE via the Chebyshev expansion

$$\dot{\tilde{\mathbf{z}}}(t) = \tilde{\mathbf{H}}(t)\tilde{\mathbf{z}}(t) = \begin{pmatrix} \mathbf{A}(t) & \mathbf{B}(t) \int_{\tau_1}^{\tau_2} \mathbf{K}(\tau) d\tau & \dots & \mathbf{B}(t) \int_{\tau_{M-1}}^{\tau_M} \mathbf{K}(\tau) d\tau \\ & & & \mathbf{D}_M \otimes \mathbf{I}_N \end{pmatrix} \tilde{\mathbf{z}}(t). \quad (6.28)$$

6. Hill-Floquet method

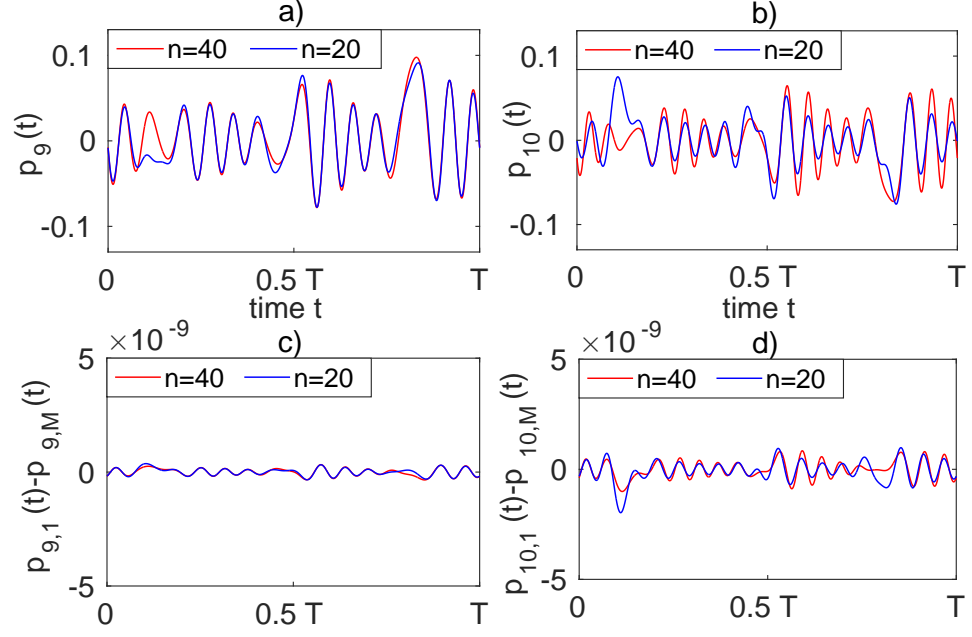


Figure 6.3.: The difference between the periodic part $\mathbf{p}_k(t)$ for $n = 20$ (blue) and $n = 40$ (red) higher harmonics increases significantly from a) $k = 9$ to b) $k = 10$, which leads to the deviations in the spectrum in Fig. 6.2b. In contrast, the tiny difference between the periodic part $\mathbf{p}_{k,j}(t)$ at two different Chebyshev nodes $j = 1$ and $j = M$ for the same eigenvectors a) $k = 9$ and d) $k = 10$ shows that the exponential part of the eigenmodes is accurately approximated for $M = 10$ Chebyshev nodes.

Now, in the first row of the coefficient matrix in Eq. 6.28 the matrix blocks are $N \times N$ dimensional, whereas the Kronecker product $\mathbf{D}_M \otimes \mathbf{I}_N$ in the second row results in a $(M - 1)N \times MN$ dimensional matrix block. In Eq. (6.28) the state \mathbf{x}_t of the original representation in one delay interval is approximated by the configurations of the system at the M Chebyshev nodes

$$\tilde{\mathbf{z}}(t) = (\mathbf{x}(t - \tau_1), \dots, \mathbf{x}_M(t - \tau_M))^T. \quad (6.29)$$

After that the Hill-Floquet transformation can be applied to the ODE Eq. (6.28) with the periodic coefficient matrix $\tilde{\mathbf{H}}(t) = \tilde{\mathbf{H}}(t + T)$, which results in the $NM(2n + 1)$ dimensional system

$$\dot{\tilde{\mathbf{z}}}_\infty(t) = \tilde{\mathbf{H}}_\infty \tilde{\mathbf{z}}_\infty(t) = \begin{pmatrix} \ddots & \vdots & \vdots & \vdots & \ddots \\ \cdots & \hat{\mathbf{H}}_0 + \mathbf{I}i\Omega & \hat{\mathbf{H}}_{-1} & \hat{\mathbf{H}}_{-2} & \cdots \\ \cdots & \hat{\mathbf{H}}_1 & \hat{\mathbf{H}}_0 & \hat{\mathbf{H}}_{-1} & \cdots \\ \cdots & \hat{\mathbf{H}}_2 & \hat{\mathbf{H}}_1 & \hat{\mathbf{H}}_0 - \mathbf{I}i\Omega & \cdots \\ \ddots & \vdots & \vdots & \vdots & \ddots \end{pmatrix} \tilde{\mathbf{z}}_\infty(t), \quad (6.30)$$

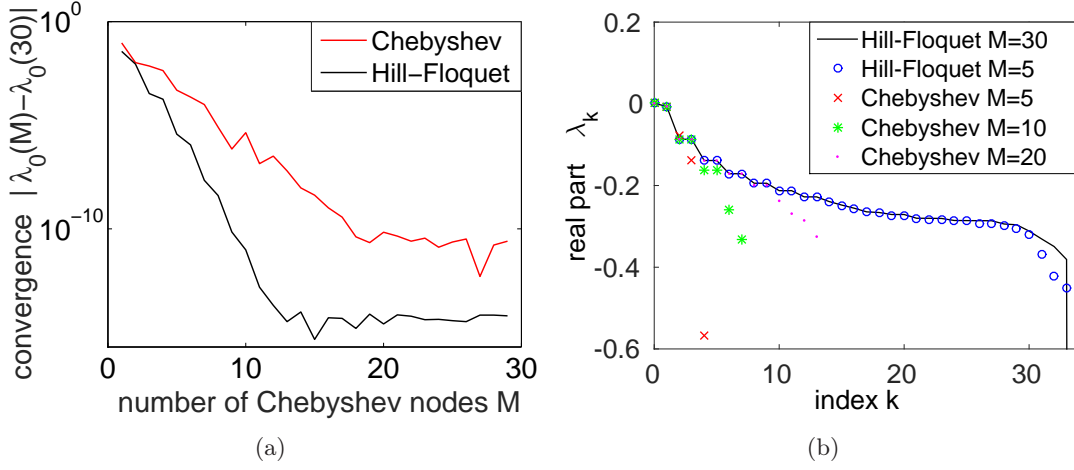


Figure 6.4.: a) Spectral convergence of the maximum Lyapunov exponent λ_0 of a periodic DDE for varying M . For Eq. (6.25) (black), i.e. the Hill-Floquet transformation is applied at first, the convergence is faster than for Eq. (6.30) (red), where the Chebyshev expansion is applied at first. b) Similarly, the exponents λ_k with $k > 0$ converges better for the Hill-Floquet transformation (black solid and blue circles) than for the Chebyshev method (red crosses, green stars, magenta dots), where only roughly $M/2$ of the exponents converge.

where \hat{H}_l denotes the l th Fourier coefficient of the matrix $\tilde{H}(t)$. The relationship between the configurations of the time-variant system Eq. (6.28) and the time-invariant system Eq. (6.30) can be given by $\tilde{z}(t) = \mathbf{F}^i(t)\tilde{z}_\infty(t)$. According to Eq. (6.8) and Eq. (6.9) the relationship between the transition matrices of the two systems is given by

$$\mathbf{F}^i(t)\tilde{H}_\infty = \tilde{H}(t)\mathbf{F}^i(t) - \dot{\mathbf{F}}^i(t). \quad (6.31)$$

In Fig. 6.4 the convergence of the Floquet exponents for the Mackey-Glass example with the same parameters as in Sec. 6.3 is presented for a fixed number of higher harmonics $n = 60$ and a varying number of Chebyshev nodes M for the two different methods. The Chebyshev expansion of the autonomous Hill-Floquet representation Eq. (6.12), which is presented in Sec. 6.3, is referred to as Hill-Floquet method, whereas the alternative method based on the Chebyshev expansion of the original DDE Eq. (3.2) with periodic coefficients and the Hill-Floquet transformation of the resulting periodic ODE Eq. (6.28) is referred to as Chebyshev method. As can be seen from Fig. 6.4a, for increasing M the real part λ_0 of the dominant eigenvalue converges exponentially, which is known as spectral convergence [54, 135]. Specifically, the dominant eigenvalue of the Hill-Floquet method (black) converges faster than the eigenvalue from the Chebyshev method (red). Moreover, by comparison of the black curve in Fig. 6.4a with Fig. 6.2a it can be concluded that the exponential rate of convergence with respect to M is much higher than the rate of convergence with respect to n , which is consistent with the conver-

6. Hill-Floquet method

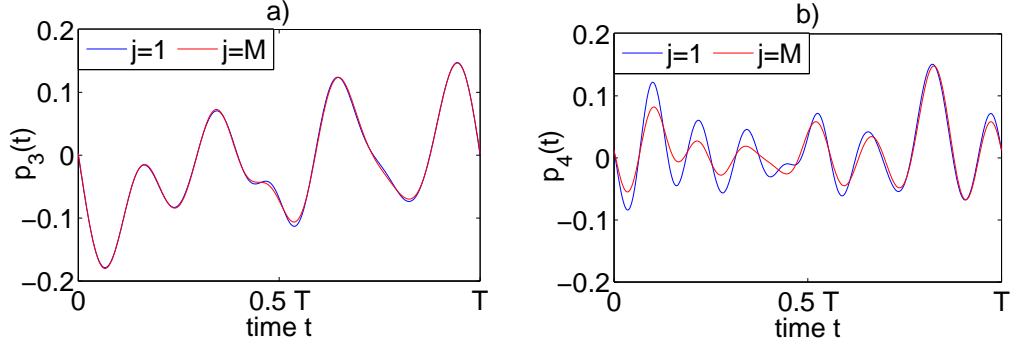


Figure 6.5.: The periodic part $p_k(t)$ is calculated from the eigenvectors of the matrix $\tilde{\mathbf{H}}_\infty$ at two different Chebyshev nodes $j = 1$ (blue) and $j = M$ (red) with $M = 10$. The difference increases significantly from a) $k = 3$ to b) $k = 4$, which is the reason for the deviations in the spectrum in Fig. 6.4b.

gence of the spectra in Fig. 6.2b and the convergence of the eigenvectors in Fig. 6.3. In Fig. 6.4b one can see that the other exponents λ_k with $k > 0$ converge much better for the Hill-Floquet method than for the Chebyshev method. In particular, for the Hill-Floquet method with $M = 5$ (blue, circles) roughly 30 exponents are converged to the exponents of the reference spectrum with $M = 30$ (black solid). In contrast, for the Chebyshev method with $M = 5$ (red crosses), $M = 10$ (green stars) and $M = 20$ (magenta dots) only 2, 4 and 10 exponents are converged to the reference spectrum, respectively. This means that for the Chebyshev method Eq. (6.30) the number of Chebyshev nodes M is also a relevant limiting parameter for the approximation. The reason for that is the qualitative difference between the different chronological order for the expansions. In fact, in the Chebyshev expansion Eq. (6.25) of the Hill-Floquet representation only the exponential part $e^{s_k t}$ of the eigenmodes must be approximated via the Chebyshev collocation method, where a small number of Chebyshev nodes M is sufficient for an accurate approximation. On the other hand, in the Chebyshev method Eq. (6.30) the complete eigenmodes $\mathbf{x}_k(t) = \mathbf{p}_k(t)e^{s_k t}$ in one delay interval including the periodic part $\mathbf{p}_k(t)$ are approximated via the Chebyshev collocation method. In this case, a larger number of Chebyshev nodes is necessary for a comparable accuracy of the approximation, because in addition to the exponential behavior also the periodic part of the eigenmodes must be approximated via the Chebyshev expansion.

This can be also seen in the redundant information on the periodic part $\mathbf{p}_k(t)$ of the eigenmodes, which is contained in the eigenvectors of the matrix $\tilde{\mathbf{H}}_\infty$ in Eq. (6.30). Specifically, the periodic part $\mathbf{p}_{k,j}(t)$ of the eigenmodes of the original system, which are defined similar to Eq. (6.27) but are now calculated for the matrix $\tilde{\mathbf{H}}_\infty$ with the fixed number of Chebyshev nodes $M = 10$, is presented for $k = 3$ and $k = 4$ at different Chebyshev nodes $j = 1$ and $j = M = 10$. In Fig. 6.5a for $k = 3$ the information on the periodic function at the most distant Chebyshev nodes $j = 1$ (blue) and $j = 10$ (red) is nearly equivalent, whereas in Fig. 6.5b for $k = 4$ there is a significant difference between

the periodic part $\mathbf{p}_{4,1}(t)$ (blue) and $\mathbf{p}_{4,M}(t)$ (red) at the first and the last Chebyshev node. This indicates that an accurate approximation with the Chebyshev expansion with $M = 10$ nodes is not possible for eigenmodes with $k \geq 4$. In fact, the deviations are by orders of magnitude larger than the deviations in Fig. 6.3c and Fig. 6.3d calculated from the eigenvectors of the matrix \mathbf{H}_∞ from Eq. (6.25) with $M = 10$, where the collocation method is used for the autonomous DDE Eq. (6.12). The deviations are also qualitatively consistent with the results on the corresponding Floquet spectrum, i.e. the green stars in Fig. 6.4b, where for $M = 10$ the approximation of the fourth exponent $k = 3$ is acceptable, whereas the exponent for $k = 4$ deviates already significantly from the reference spectrum. Thus, it is advisable to apply the Hill-Floquet transformation at first and use the autonomous DDE Eq. (6.12) for the stability analysis of periodic DDEs.

6.5. Discussion of the two separate expansions

In this thesis two separate expansions for the reduction of a periodic DDE to an autonomous ODE are proposed. The Hill-Floquet method in Sec. 6.1 transforms the DDE with periodic coefficients Eq. (3.2) to the autonomous DDE with constant coefficients Eq. (6.12), whereby the dimension of the system is increased by a factor $(2n + 1)$. In a second step, a collocation method is used in Sec. 6.3 for the approximation of the autonomous DDE Eq. (6.12) by an autonomous ODE Eq. (6.25). The collocation method further increases the dimension of the system by a factor M . At first, it should be made clear why a second expansion of the Hill-Floquet representation Eq. (6.12) is necessary. In fact, the configuration $\mathbf{x}_\infty(t)$ of the Hill-Floquet representation Eq. (6.12) at time t contains some information on the solution not only at time t but also at the delayed times $t - \tau$. In particular, the complete information on the periodic part $\mathbf{p}_k(t)$ of the eigenmodes for $0 \leq t < \infty$ is stored in the vectors $\mathbf{q}_{\infty,k}(t)$. However, this information is not sufficient to specify the past solution $\mathbf{x}_\infty(t - \tau)$ of the DDE because no information on the exponential behavior $e^{s_k t}$ of the eigenmodes is available.

On the other hand, the question arises why not only one expansion is used for the reduction of the periodic DDE Eq. (3.2) to an autonomous ODE? In fact, such methods exist and are commonly used for the stability analysis of linear periodic DDEs (see Sec. 5.2.2). For example, the Chebyshev collocation method can be used for a finite dimensional approximation of the solution $\mathbf{x}(t)$ of the original non-autonomous system Eq. (3.2) in one delay interval similar to Eq. (6.29). Then, in contrast to the additional Hill-Floquet transformation of the non-autonomous ODE Eq. (6.28), which is presented in Sec. 6.4, the Floquet exponents can be also calculated from the eigenvalues of the monodromy matrix. The monodromy matrix is the transition matrix for the evolution of the solution of the non-autonomous ODE Eq. (6.28) over one period. In this case, the dimension of the system increases only by a factor M but an additional numerical effort is necessary for the calculation of the monodromy matrix for the periodic ODE Eq. (6.28), which can become very time-consuming if the principle period is much larger than the maximum delay $T \gg \tau_{\max}$. Moreover, as can be seen already from the results in Sec. 6.4 the number of Chebyshev nodes M for the expansion of the original non-autonomous

6. Hill-Floquet method

system Eq. (3.2) must be larger than the number of Chebyshev nodes for the expansion of the autonomous Hill-Floquet system Eq. (6.12) for obtaining comparable convergence rates. Nevertheless, the direct application of the Chebyshev collocation method is suitable for the specific case, where only a single discrete delay τ_0 appears that is equal to the principle period $\tau_0 = T$, because in this case a simple and accurate expression can be derived for the monodromy matrix of the system [73]. Nevertheless, the main advantage of the Hill-Floquet method lies in the fact that a construction of the monodromy matrix is not necessary. In fact, there exists a large variety of efficient methods for the analysis of linear autonomous DDEs, which can be combined with the Hill-Floquet method. Some of them are listed in Sec. 5.1.4. Moreover, it should be emphasized that the FFT algorithm can be used for the expansion of the periodic coefficients of the DDE in a Fourier series, which makes the numerical implementation of the Hill-Floquet transformation very efficient.

6.6. Solution operator from the Hill-Floquet method

In this section the approximation of the solution operator based on the Hill-Floquet method is presented for periodic time delay systems. This is useful in applications, where the explicit form of the perturbations must be known. Moreover, the solution operator gives a relationship between the Hill-Floquet transformation and the Lyapunov-Floquet transformation and can be used for a comparison of the Hill-Floquet method with existing methods for the stability analysis, which are based on the construction of the monodromy matrix.

6.6.1. Fundamental matrix solution

The fundamental matrix solution \mathbf{M}_H of the autonomous ODE Eq. (6.25) is translation invariant and can be given by

$$\mathbf{z}_\infty(t) = \mathbf{M}_H(t)\mathbf{z}_\infty(0) = e^{t\mathbf{H}_\infty}\mathbf{z}_\infty(0). \quad (6.32)$$

The initial condition $\mathbf{z}_\infty(0)$ can be specified by using Eq. (6.24) and Eq. (6.20) for the determination of the initial configurations of the Hill-Floquet representation $\mathbf{x}_\infty(-\tau_j)$ at the Chebyshev nodes $j = 1, \dots, M$. In the Chebyshev expanded Hill-Floquet representation with the solution operator Eq. (6.32) the evolved state of the original system \mathbf{x}_t at time t is approximated by the configurations of the Hill-Floquet system at the Chebyshev nodes $\mathbf{x}_\infty(t - \tau_j)$, $j = 1, \dots, M$. The solution $\mathbf{x}(t)$ of the original system at time t can be calculated with the inverse Hill-Floquet transformation Eq. (6.5). Typically, the matrix \mathbf{H}_∞ is diagonalizable and the spectral representation of the fundamental matrix solution can be given as

$$\mathbf{M}_H(t) = \mathbf{P}_H e^{t\mathbf{S}_\infty} \mathbf{P}_H^{-1}, \quad (6.33)$$

where the matrices \mathbf{P}_H , \mathbf{P}_H^{-1} contain the right and the left eigenvectors of the matrix \mathbf{H}_∞ , and the matrix \mathbf{S}_∞ is a diagonal matrix with the eigenvalues. Thus, the columns of the matrix \mathbf{P}_H are equal to the eigenvectors $\mathbf{h}_{\infty,k}$ defined in Eq. (6.26). The corresponding

6.6. Solution operator from the Hill-Floquet method

eigenvalues are the Floquet exponent s_k of the DDE. The matrices \mathbf{S}_∞ and \mathbf{P}_H contain the eigenvalues and the eigenvectors associated with the reference and the redundant Floquet exponents of the system (see Sec. 6.2).

The transformation between the fundamental solution $\mathbf{M}_H(t)$ of the Hill-Floquet representation Eq. (6.25) and the fundamental solution $\mathbf{M}(t, 0)$ of the original representation can be obtained by

$$\mathbf{z}_\infty(t) = \mathbf{F}_H \mathbf{z}(t), \quad \text{and} \quad \mathbf{z}(t) = \mathbf{F}_H^i(t) \mathbf{z}_\infty(t), \quad (6.34)$$

where, according to the definition Eq. (6.24) of the vector $\mathbf{z}_\infty(t)$, the matrices \mathbf{F}_H and $\mathbf{F}_H^i(t)$ are specified by

$$\mathbf{F}_H = \begin{pmatrix} \mathbf{F}_0 & \mathbf{0} & \cdots & \mathbf{0} \\ \mathbf{0} & \mathbf{F}_0 & \cdots & \mathbf{0} \\ \vdots & \vdots & \ddots & \vdots \\ \mathbf{0} & \mathbf{0} & \cdots & \mathbf{F}_0 \end{pmatrix}, \quad \text{and} \quad \mathbf{F}_H^i(t) = \begin{pmatrix} \mathbf{F}^i(t) & \mathbf{0} & \cdots & \mathbf{0} \\ \mathbf{0} & \mathbf{F}^i(t - \tau_2) & \cdots & \mathbf{0} \\ \vdots & \vdots & \ddots & \vdots \\ \mathbf{0} & \mathbf{0} & \cdots & \mathbf{F}^i(t - \tau_M) \end{pmatrix}, \quad (6.35)$$

where the matrix blocks are given by Eq. (6.20) and Eq. (6.5), respectively. The vector $\mathbf{z}(t)$ contains the configurations of the original system at the Chebyshev nodes similar to the definition of $\tilde{\mathbf{z}}(t)$ in Eq. (6.29) for the alternative method. However, in contrast to the alternative method with the configuration $\tilde{\mathbf{z}}(t)$ the solution $\mathbf{z}(t)$ in Eq. (6.34) is not obtained via the alternative method from Sec. 6.4, but rather via the solution of the autonomous ODE Eq. (6.25) and an additional inverse Hill-Floquet transformation with the matrix $\mathbf{F}_H^i(t)$. If Eq. (6.32) is multiplied with $\mathbf{F}_H^i(t)$ from the left and Eq. (6.34) is used, the fundamental matrix solution $\mathbf{M}(t, 0)$ in the time domain can be expressed as

$$\mathbf{z}(t) = \mathbf{F}_H^i(t) \mathbf{M}_H(t) \mathbf{F}_H \mathbf{z}(0) = \mathbf{M}(t, 0) \mathbf{z}(0). \quad (6.36)$$

If the spectral representation Eq. (6.33) of the matrix $\mathbf{M}_H(t)$ is substituted in Eq. (6.36), the solution operator can be written as

$$\mathbf{M}(t, 0) = \mathbf{P}_\infty(t) e^{t\mathbf{S}_\infty} \mathbf{P}_\infty^i(0), \quad (6.37)$$

where the matrices of the right and the left eigenvectors are defined as

$$\mathbf{P}_\infty(t) = \mathbf{F}_H^i(t) \mathbf{P}_H, \quad \text{and} \quad \mathbf{P}_\infty^i(0) = \mathbf{P}_H^{-1} \mathbf{F}_H. \quad (6.38)$$

The eigenvector matrices $\mathbf{P}_\infty(t)$ and $\mathbf{P}_\infty^i(0)$ still contain the redundant eigenvectors and are, in general, no square matrices, which means that $\mathbf{P}_\infty^i(0)$ is not the inverse of the matrix $\mathbf{P}_\infty(0)$. In fact, due to the redundant nature of the Hill-Floquet representation, similar to Eq. (6.23) only the identity condition $\mathbf{P}_\infty(t) \mathbf{P}_\infty^i(0) = \mathbf{I}$ holds, whereas the opposite is not true.

A further simplification of the fundamental matrix solution is possible if only the reference eigenvectors $\mathbf{P}(t)$ and exponents \mathbf{S} are used. In particular, the matrix \mathbf{S} contains only the NM reference Floquet exponents of the matrix \mathbf{S}_∞ on the main diagonal, and

6. Hill-Floquet method

the matrix $\mathbf{P}(t)$ contains only the NM columns of the matrix $\mathbf{P}_\infty(t)$ with the reference eigenvectors. In this case, the spectral representation of the matrix fundamental solution can be written as

$$\mathbf{M}(t, 0) = \mathbf{P}(t)e^{t\mathbf{S}}\mathbf{P}^{-1}(0), \quad (6.39)$$

where now $\mathbf{P}^{-1}(0)$ is the inverse of the $NM \times NM$ dimensional square matrix $\mathbf{P}(0)$.

6.6.2. Monodromy matrix

The monodromy matrix of a periodic DDE Eq. (3.2) is given by the transition matrix $\mathbf{M}(T, 0)$ over one period of the system. In particular, by combining Eq. (6.32) and Eq. (6.36) the monodromy matrix can be given by

$$\mathbf{M}(T, 0) = \mathbf{F}_H^i(T)e^{T\mathbf{H}_\infty}\mathbf{F}_H. \quad (6.40)$$

Eq. (6.40) can be used for the calculation of the characteristic exponents of the periodic delay system. In contrast to the $N(2n + 1)M$ dimensional eigenvalue problem for the matrix \mathbf{H}_∞ in Eq. (6.25), the NM dimensional matrix $\mathbf{M}(T, 0)$ contains only NM Floquet multipliers $e^{s_k T}$ and no redundant information. However, there is no advantage in the computing time because for the determination of the lower dimensional matrix $\mathbf{M}(T, 0)$ with Eq. (6.40) the matrix exponential of the matrix \mathbf{H}_∞ must be calculated, which is typically based on the eigenvalue decomposition of the high dimensional matrix \mathbf{H}_∞ . Alternatively, the monodromy matrix can be also calculated from Eq. (6.39) with $t = T$, where only the reference Floquet exponents and the associated eigenvectors of the matrix \mathbf{H}_∞ are used.

6.6.3. Lyapunov-Floquet transformation

The Hill-Floquet method converts a system with periodic coefficients to a system with constant coefficients. A closely related transformation is the Lyapunov-Floquet transformation. The Lyapunov-Floquet transformation is based on the Floquet theory, that is a factorization of the fundamental matrix solution $\mathbf{M}(t, 0)$ of a linear periodic ODE in a periodic part $\mathbf{Q}(t) = \mathbf{Q}(t + T)$ and a matrix exponential of the time-invariant matrix \mathbf{R} as [169]

$$\mathbf{M}(t, 0) = \mathbf{Q}(t)e^{t\mathbf{R}}, \quad \text{with} \quad \mathbf{Q}(0) = \mathbf{I}. \quad (6.41)$$

If the factorization Eq. (6.41) is put into Eq. (4.12), the following ODE can be derived for the evolution of the periodic matrix $\mathbf{Q}(t)$ [75]

$$\dot{\mathbf{Q}}(t) = \mathbf{A}(t)\mathbf{Q}(t) - \mathbf{Q}(t)\mathbf{R}. \quad (6.42)$$

As a consequence, a linear periodic ODE $\dot{\mathbf{x}}(t) = \mathbf{A}(t)\mathbf{x}(t)$ can be converted with the Lyapunov-Floquet transformation into the system

$$\dot{\mathbf{x}}_R(t) = \mathbf{R}\mathbf{x}_R(t), \quad (6.43)$$

where $\mathbf{x}(t) = \mathbf{Q}(t)\mathbf{x}_R(t)$ is substituted in the periodic ODE. The emerging N dimensional configuration $\mathbf{x}_R(t)$ in the linear time-invariant ODE Eq. (6.43) contains only the

information on the exponential behavior of the eigenmodes $\mathbf{x}_k(t)$ of the original periodic system. The periodic part of the eigenmodes $\mathbf{p}_k(t)$ is encoded in the periodic coordinate transformation $\mathbf{Q}(t)$.

A relationship between the Hill-Floquet transformation and the Lyapunov-Floquet transformation can be obtained by considering the monodromy matrix Eq. (6.41) of a periodic ODE for the time evolution over one period

$$\mathbf{M}(T, 0) = \mathbf{Q}(T)\mathbf{e}^{T\mathbf{R}} = \mathbf{e}^{T\mathbf{R}}. \quad (6.44)$$

The comparison of the monodromy matrix Eq. (6.44) from the Lyapunov-Floquet representation with the monodromy matrix Eq. (6.39) from the Hill-Floquet representation together with the periodicity condition $\mathbf{P}_\infty(T) = \mathbf{P}_\infty(0)$ leads to

$$\mathbf{R} = \mathbf{P}(0)\mathbf{S}\mathbf{P}^{-1}(0), \quad \text{and} \quad \mathbf{Q}(t) = \mathbf{P}(t)\mathbf{P}^{-1}(0). \quad (6.45)$$

Eq. (6.45) can be used for the calculation of the Lyapunov-Floquet transformation from the solution operator of the Hill-Floquet representation.

6.7. Summary

In this chapter, the so-called Hill-Floquet transformation was introduced in Sec. 6.1. It is based on Hill's method and transforms non-autonomous systems with periodic coefficients Eq. (3.2) to autonomous systems with constant coefficients Eq. (6.12). In particular, Floquet theory was used to decompose the solution of a periodic system into a periodic part and an exponential part similar to Eq. (6.1). The periodic part is expanded into a Fourier series, whereas the exponential behavior of the Fourier coefficients is described in the time domain by the autonomous DDE Eq. (6.12).

In Sec. 6.2 it was shown that the Floquet exponents and the corresponding eigenvectors, which can be obtained from the Hill-Floquet representation are not unique. This means that multiple eigenvalues of the matrix \mathbf{H}_∞ in combination with the corresponding eigenvectors describe the same eigenmode $\mathbf{x}_k(t)$ of the original time delay system. This is equivalent to the Brillouin zones in solid state physics. In fact, the information in the first Brillouin zone is sufficient for a complete description of the periodic crystal. Here, the Floquet exponents s_k in the first Brillouin zone, which are called reference Floquet exponents, are sufficient for the description of the solution of the periodic system. The redundant information in the eigenvalue decomposition of the matrix \mathbf{H}_∞ can be used to check the accuracy of a finite dimensional approximation of the Hill-Floquet transformation.

After applying the Hill-Floquet transformation to a DDE with periodic coefficients, the resulting autonomous DDE can be analyzed by existing methods for autonomous DDEs. In Sec. 6.3, the Chebyshev collocation method was used for the stability analysis of the autonomous Hill-Floquet system Eq. (6.12), which transform the autonomous DDE to an autonomous ODE Eq. (6.25). In particular, the dominant Floquet exponents of the original system are approximated by the eigenvalues of the coefficient matrix \mathbf{H}_∞

6. Hill-Floquet method

of the Chebyshev-expanded Hill-Floquet representation Eq. (6.25). It is shown that the presented Hill-Floquet transformation in combination with the Chebyshev collocation method is an efficient and reliable method for the calculation of the Floquet exponents for periodic DDEs with distributed delay. Only the number of higher harmonics n and the number of Chebyshev nodes M for the two expansions must be specified. The corresponding coefficient matrices \mathbf{A}_∞ and $\mathbf{B}_\infty(\tau)$ of the autonomous DDE can be calculated very efficiently with the FFT algorithm and an algorithm for the construction of the Chebyshev spectral differentiation matrix \mathbf{D}_M can be taken from [166]. The eigenvalues of the matrix \mathbf{H}_∞ approximate automatically the most dominant Floquet exponents of the original periodic DDE, which is the main advantage of the Hill-Floquet method in contrast to root finding algorithms for the infinite dimensional characteristic equation (cf. [42]), where it is not clear whether the dominant characteristic roots are found. In addition, the Hill-Floquet method does not require the calculation of the solution operator or the monodromy matrix, which is the main advantage in comparison to time domain approaches for the analysis of periodic DDEs such as, for example, the semidiscretization method [3].

7. Applications

In this chapter the methods for the analysis of time delay systems, which are presented in this thesis, are applied for specific time delay systems in biology, engineering and physics. In particular, in Sec. 7.1 diffusion-driven instabilities in delayed reaction-diffusion systems are studied, in Sec. 7.2 the stability lobes for machine tool vibrations are calculated and in Sec. 7.3 the stability of synchronized solutions of a Hodgkin-Huxley neuronal network is analyzed. For the delayed reaction-diffusion systems and the machine-tool models the results from Chapter 2 on the approximations of systems with variable delays and the transformation from variable delays to constant delays are used. In all examples, the D-subdivision method from Sec. 5.3 is used for the calculation of stability charts of equilibria. Moreover, the Hill-Floquet method from Chapter 6 for periodic time delay systems is used for the stability analysis of turning with spindle speed variation and for the stability of synchronized periodic solutions in the Hodgkin-Huxley neuronal network.

7.1. Delayed reaction-diffusion systems

Reaction-diffusion systems are typical models for pattern formation. It has been shown in 1952 that, counterintuitively, a stable equilibrium of a system without diffusion, can become unstable in the presence of diffusion [170]. If a dominant characteristic exponent s_0 crosses the imaginary axis through the origin with $s_0 = 0$ due to the presence of diffusion, the instability is called Turing instability and the resulting spatially inhomogeneous time-invariant pattern is known as Turing pattern. If there is a complex-conjugate pair of characteristic exponents which crosses the imaginary axis, the instability is called wave instability. The resulting patterns that occur from a wave instability are traveling or standing waves [171]. Whereas in classical reaction-diffusion systems the reaction depends instantaneously on the concentration of the reactants, it is often more realistic that the effect of time delays play a significant role in the reaction dynamics. For example, time-delayed population models can describe the oscillations in single species dynamics very well [38]. Delayed reaction-diffusion systems have been studied in [172, 173, 174]. In addition, time-delayed feedback control of spatially inhomogeneous structures in reaction-diffusion systems has been investigated [175]. In the classical paper about the Turing instability [170] it has been proved that a Turing or a wave instability is only possible for reaction-diffusion systems with at least two or at least three components, respectively. However, it is known that the introduction of time delays leads to an infinite dimension of the system. This was the motivation for studying the existence of diffusion-driven instabilities in single species reaction-diffusion systems with delay. The results are closely related to the work on the occurrence of Turing pattern in a high-dimensional system with one diffuser [176], because as mentioned above in Sec. 6.3 a time delay system can

7. Applications

be approximated by a high dimensional system of ODEs. Recently, some interesting results on delay-induced Turing-like waves for reaction-diffusion models on a network were published [90]. It is shown that a diffusion-induced instability cannot occur if there is only a single delay in the reaction term but diffusion-induced traveling waves were found if there is a time delay in a discrete diffusion process on a complex network.

7.1.1. Stability analysis for homogeneous equilibria

In this thesis the possibility for the occurrence of diffusion-driven instabilities for single species reaction-diffusion systems with a distributed delay or a time-varying delay in the reaction term is investigated. Detailed results on this study are presented in [177]. In the following, the stability of time-invariant homogeneous solutions of the system are analyzed, which are spatially homogeneous equilibria of the delay partial differential equation

$$\frac{\partial u(\theta, t)}{\partial t} = f(u(\theta, t), r_u(\theta, t)) + D\Delta u(\theta, t). \quad (7.1)$$

In Eq. (7.1), $u(\theta, t)$ is the population density of a species at time t and location θ , the function f describes the reaction dependent on the instantaneous density u and the delayed density r of the population, D is the diffusion coefficient, and Δ is the Laplace operator. For brevity, only one spatial dimension is considered, but the extension to more spatial dimensions is straightforward. According to Sec. 3.3.2, the dynamics of infinitesimal perturbations x around an equilibrium $u(\theta, t) = u^*$ of Eq. (7.1) can be described by the linear delay partial differential equation

$$\frac{\partial x(\theta, t)}{\partial t} = (A + D\Delta)x(\theta, t) + Br_x(\theta, t), \quad (7.2)$$

where the scalars A and B are the derivatives of the function f at the equilibrium u^* with respect to the first and the second argument, respectively. If the Fourier transform Eq. (5.11) with respect to the spatial variable θ is applied to Eq. (7.2), the Laplace operator is decomposed into its eigenmodes. The dynamics of the Fourier modes $\hat{x}(k, t)$ dependent on the wavenumber k is characterized by

$$\dot{\hat{x}}(t) = (A - Dk^2)\hat{x}(t) + Br_x(t), \quad (7.3)$$

where the additional argument k and the hat were immediately dropped from the Fourier modes $\hat{x}(k, t) = x(t)$. Thus, the dynamics of the Fourier modes, i.e. the eigenfunctions of the Laplace operator, can be described by the scalar autonomous DDE Eq. (7.3), where $-k^2$ are the eigenvalues of the Laplace operator. In practice, the possible value for the wavenumber k depends on the boundary condition of the reaction-diffusion system. For example, for periodic boundary conditions only a discrete set of wavenumbers k is possible. For the analysis of diffusion-driven instabilities in this thesis, the more general case of a continuous set of wavenumbers $k \in \mathbb{R}$ is considered.

A stability chart for the reaction-diffusion system Eq. (7.3) can be calculated with the D-subdivision method as described in Sec. 5.3. The characteristic equation for the

D-curves with $s = i\omega$ is given by

$$i\omega - A + Dk^2 - B\bar{K}(i\omega) = 0, \quad (7.4)$$

where $\bar{K}(i\omega)$ is the Laplace transform of the delay distribution $K(\tau)$ in the memory $r(x_t)$ of the system. The Laplace transform of the delay distribution is written as

$$\bar{K}(i\omega) = e^{-i\omega\tau_0} \int_{-\tau_0}^{\tau_{\max}-\tau_0} K(\tau_0 + \tau) e^{-i\omega\tau} d\tau = R_K(\omega) e^{i(\phi_K(\omega) - \omega\tau_0)}, \quad (7.5)$$

where τ_0 is a delay offset, $R_K(\omega)$ is the modulus and $\phi_K(\omega)$ the phase of the typically complex valued Laplace transform of the τ_0 -shifted delay distribution. If the offset τ_0 for symmetric delay distributions $K(\tau_0 - \tau) = K(\tau_0 + \tau)$ is equal to the mean delay, the Laplace transform of the τ_0 -shifted delay distribution is real, which means that the phase $\phi_K(\omega)$ can adopt only the two values 0 and π . Without loss of generality the mean delay is set to one $\tau_0 = 1$, which can be obtained by rescaling the parameters A , B and D of the system. After substituting Eq. (7.5) with $\tau_0 = 1$ in Eq. (7.4) the D-curves can be determined by

$$\left. \begin{aligned} B &= Dk^2 - A, \quad \text{for } \omega = 0, \\ \left. \begin{aligned} A - Dk^2 &= \frac{\omega}{\tan(\omega - \phi_K(\omega))} \\ B &= -\frac{\omega}{R_K(\omega) \sin(\omega - \phi_K(\omega))} \end{aligned} \right\}, \quad \text{for } \omega \neq 0. \end{aligned} \right\} \quad (7.6)$$

If a delay distribution is specified by the functions $R_K(\omega)$ and $\phi_K(\omega)$, the D-curves can be determined from Eq. (7.6) in a two dimensional parameter space by sweeping the frequency ω and calculating the corresponding values for the parameters $A - Dk^2$ and B , where one characteristic exponent of the system crosses the imaginary axis.

7.1.2. Diffusion-driven instabilities

The stability chart for the homogeneous equilibria u^* of the reaction-diffusion system Eq. (7.1) for a discrete delay $K(\tau) = \delta(\tau - \tau_0)$, where $R_K(\omega) = 1$ and $\phi_K(\omega) = 0$, is shown in Fig. 7.1a. The D-curves (blue curves) specify the parameters, where one or two complex conjugated characteristic exponents cross the imaginary axis. Parameters in the white region corresponds to a stable equilibrium, where all characteristic exponents have a negative real part. The shaded area indicates an unstable equilibrium, where at least one characteristic exponent has a positive real part. A diffusion-driven instability is possible if an equilibrium is stable for $k = 0$ and unstable for $k > 0$. Such a situation occurs if a parameter point in the white region of Fig. 7.1a, corresponding to a stable equilibrium with $k = 0$ and fixed parameters A and B , crosses a D-curve for increasing k or decreasing $A - Dk^2$, respectively. Obviously, this is not possible in Fig. 7.1a for a single discrete delay and can be proven rigorously if a series expansion of the Lambert W function in Eq. (5.8) is used for the description of the characteristic roots (see [90]). Note, that the stability chart in Fig. 7.1a holds, in general, for an arbitrary equilibrium of an

7. Applications

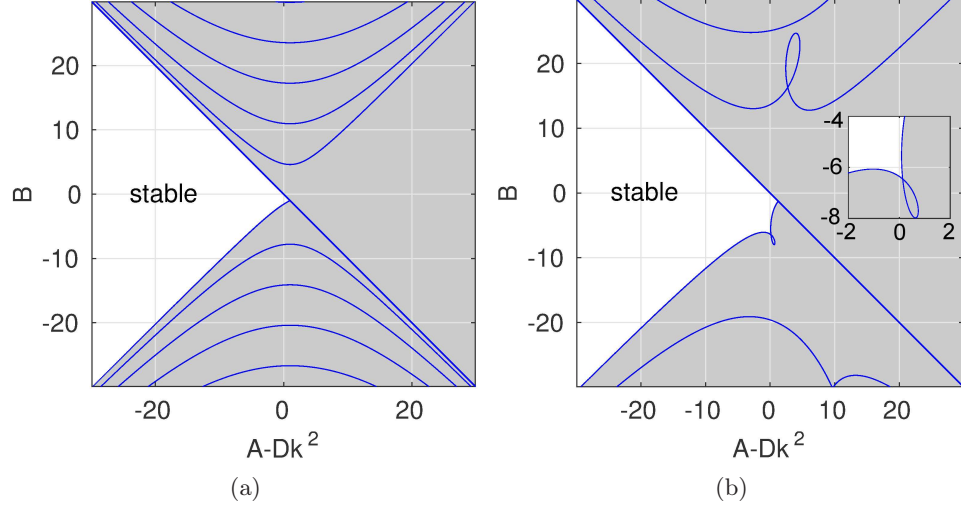


Figure 7.1.: General stability chart for equilibria of a single species reaction-diffusion system Eq. (7.1) for a) a single discrete delay, and b) the asymmetrically distributed delay Eq. (7.7).

arbitrary single species reaction-diffusion system Eq. (7.1) with discrete delay. Switching between the equilibria of a system, changing the nonlinear function f that describes the reaction of the system, or changing the discrete delay τ_0 does only change the parameters A , B and D in Eq. (7.6).

Similar stability charts can be calculated from Eq. (7.6) for any other distributed delay. As mentioned above, for symmetric delay distributions the phase $\phi_K(\omega)$ can only adopt the values 0 and π . As a consequence, for the D-curves the dependence of $A - Dk^2 := \alpha$ on the frequency ω is the same as for a single discrete delay. Moreover, according to Eq. (7.6) it can be shown that the condition $\alpha'(\omega) \leq 0$ holds for the derivative of the parametric function. This might be the reason why in extensive numerical simulations with various symmetrical delay distributions no Turing or wave instabilities were detected. For asymmetric delay distributions the situation is different. In this case also loops of the D-curves with $\alpha'(\omega) > 0$ are possible. If such a loop appears in the D-curve that separates stable from unstable behavior, diffusion-driven instabilities are likely to be possible. In fact, a Turing or wave instability is only possible if an initially stable system becomes unstable after moving on a horizontal line to the left in the stability charts similar to Fig. 7.1. An appropriate example for a diffusion-driven instability is shown in Fig. 7.1b. In this case the distributed delay is composed of two asymmetrically weighted delta peaks, where the delay distribution is given by

$$K(\tau) = 0.7\delta(\tau - 0.48) + 0.3\delta(\tau - 1.52). \quad (7.7)$$

The inset in Fig. 7.1b shows an enlarged version of the loop that is responsible for a wave instability. The non-monotonic behavior of the D-curve, which separates stable from unstable regions, enables the occurrence of a diffusion-induced instability. In particular,

for $A = 0$ and $-6.2 < B < -6$ slightly above the loop of the specific D-curve, the system is stable for $k = 0$ but becomes unstable for some $k > 0$. In this case, a pair of complex conjugated characteristic exponents with $\omega \neq 0$ crosses the imaginary axis in the complex plane at a finite wavenumber $k > 0$, which means that a wave instability appears. In general, classical Turing instabilities with $\omega = 0$ are not possible in one component reaction-diffusion systems with delay because according to Eq. (7.6) the D-curve for $\omega = 0$ is a strictly decreasing function independent of the delay distribution.

7.1.3. Turing-like traveling waves

An example of the corresponding oscillatory Turing-like pattern is shown for the Hutchinson equation with distributed delay and diffusion. The Hutchinson equation is typically used as a model for single species dynamics that can describe oscillatory behavior [106]. Originally, it was defined with a single discrete delay and without diffusion. The Hutchinson equation with a distributed delay similar to Eq. (7.7) and with diffusion is given by

$$\frac{\partial u(\theta, t)}{\partial t} = -Bu(\theta, t)(1 - 0.7u(\theta, t - 0.48) - 0.3u(\theta, t - 1.52)) + D\Delta u(\theta, t). \quad (7.8)$$

Eq. (7.8) can be also interpreted as a generalization of the Fisher-KPP equation to a system with distributed delay [178, 179]. A realistic population model implies a positive growth rate with $B < 0$. In this case the trivial equilibrium $u(\theta, t) = 0$ of Eq. (7.8) is always unstable. For the non-trivial equilibrium $u^* = 1$ the linear variational system in Fourier space can be given by

$$\dot{x}(t) = -Dk^2x(t) + B(0.7x(t - 0.48) + 0.3x(t - 1.52)). \quad (7.9)$$

According to the stability chart Fig. 7.1b the growth rate $B = -6.1$ is chosen, where the equilibrium is stable for $k = 0$ and becomes unstable for perturbations with some wavenumber $k > 0$. The emerging pattern with $D = 0.1$ in one space dimension with periodic boundary condition is shown in Fig. 7.2. Indeed, a traveling wave can be observed. From the linear stability analysis of Eq. (7.3) for $D = 0.1$ it follows that, theoretically, the most unstable Fourier mode that occurs for periodic boundary conditions with a spatial period 32 is the mode with the wavenumber $k_u = \pi$ (cf. black dotted curve in Fig. 7.3). The frequency ω_u of this most unstable Fourier mode is $\omega_u = 4.55$. In fact, these values from the linear theory coincide very well with the numerical values for the wavenumber $k_s = \pi$ and the frequency $\omega_s = 4.56$ that can be extracted from the resulting traveling wave in the nonlinear system Eq. (7.8) in Fig. 7.2.

7.1.4. Diffusion-driven instabilities in systems with time-varying delay

In Sec. 2.4.2 it was shown that a system with slowly time-varying delay can be approximated by a sequence of systems with discrete delays similar to Eq. (2.46). Therefore, the dominant Floquet exponent of the system with a slowly time-varying delay can be approximated by an average of the dominant characteristic exponents for the system with all adopted discrete delays. Since one-component reaction-diffusion systems with

7. Applications

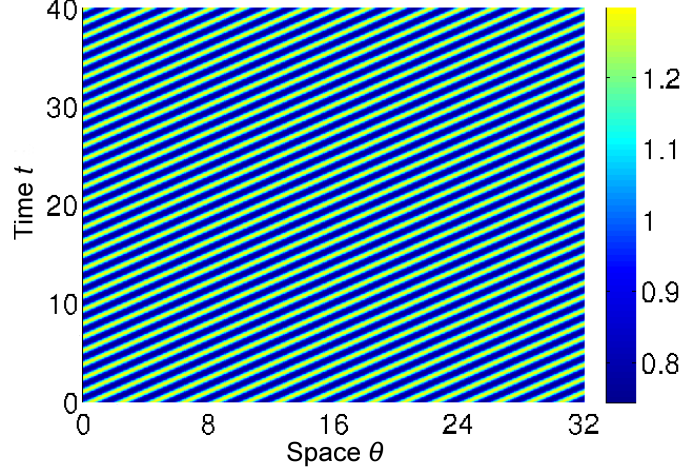


Figure 7.2.: Turing-like traveling wave that appears in the Fisher-KPP equation Eq. (7.8) with the delay distribution Eq. (7.7), where diffusion leads to an instability of the homogeneous equilibrium $u^* = 1$. The parameters $D = 0.1$, $B = -6.1$, and one spatial dimension with periodic boundary conditions $u(\theta, t) = u(\theta + 32, t)$ are used.

an arbitrary time-invariant discrete delay does not admit Turing or wave instabilities, it follows immediately that diffusion-induced instabilities cannot occur in systems with slowly time-varying delays (cf. [177]).

However, a system with fast time-varying delay can be approximated by the same system with a time-averaged delay distribution as described in Sec. 2.4.1. Thus, a wave instability should be possible in a single species reaction-diffusion system with an asymmetric fast time-varying delay, where the corresponding averaged delay distribution $K_{\text{av}}(\tau)$ is equivalent to Eq. (7.7) that admits diffusion-driven instabilities. Such an asymmetric delay distribution, can be given by

$$K_{\text{var}}(t, \tau) = \begin{cases} \delta(\tau - 0.48), & \text{if } \text{mod}(t, T) < 0.7T \\ \delta(\tau - 1.52), & \text{otherwise.} \end{cases} \quad (7.10)$$

In Eq. (7.10) T denotes the period of the delay variation. In Fig. 7.3 the largest real part λ_0 of the characteristic exponents of the reaction-diffusion system with time-varying delay distribution Eq. (7.10) as a function of the value Dk^2 of the harmonic perturbation is shown for various periods T of the delay variation. The parameter $B = -6.1$ is chosen equal to Fig. 7.2, where a wave instability is possible for the system with distributed delay. The curves in Fig. 7.3 are an illustration of the dispersion relation $\lambda_0(k)$ on a quadratic abscissa scaled by the diffusion coefficient D . The curves are calculated with the semidiscretization method [180], because the linear DDE Eq. (7.3) with time-varying rectangular delay cannot be put into the standard form Eq. (3.2) for the stability analysis with the Hill-Floquet method. Nevertheless, the dispersion relation for the case $T \rightarrow 0$ (black dotted curve in Fig. 7.3), that corresponds to the distributed delay comparison

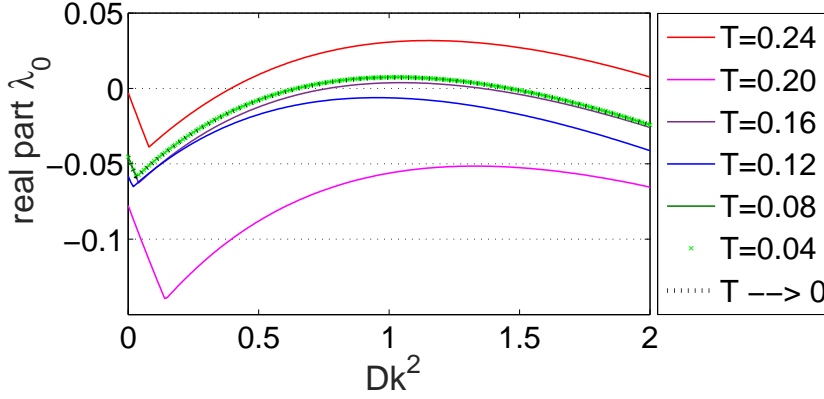


Figure 7.3.: Maximum growth rate λ_0 of the perturbations Eq. (7.3) for varying periods T of the periodically-varying delay Eq. (7.10) as a function of Dk^2 ($A = 0$, $B = -6.1$). For decreasing T the curves converge to the black dotted curve from the system with the distributed delay Eq. (7.7). A wave instability is possible if $\lambda_0 < 0$ for $k = 0$ and $\lambda_0 > 0$ for some wavenumber with $k > 0$.

system with the time-invariant delay distribution Eq. (7.7), can be calculated with the frequency domain methods for autonomous DDEs, which are described in Sec. 5.1.4.

As can be seen from Fig. 7.3, in fact, for decreasing periods of the delay variation the curves converge to the dispersion relation of the distributed delay comparison system. However, for $T > 0.1$ the convergence is not uniform and the specific behavior depends sensitively on the exact value of the period T . In particular, the discrepancy between the curve for $T = 0.24$ (red) and the asymptotic behavior is smaller than the discrepancy between the curve for $T = 0.20$ (magenta) and the asymptotic behavior, even though the delay variation for $T = 0.20$ is faster than for $T = 0.24$. Moreover, similar to the asymptotic behavior for a distributed delay, a wave instability is possible for the variable delay with $T = 0.24$ (red) and $T = 0.16$ (purple) but not possible for $T = 0.20$ (magenta) and $T = 0.12$ (blue). For $T \leq 0.1$ the curves are very close to the dispersion relation of the distributed delay comparison system, which can be seen from Fig. 7.3 for $T = 0.08$ (dark green) and $T = 0.04$ (crosses).

7.2. Metal cutting vibrations

Metal cutting processes are one of the most important manufacturing processes in industry. The efficiency and productivity of metal cutting processes is often limited by machine tool chatter, which are periodic, quasi-periodic or chaotic large-amplitude vibrations between the cutting tool and the workpiece. Chatter leads to noise, bad surface finish and increased tool wear. Numerical simulations of the dynamic interactions between the cutting tool and the workpiece can be used for increasing the productivity of machine-tools and the quality of the parts. In particular, the prediction of the so-called stability lobes are used for an optimization of the cutting process. The stability lobes are the stability

7. Applications

chart in the parameter plane of spindle speed Ω_0 and chip width b . Since more than 50 years, it is well-accepted in industry that the dynamics of the machine tool vibrations depends not only on the current position of the cutting tool but also on time-delayed positions of the tool, which are relevant due to the waviness of the outer surface of the chip (see Fig. 1.1). This is also known as regenerative effect [4, 5]. Roughly speaking, machine tool chatter occurs if the wavy outer surface of the chip due to vibrations at the previous cut generates significant dynamic variations of the cutting force, and the amplitude of the vibrations due to the force variations at the present cut is larger than the amplitude at the previous cut.

An overview on the stability lobe theory for different metal cutting and grinding processes is given in [2, 181]. Current research in the field is dedicated, but not limited, to the stability analysis of parallel turning [91, 92, 182] and milling processes [183, 184, 185, 186], and the effect of a variable spindle speed on the stability lobes in metal cutting [23, 26, 180]. In this thesis, the stability analysis of metal cutting vibrations is presented for two examples. The efficient numerical calculation of the stability charts with the D-subdivision method from Sec. 5.3 is shown for a parallel turning process with multiple delays, and the implementation of the Hill-Floquet method from Chapter 6 is shown for turning processes with a variable transport delay due to an active spindle speed variation.

7.2.1. Parallel turning

The simplified kinematics of a parallel turning process is illustrated in Fig. 7.4a. Two inserts are cutting simultaneously the same surface at different angular positions of the workpiece. Hence, the coupled regenerative effect at the two cuts must be taken into account for an accurate stability analysis of the parallel turning process. A common and reasonable approximation is made by the two assumptions that the angular velocity Ω_0 of the spindle is perfectly constant, and that vibrations in the y - z plane does not affect the cutting force. As a consequence, only the vibrations in x -direction are self-excited vibrations and are relevant for the stability analysis, whereas the vibrations in the y - z -plane are only forced vibrations.

The modulus of the cutting force $F_i(t)$ at the i th cut can be determined by

$$F_i(t) = b f_c(h_i(t)), \quad i = 1, 2, \quad (7.11)$$

where b specifies the depth of cut and $h_i(t)$ is the chip thickness at the i th cut. The function f_c characterizes the cutting force law. An overview on some realistic cutting force laws can be found in [187]. The chip thicknesses at the two cuts can be given by

$$h_1(t) = v_f \tau_1 + u_2(t - \tau_1) - u_1(t), \quad h_2(t) = v_f \tau_2 + u_1(t - \tau_2) - u_2(t). \quad (7.12)$$

where v_f is the feed velocity and u_1 and u_2 are the relative displacements in x -direction between the workpiece and the first and the second tool tip, respectively. The time delays τ_1 and τ_2 can be given by

$$\tau_1 = \frac{\gamma}{\Omega_0}, \quad \tau_2 = \frac{2\pi - \gamma}{\Omega_0}, \quad (7.13)$$

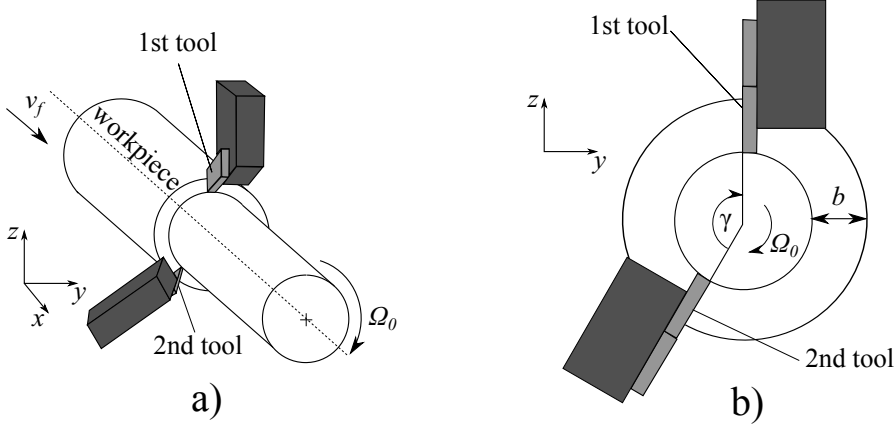


Figure 7.4.: a) Kinematics of a parallel turning process with two tools cutting the same surface. b) The angle γ between the two tools determines the time delays τ_1 and τ_2 at the first and second tool.

which means that they are equal to the time for the rotation of the workpiece by the angles γ and $(2\pi - \gamma)$, respectively. As can be seen in Fig. 7.4b γ is the angle between the second and the first tool. For $\gamma = \pi$ as it was assumed in [182], the two delays are equal $\tau_1 = \tau_2 = \pi/\Omega_0$. For the theoretical analysis in this thesis an arbitrary angle γ between the two tools is considered. The structural dynamics of the tool tip displacements in response to a cutting force are assumed to be linear and can be specified in the frequency domain by

$$\begin{aligned} \hat{\mathbf{u}}(\omega) &= \mathbf{G}(\omega) \hat{\mathbf{F}}(\omega), \\ \begin{pmatrix} \hat{u}_1(\omega) \\ \hat{u}_2(\omega) \end{pmatrix} &= \begin{pmatrix} G_{11}(\omega) & G_{12}(\omega) \\ G_{21}(\omega) & G_{22}(\omega) \end{pmatrix} \begin{pmatrix} \hat{F}_1(\omega) \\ \hat{F}_2(\omega) \end{pmatrix}. \end{aligned} \quad (7.14)$$

The frequency response function $G_{ij}(\omega)$ specifies the x -displacements at the i th tool tip in response to a harmonic excitation with frequency ω at the j th cut. The excitation at the j th cut is considered in the cutting force direction, which means that $\mathbf{G}_{ij}(\omega)$ is a matrix of oriented transfer functions [2, 181]. In the time domain Eq. (7.14) can be described by a system of harmonic oscillators, where the mass, damping and stiffness parameters of the oscillators are equal to the modal parameters of the eigenmodes of the structure at the tool tip.

The system has a non-trivial equilibrium $\mathbf{u}^* = \text{col}(u_1^*, u_2^*)$, which is desired to be stable for a high-quality implementation of the parallel turning process. The equilibrium specifies the static displacements of the tools during cutting and can be derived from the solution of the system of nonlinear equations

$$\mathbf{u}^* = \mathbf{G}(0) \mathbf{F}_{\text{stat}}(\mathbf{u}^*), \quad \mathbf{F}_{\text{stat}}(\mathbf{u}^*) = b \begin{pmatrix} f_c(v_f \tau_1 + u_2^* - u_1^*) \\ f_c(v_f \tau_2 + u_1^* - u_2^*) \end{pmatrix}. \quad (7.15)$$

The vector $\mathbf{F}_{\text{stat}}(\mathbf{u}^*)$ determines the static part of the cutting force that appears if the perturbations $\mathbf{x}(t) = \mathbf{u}(t) - \mathbf{u}^*$ at the non-trivial equilibrium can be neglected. In

7. Applications

general, the static stiffness $\mathbf{G}(0)$ and the static forces \mathbf{F}_{stat} are different for the first and the second tool, which means that there is also a difference in the static displacements of the structure u_1^* and u_2^* at the two cuts. The linearization around the equilibrium as described in Sec. 3.3.2 leads to the dynamic cutting force

$$\mathbf{F}_{\text{dyn}}(t) = b \begin{pmatrix} P_1(x_2(t - \tau_1) - x_1(t)) \\ P_2(x_1(t - \tau_2) - x_2(t)) \end{pmatrix}, \quad (7.16)$$

where P_1 and P_2 are the specific cutting pressures at the first and the second cut. The specific cutting pressures P_i are equal to the slope of the cutting force law at the static chip thickness h_i^* , and are defined by

$$P_1 = f'_c(v_f \tau_1 + u_2^* - u_1^*), \quad P_2 = f'_c(v_f \tau_2 + u_1^* - u_2^*). \quad (7.17)$$

The dynamic cutting force $\mathbf{F}_{\text{dyn}}(t)$ is the part of the cutting force that is induced only by the perturbations $\mathbf{x}(t) = \text{col}(x_1(t), x_2(t))$ of the equilibrium \mathbf{u}^* .

7.2.2. Stability lobes for parallel turning

The D-subdivision method that is described in Sec. 5.3 is used for the stability analysis, which means that the parameters are identified, where the eigenmodes are periodic functions $\mathbf{x}_k(t) = \mathbf{q}_k e^{i\omega_k t}$. If Eq. (7.13) is used for the time delays and Eq. (7.16) is transformed into the frequency domain and put into Eq. (7.14), an eigenvalue equation can be obtained for the eigenmodes of the time delay system

$$\mathbf{q}_k = b\mathbf{G}(\omega_k)\mathbf{P}(\omega_k, \Omega_0)\mathbf{q}_k, \quad \mathbf{P}(\omega, \Omega_0) = \begin{pmatrix} -P_1 & P_1 e^{-i\gamma \frac{\omega}{\Omega_0}} \\ P_2 e^{-i(2\pi - \gamma) \frac{\omega}{\Omega_0}} & -P_2 \end{pmatrix}, \quad (7.18)$$

where the matrix \mathbf{P} is the force coefficient matrix. In Eq. (7.18) there are three free parameters b , ω_k and Ω_0 and two scalar equations for the real and the imaginary part of the eigenvalue equation. The stability lobes in the Ω_0 - b -plane for the parallel turning process can be calculated very efficiently with the method described in [188], that can be described as follows. At first, the two eigenvalues $\sigma_{1/2}(\omega, \Omega_0)$ of the matrix product $\mathbf{G}(\omega)\mathbf{P}(\omega, \Omega_0)$ are calculated analytically. Then, a spindle speed Ω_0 is selected. Since b is a real parameter, the frequencies ω_k of the eigenmodes are a discrete set, where the imaginary part of one of the two eigenvalues vanishes, $\text{Im}(\sigma_{1/2}(\omega_k, \Omega_0)) = 0$. If the frequencies ω_k of the eigenmodes are identified, the corresponding critical chip widths b can be calculated from the real part of the eigenvalues as $b = 1/\text{Re}(\sigma_{1/2}(\omega_k, \Omega_0))$. This method can be also applied if the chip width is different at the two different cuts. The method is much simpler than the method proposed in [92, 182], where an additional numerical search algorithm is used to find the solutions of the eigenvalue Eq. (7.18). Moreover, the method can be also used for milling with variable pitch or variable helix tools because in both cases the stability lobes can be approximated very well with time-invariant force coefficient matrices \mathbf{P} [40, 41].

In some situations it is reasonable that the cross FRFs are much smaller than the direct FRFs and can be neglected $G_{12}(\omega) = G_{21}(\omega) = 0$. This means that a cutting force at

Table 7.1.: Structural parameters for the parallel turning process

FRF	Eigenfrequency (Hz)	Damping (N s/m)	Mass (kg)
$G_{11}(\omega)$	120	1800	30
$G_{22}(\omega)$	130	1800	30
$G_{12}(\omega)$	477	1800	10
$G_{21}(\omega)$	477	1800	10

the first tool does not lead to a structural response at the second tool and vice versa. In this case the two eigenvalues $\sigma_{1/2}(\omega, \Omega_0)$ can be given by

$$\sigma_{1/2} = \frac{1}{2} \left(G_1 P_1 + G_2 P_2 \pm \sqrt{(G_1 P_1 - G_2 P_2)^2 + 4 G_1 G_2 P_1 P_2 e^{-i2\pi \frac{\omega}{\Omega_0}}} \right). \quad (7.19)$$

For the sake of clarity, the arguments of the transfer functions were dropped in Eq. (7.19). It turns out that for an uncoupled structural behavior, where the cross FRFs are zero, only the product of the off-diagonal terms of the matrix $\mathbf{P}(\omega, \Omega_0)$ appears in the eigenvalues in Eq. (7.19). As a consequence, the angular displacement γ between the two cutting tools does not affect the stability, even though the process is coupled and the two tools are cutting the same surface. Nevertheless, for a significant structural coupling between the displacements at the two cutting tools, $G_{12}(\omega) \neq 0$ and/or $G_{21}(\omega) \neq 0$, the angle γ between the two tools does also affect the stability lobes.

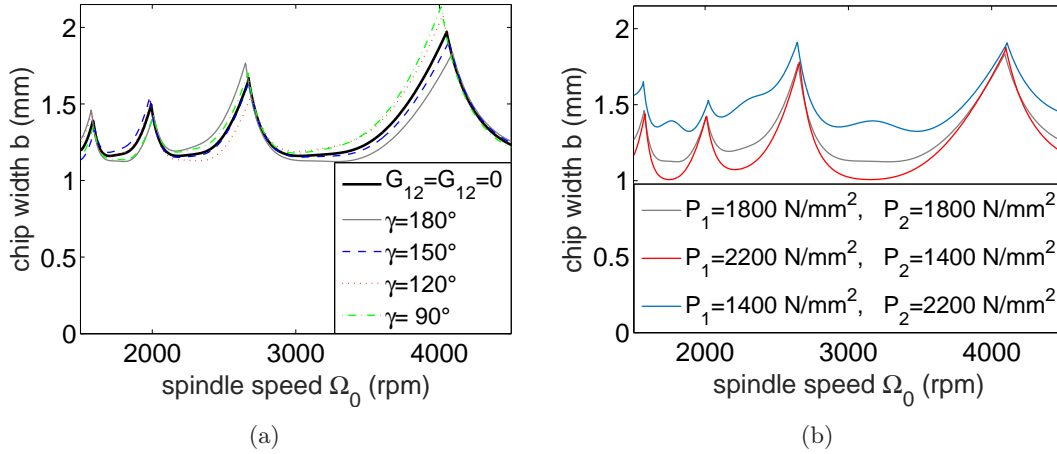


Figure 7.5.: Stability lobes for parallel turning with parameters from Table 7.1. a) For $P_1 = P_2 = 1800 \text{ N/mm}^2$ a varying angle γ between the two tools does not change the stability lobes significantly. b) The process can be stabilized (destabilized) by decreasing (increasing) the cutting force pressure P_1 at the first cut as can be seen from the blue (red) lobes.

7. Applications

A numerical example is considered to present concrete results on the frequency domain stability analysis. The direct FRFs for the dynamic behavior of the two tools and the cross FRFs for the structural coupling between the tools are modeled by single harmonic oscillators. The structural parameters for the oscillators are given in Table 7.1 and are taken from [91]. The stability lobes for the parallel turning process are shown in Fig. 7.5. The process is stable if a chip width b below the stability lobes is chosen. The dependence of the stability lobes on the angle γ between the two tools is shown in Fig. 7.5a for equivalent specific cutting force pressures $P_1 = P_2 = 1800 \text{ N/mm}^2$ at the two tools. As can be derived from Eq. (7.19) the angle γ does not affect the stability if the structure is uncoupled $G_{12} = G_{21} = 0$ (black thick). For non-vanishing cross coupling with the structural parameters from Table 7.1, the stability lobes change with varying γ but the variation is very small. This is due to the fact, that the magnitude of the direct FRFs G_{11} and G_{22} is much larger than the magnitude of the cross FRFs G_{12} and G_{21} , which are responsible for the γ -dependence of the stability lobes. Note, that in this simplified numerical example there is a symmetry with respect to $\gamma = 180^\circ$, which means that, for example, the lobes for $\gamma = 150^\circ$ are equivalent to the lobes for $\gamma = 210^\circ$. In Fig. 7.5b a fixed angle $\gamma = 180^\circ$ was used, and the dependence of the stability lobes on the specific cutting force pressures P_1 and P_2 is illustrated. The mean cutting force pressure is fixed at $(P_1 + P_2)/2 = 1800 \text{ N/mm}^2$. If the two cutting force pressures are equal, the stability lobes are equivalent to the gray solid lobes in Fig. 7.5a. If P_1 is increased and P_2 is decreased, the limiting chip width b becomes smaller (red). In contrast, the process can be stabilized significantly by decreasing the pressure P_1 at the first tool and increasing P_2 (blue). The reason behind this is the lower eigenfrequency of the eigenmode at the first tool, which is equivalent to a lower dynamic stiffness. In other words, the main reason for chatter in this example with the structural parameters from Table 7.1 are unstable self-excited vibrations at the first tool. This means that the process can be stabilized (destabilized) by decreasing (increasing) the specific cutting force pressure P_1 at the first tool, whereas the specific cutting force pressure P_2 at the second tool has only a minor influence on the stability behavior. Different cutting force pressures occur due to the nonlinear cutting force behavior $f_c(h_i)$ and different static chip thicknesses h_1^* and h_2^* at the first and the second tool. In fact, the static chip thicknesses h_i^* at the two cutting tools depend mainly on the angle γ between the two tools, which is the reason for another γ -dependence of the stability lobes in real parallel turning processes.

7.2.3. Turning with spindle speed variation

As a second machining example, a turning process with spindle speed variation (SSV) is studied. A passive SSV occurs in real cutting processes due to an excitation of the spindle drive via a non-stationary process torque [26, 189]. Moreover, an active SSV is used in the industry for a stabilization of cutting processes [22, 23]. The kinematics of the process is similar to the parallel turning process that is shown in Fig. 7.4, where only the first tool is cutting. The time delay in metal cutting is a variable transport delay as described in Sec. 2.2.1. A variation of the spindle speed can lead to a variable delay $\tilde{\tau}(\tilde{t})$ in the physical time \tilde{t} , which is equivalent to a variable time for one revolution of

the spindle. However, if the process is described in terms of the spindle angle t , the delay for the turning process in the so-called internal clock t is always constant $\tau(t) = \tau$. The transformation from elapsed physical time \tilde{t} to the spindle angle t is given by the monotonic increasing function $\Phi(\tilde{t})$ in Eq. (2.3). The derivative of the function $\Phi(\tilde{t})$ is the angular velocity $\Omega(\tilde{t})$ of the spindle. An active SSV is considered, where the angular velocity is assumed to be sinusoidal in the physical time

$$\Omega(\tilde{t}) = \Omega_0(1 + A_\Omega \cos(2\pi f_\Omega \tilde{t})). \quad (7.20)$$

In Eq. (7.20) A_Ω and f_Ω are the relative amplitude and the frequency of the SSV.

A concrete numerical example is considered, where the structural dynamics can be described by one dominant eigenmode with eigenfrequency ω_n and damping ratio ζ . In the physical time the system can be described by a DDE with time-varying delay [180]

$$\begin{aligned} \tilde{\mathbf{x}}'(\tilde{t}) &= \tilde{\mathbf{A}}\tilde{\mathbf{x}}(\tilde{t}) + \tilde{\mathbf{B}}\tilde{\mathbf{x}}(\tilde{t} - \tilde{\tau}(\tilde{t})), \\ \tilde{\mathbf{A}} &= \begin{pmatrix} 0 & 1 \\ -\omega_n^2(1+w) & -2\zeta\omega_n \end{pmatrix}, \quad \tilde{\mathbf{B}} = \begin{pmatrix} 0 & 0 \\ \omega_n^2 w & 0 \end{pmatrix}. \end{aligned} \quad (7.21)$$

The variable transport delay $\tilde{\tau}(\tilde{t})$ in the physical time can be calculated by Eq. (2.7) with the constant delay $\tau = 2\pi$, that is the angle for one spindle revolution. The two dimensional configuration $\tilde{\mathbf{x}}(\tilde{t})$ specifies the velocity and the displacement of the tool tip perturbations in x -direction dependent on the physical time \tilde{t} . In Eq. (7.21) w is the dimensionless chip width that is proportional to the real chip width b . The exact relationship between the dimensionless and the real chip width depends on the cutting force coefficient and the properties of the dominant eigenmode of the structure¹. Since the delay in system Eq. (7.21) is defined by a variable transport over the constant distance $\tau = 2\pi$, the system can be transformed to standard form Eq. (2.1) in the angular domain or the internal clock with constant delay and periodic coefficients

$$\dot{\mathbf{x}}(t) = \mathbf{A}(t)\mathbf{x}(t) + \mathbf{B}(t)\mathbf{x}(t - 2\pi). \quad (7.22)$$

By comparison of Eq. (7.22) and Eq. (7.21) with their general counterparts Eq. (2.1) and Eq. (2.14), respectively, the coefficient matrices can be identified as

$$\mathbf{A}(t) = \frac{1}{\Omega(\Phi^{-1}(t))}\tilde{\mathbf{A}}, \quad \mathbf{B}(t) = \frac{1}{\Omega(\Phi^{-1}(t))}\tilde{\mathbf{B}}. \quad (7.23)$$

The stability analysis of turning with SSV in the angular domain with Eq. (7.22) with a constant angular delay was at first shown in [70]. However, the authors have considered a variable spindle speed $\Omega(t)$ that varies sinusoidally in the internal clock t , which is not the generic case for an application. A more detailed description of the transformation of dynamical systems from the physical time \tilde{t} to the internal clock t can be found in [26, 94], where also the stability lobes for the equivalent systems Eq. (7.21) and Eq. (7.22) are compared.

¹In particular, the orientation, the modal mass and the eigenfrequency of the mode are relevant

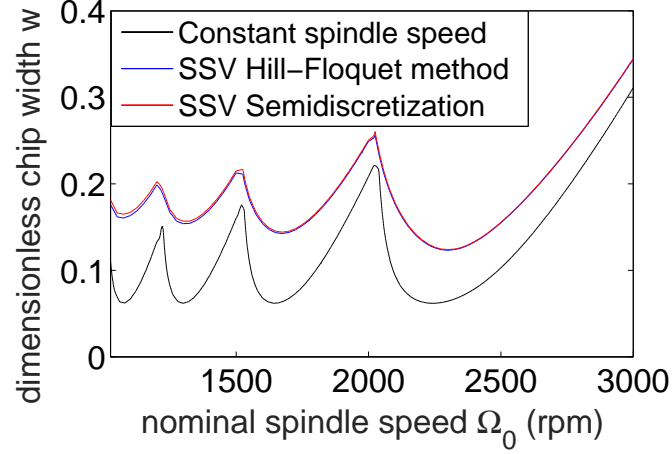


Figure 7.6.: The stability lobes for a turning process with SSV calculated with the Hill-Floquet method (blue) coincide well with the results from [26] (red), which were calculated with the semidiscretization method. The stability lobes for the process with constant spindle speed (black) were also shown.

7.2.4. Stability lobes for turning with spindle speed variation

In this thesis, the example from Ref. [26] is chosen for the calculation of the stability lobes with the Hill-Floquet method from Eq. (7.22) as described in Sec. 6.3. The relative amplitude and the frequency of the spindle speed modulation are given by $A_\Omega = 0.15$ and $f_\Omega = 1$ Hz. The parameters for the structural dynamics are $\omega_n = 2\pi 100s^{-1}$ and $\zeta = 0.03$. The stability lobes are calculated for $n = 150$ higher harmonics and $M = 3$ Chebyshev nodes. The results from the Hill-Floquet method (blue) are shown in Fig. 7.6 and compared to the results from Ref. [26] (red) that were calculated with the semidiscretization method [190]. In addition, the stability lobes for the system with constant spindle speed $A_\Omega = 0$ (black) are shown. The results from both methods coincide very well, even though the number of Chebyshev nodes $M = 3$ is very low. A bottle neck in the Hill-Floquet method is the large number of higher harmonics that must be used, because the frequency f_Ω of the SSV is much lower than the eigenfrequency of the structure. This leads to a worse numerical performance for this specific example with a low modulation frequency.

Nevertheless, the Hill-Floquet method becomes advantageous for very low spindle speeds, because with the Hill-Floquet method the system is transformed to an autonomous system and no monodromy matrix must be calculated. In particular, for lower spindle speeds the delay becomes larger, whereas the frequency of the tool vibrations remains in the neighborhood of the eigenfrequency of the structure. This means that more collocation points are necessary for an approximation of the solution in one delay interval with the semidiscretization. The higher dimension of the transition matrices of the semidiscretization method for low spindle speeds leads to an increasing numerical effort for the calculation of the monodromy matrix and their eigenvalues. Specifically,

for the calculation of the stability lobes in Fig. 7.6 the number of collocation points for the semidiscretization method was fixed to $M = 100$. As a consequence, the accuracy of the semidiscretization (red) decreases for low spindle speeds resulting in very small deviations between the red and the blue curve that can be seen in Fig. 7.6 for low spindle speeds. In contrast, the accuracy of the Hill-Floquet method is very high and does not significantly depend on the nominal spindle speed Ω_0 .

7.3. Networks with heterogeneous coupling delays

Synchronization in complex networks is a well-known phenomena that can be found, for example, in social systems [191, 192], in engineering [193, 194, 195, 196], in biology [156, 197, 198] or in physics [199, 200, 201]. An overview on the synchronization phenomena in classical networks with instantaneous coupling can be found in [202, 203]. However, synchronization is also possible in networks with time-delayed couplings [15, 93]. In some technical applications, for example, in delay-coupled semiconductor lasers [199, 200, 201], the time-delays in the network can be tuned to be homogeneous. However, in real world systems, such as neuronal networks, social networks or connected vehicle systems, the delays in the network are typically heterogeneous, i.e. there are couplings with different delays between different nodes of the network [195]. Such a situation is studied here, where a specific method for the decomposition of the network dynamics for the case of heterogeneous coupling delays is introduced.

7.3.1. Synchronization in heterogeneously delay-coupled networks

In general, the dynamics of a network with d identical oscillators with heterogeneous linear delay coupling can be described by

$$\dot{\mathbf{u}}_i(t) = \mathbf{f}(\mathbf{u}_i(t)) + \frac{1}{d} \sum_{j=1}^d c_{ij} \mathbf{B} \mathbf{u}_j(t - \tau_{ij}), \quad (7.24)$$

where $\mathbf{u}_i \in \mathbb{R}^N$ specifies the configuration of the $i = 1, \dots, d$ oscillators. The solution of the uncoupled oscillators is described by the nonlinear ODE $\dot{\mathbf{u}}_i = \mathbf{f}(\mathbf{u}_i)$. The dynamics of the each oscillator in the network is affect by an additional term corresponding to the delayed coupling with other oscillators. The coupling is specified by the $d \times d$ dimensional adjacency matrix \mathbf{C} and the coupling matrix \mathbf{B} . The elements c_{ij} of the adjacency matrix are equal to one if the current configuration of node i at time t is affected by the configuration of node j at the delayed time $t - \tau_{ij}$, or zero if there is no coupling between the nodes i and j .

A complete synchronized solution, $\mathbf{u}_i(t) = \mathbf{u}_s(t)$ for $i = 1, \dots, d$, is only possible if there is a uniform delay distribution $K_i(\tau) = K(\tau)$ independent of the specific node index i , which is defined by the sum over all discrete delays in the coupling term of one node

$$K_i(\tau) := \frac{1}{d} \sum_{j=1}^d c_{ij} \delta(\tau - \tau_{ij}) = K(\tau). \quad (7.25)$$

7. Applications

Eq. (7.25) is the generalization of the constant row sum condition [93, 204] for networks without delay or networks with homogeneous delays to networks with heterogeneous delays in the coupling. With Eq. (7.25) the dynamics within the so-called synchronization manifold $\mathbf{u}_s(t)$ can be described by the nonlinear DDE with distributed delay

$$\dot{\mathbf{u}}_s(t) = \mathbf{f}(\mathbf{u}_s(t)) + \mathbf{B} \int_0^{\tau_{\max}} K(\tau) \mathbf{u}_s(t - \tau) d\tau. \quad (7.26)$$

The linear variational system can be obtained by studying the behavior of infinitesimal perturbations around the synchronized solution $\mathbf{x}_i(t) = \mathbf{u}_s(t) - \mathbf{u}_i(t)$. In particular, the linearized dynamics can be characterized by

$$\dot{\mathbf{x}}_i(t) = \mathbf{A}(t) \mathbf{x}_i(t) + \frac{1}{d} \sum_{j=1}^d c_{ij} \mathbf{B} \mathbf{x}_j(t - \tau_{ij}), \quad (7.27)$$

where $\mathbf{A}(t)$ is the Jacobian of \mathbf{f} at the synchronized solution $\mathbf{u}_s(t)$ (cf. Sec. 3.3.2).

7.3.2. Representation with the adjacency lag operator

For networks with heterogeneous delays a representation of the coupling terms with lag operators is suitable [195, 205]. The lag operator $\mathcal{S}(\tau)$ is defined as

$$\mathcal{S}(\tau) \mathbf{x}(t) = \mathbf{x}(t - \tau). \quad (7.28)$$

Alternatively, in quantum mechanics the lag operator is defined as $\mathcal{S}(\tau) = e^{-\tau \frac{\partial}{\partial t}}$, which is equivalent to Eq. (7.28). The eigenfunctions of the lag operator are exponential functions $\mathbf{x}(t) = \mathbf{q} e^{st}$

$$\mathcal{S}(\tau) \mathbf{q} e^{st} = e^{-s\tau} \mathbf{q} e^{st}. \quad (7.29)$$

In Eq. (7.29) the eigenvalue $e^{-s\tau}$ depends on the argument τ of the lag operator, whereas the eigenfunctions are exponential functions independent of the argument τ . As a consequence, lag operators with different arguments commute with each other and fulfill the relation

$$\mathcal{S}(\tau_1) \mathcal{S}(\tau_2) = \mathcal{S}(\tau_2) \mathcal{S}(\tau_1) = \mathcal{S}(\tau_1 + \tau_2). \quad (7.30)$$

From Eq. (7.30) it follows that $\mathcal{S}^n(\tau) = \mathcal{S}(n\tau)$, which can be used to calculate roots and the inverse of lag operators. The identity element is given by $\mathcal{S}(0) \mathbf{x}(t) = \mathbf{x}(t)$. Furthermore, the lag operator commutes with the differential operator $\frac{d}{dt} \mathcal{S}(\tau) = \mathcal{S}(\tau) \frac{d}{dt}$, because they share the same eigenfunctions.

With the lag operators Eq. (7.27) can be written as

$$\dot{\mathbf{x}}(t) = (\mathbf{I} \otimes \mathbf{A}(t)) \mathbf{x}(t) + (\mathcal{C} \otimes \mathbf{B}) \mathbf{x}(t), \quad (7.31)$$

where \otimes denotes the direct product and the Nd dimensional vector $\mathbf{x} = \text{col}(\mathbf{x}_1, \dots, \mathbf{x}_d)$ contains the perturbations at all nodes of the network. The matrix of lag operator \mathcal{C} is

called adjacency lag operator and the elements of the adjacency lag operator are given by

$$\{\mathcal{C}\}_{ij} = \frac{1}{d} c_{ij} \mathcal{S}(\tau_{ij}). \quad (7.32)$$

On the one hand, the adjacency lag operator describes the topology of the network, which is characterized by the matrix \mathbf{C} . In addition, the adjacency lag operator contains the information on the coupling delays. For complex networks a decomposition of the dynamics into network eigenmodes is suitable, which is shown next.

7.3.3. Decomposition into network eigenmodes

Many efforts have been made for the stability analysis of the synchronized solution of complex networks based on the eigenmode decomposition of the perturbations \mathbf{x} into network eigenmodes. Note that the network eigenmodes are not to be confused with the eigenmodes of a DDE, which are functions in one delay interval and are described in Sec. 4.4. Instead, the network eigenmodes are in the simplest case the eigenfunctions of the adjacency matrix \mathbf{C} . The stability analysis based on the eigenmode decomposition was at first presented in [204, 206] for networks with instantaneous coupling. The so-called master stability function can be used to analyze the stability of the network dependent on the eigenvalues of the adjacency matrix \mathbf{C} . Later, the master stability approach was extended to the decomposition of the network dynamics in case of parameter mismatches [207, 208] and for the decomposition around cluster states [209]. The master stability function can be also used for networks with delay couplings, as it was presented for homogeneous delay couplings in [93]. For heterogeneous delay couplings, however, the application of the master stability function is restricted to the case, where the separate adjacency matrices for each discrete delay in the coupling commute [210]. In [211] an approach for the eigenmode decomposition was presented for hierarchical networks with a small delay in some subnetworks and a much longer delay for the coupling between the subnetworks. A general approach for the decomposition of the dynamics of heterogeneously delay-coupled networks based on a diagonalization of the operator \mathcal{C} has been shown in [195]. This method can be applied for the decomposition of the network dynamics into eigenmodes for synchronized equilibria but the extension to synchronized time-dependent solutions is not straightforward. In this thesis, the eigenmode decomposition is shown for synchronized time-dependent solutions in networks with arbitrary heterogeneous delays in the coupling.

It is assumed that the adjacency lag operator can be diagonalized as

$$\mathbf{U}(t) \mathcal{C} \mathbf{V}(t) = \mathbf{L}, \quad (7.33)$$

where $\mathbf{U}(t)$ and $\mathbf{V}(t)$ is the matrix of the left and the right eigenvectors and \mathbf{L} is a diagonal matrix with the eigenvalues of the adjacency lag operator on the main diagonal. Since exponential functions are always eigenfunctions of the lag operators $\mathcal{S}(\tau)$ independent of the delay τ in the argument, the eigenfunctions and the eigenvalues of the adjacency lag operator can be written as

$$\mathbf{U}(t) = e^{-st} \mathcal{U}, \quad \mathbf{V}(t) = \mathcal{V} e^{st}, \quad \text{and} \quad \mathbf{L} = e^{-st} \mathcal{L} e^{st}. \quad (7.34)$$

7. Applications

The matrix operators \mathcal{U} , \mathcal{V} contain lag operators equivalent to the formal left and the formal right eigenvectors of the matrix operator \mathcal{C} , and they diagonalize the adjacency lag operator as

$$\mathcal{U}\mathcal{C}\mathcal{V} = \mathcal{L}, \quad (7.35)$$

where \mathcal{L} is a diagonal operator and $\mathcal{U}\mathcal{V} = \mathbf{I}$. With the operators \mathcal{U} and \mathcal{V} the modal coordinates $\mathbf{y}(t)$ on the network level can be defined as

$$\mathbf{x}(t) = (\mathcal{V} \otimes \mathbf{I}) \mathbf{y}(t), \quad \mathbf{y}(t) = (\mathcal{U} \otimes \mathbf{I}) \mathbf{x}(t). \quad (7.36)$$

With Eq. (7.35) and the coordinate transformations in Eq. (7.36) the network dynamics Eq. (7.31) in modal coordinates can be described by

$$\dot{\mathbf{y}}(t) = (\mathcal{U} \otimes \mathbf{I}) (\mathbf{I} \otimes \mathbf{A}(t)) (\mathcal{V} \otimes \mathbf{I}) \mathbf{y}(t) + (\mathcal{L} \otimes \mathbf{B}) \mathbf{y}(t). \quad (7.37)$$

The main difference between the decomposition for equilibria with a time-invariant coefficient matrix $\mathbf{A}(t) = \mathbf{A}_0$ and the decomposition for periodic orbits with a time-varying matrix $\mathbf{A}(t)$ can be seen in the first term on the right hand side of Eq. (7.37). For a constant matrix \mathbf{A}_0 the lag operators in \mathcal{U} or \mathcal{V} always commute with the constant matrix \mathbf{A}_0 and the term can be simplified to $(\mathbf{I} \otimes \mathbf{A}_0)$, which results in d decoupled equations of dimension N in Eq. (7.37). However, this is not true for time-varying matrices $\mathbf{A}(t)$ because, in general, they do not commute with the operators \mathcal{U} or \mathcal{V} . This can be illustrated by the following paradigmatic example. Whereas for constant matrices the term $\mathcal{S}(-\tau)\mathbf{A}_0\mathcal{S}(\tau)\mathbf{x}(t)$ can be simplified to $\mathbf{A}_0\mathbf{x}(t)$, the equivalent relation with a time-varying matrix is not true

$$\mathcal{S}(-\tau)\mathbf{A}(t)\mathcal{S}(\tau)\mathbf{x}(t) = \mathbf{A}(t+\tau)\mathbf{x}(t) \neq \mathbf{A}(t)\mathbf{x}(t). \quad (7.38)$$

As a consequence, for a time-varying coefficient matrix $\mathbf{A}(t)$, in general, the equations in modal coordinates in Eq. (7.37) cannot be decoupled with the eigenfunctions of the adjacency lag operator on the network level. Nevertheless, for the dynamics can be separated on the network level if the elements \mathcal{L}_k of the diagonalized adjacency lag operator \mathcal{L} can be characterized by a linear combination

$$\mathcal{L}_k = \sum_{i,j} \rho_{ij} \mathcal{S}(\tau_{ij}), \quad \rho_{ij} \in \mathbb{C}, \quad (7.39)$$

which contains only time lag operators $\mathcal{S}(\tau_{ij})$ with the coupling delays τ_{ij} . In this case, it can be shown that either the corresponding column \mathcal{V}_k in the matrix operator \mathcal{V} or the corresponding row \mathcal{U}_k^T in the matrix operator \mathcal{U} contain only complex numbers but no lag operators. In this case, the modal dynamics is decoupled and can be described by

$$\dot{\mathbf{y}}_k(t) = \mathbf{A}(t)\mathbf{y}_k(t) + \mathcal{L}_k \mathbf{B}\mathbf{y}_k(t), \quad (7.40)$$

where $\mathbf{y}_k(t)$ is the N dimensional vector of the perturbations in modal coordinates corresponding to the k th network eigenmode. For the tangential eigenmode, that describes perturbations within the synchronization manifold, the corresponding scalar operator \mathcal{L}_{\parallel}

7.3. Networks with heterogeneous coupling delays

can be always written as a linear combination similar to Eq. (7.39). For example, in Eq. (7.39) the coefficients of the lag operator $\mathcal{L}_k = \mathcal{L}_\parallel$ can be given by $d\rho_{ij} = c_{ij}\delta_{i1}$. The eigenvector of the adjacency lag operator corresponding to the tangential eigenmode is characterized by $\mathcal{V}_k = \text{col}(1, \dots, 1)$, which is equivalent to the eigenvector for the tangential eigenmode in networks with homogeneous coupling delays.

Eq. (7.40) is related to the well-known master stability function. For networks without delay the scalar operators \mathcal{L}_k are simply complex numbers without any lag operator [204]. For networks with a homogeneous delay in the coupling, the scalar operators \mathcal{L}_k are a product of the lag operator for the homogeneous delay and a complex number. Thus, in both cases the modal equations for different eigenmodes differ only in a complex number given by different eigenvalues of the adjacency matrix \mathbf{C} . In contrast, for heterogeneous delay couplings the scalar operators \mathcal{L}_k can contain an arbitrary combination of different lag operators, which means that the modal dynamics for varying k can be specified by a DDE with different multiple or distributed delays.

For illustration, a concrete coupling scheme with $N = 5$ nodes and two different delays $\tau_{ij} \in \{\tau_1, \tau_2\}$ is studied. In particular, all nodes are coupled to all other nodes of the network and the adjacency lag operator \mathcal{C} is given by

$$\mathcal{C} = \begin{pmatrix} 0 & \mathcal{S}(\tau_1) & \mathcal{S}(\tau_1) & \mathcal{S}(\tau_1) & \mathcal{S}(\tau_2) \\ \mathcal{S}(\tau_1) & 0 & \mathcal{S}(\tau_2) & \mathcal{S}(\tau_1) & \mathcal{S}(\tau_1) \\ \mathcal{S}(\tau_1) & \mathcal{S}(\tau_2) & 0 & \mathcal{S}(\tau_1) & \mathcal{S}(\tau_1) \\ \mathcal{S}(\tau_1) & \mathcal{S}(\tau_1) & \mathcal{S}(\tau_1) & 0 & \mathcal{S}(\tau_2) \\ \mathcal{S}(\tau_2) & \mathcal{S}(\tau_1) & \mathcal{S}(\tau_1) & \mathcal{S}(\tau_1) & 0 \end{pmatrix}. \quad (7.41)$$

The corresponding diagonalized operator \mathcal{L} can be specified by the diagonal elements

$$\begin{aligned} \mathcal{L}_\parallel = \mathcal{L}_1 &= 3\mathcal{S}(\tau_1) + \mathcal{S}(\tau_2), & \mathcal{L}_3 &= -\mathcal{S}(\tau_1), \\ \mathcal{L}_2 &= -2\mathcal{S}(\tau_1) + \mathcal{S}(\tau_2), & \mathcal{L}_{4,5} &= -\mathcal{S}(\tau_2). \end{aligned} \quad (7.42)$$

According to Eq. (7.42), in this case all entries \mathcal{L}_k of the diagonal operator \mathcal{L} can be written as a linear combination of the two lag operators $\mathcal{S}(\tau_1)$ and $\mathcal{S}(\tau_2)$, which means that the decoupled modal equations Eq. (7.40) can be used for the description of the network dynamics in modal coordinates.

For example, the column vector \mathcal{V}_3 corresponding to the third network eigenmode with the scalar operator \mathcal{L}_3 in Eq. (7.42) is determined by

$$\mathcal{V}_3 = \text{col}(1, 1, 1, -3 - \mathcal{S}(\tau_2 - \tau_1), 1). \quad (7.43)$$

This means that if the transversal network eigenmode $\mathbf{q}_3(t)$ becomes unstable in a network with the adjacency lag operator \mathcal{C} from Eq. (7.41), the network dynamics can be characterized by four nodes that remain synchronized $\mathbf{y}_i(t) = \mathbf{q}_3(t)$ for $i = 1, 2, 3, 5$ and one node that can be characterized by $\mathbf{y}_4(t) = -3\mathbf{q}_3(t) - \mathbf{q}_3(t - \tau_2 + \tau_1)$. Such a time-shifted relation between the dynamics at different nodes for the transversal network eigenmodes is not possible in networks with homogeneous delays but can occur in networks with heterogeneous delay couplings. The second fundamental difference in contrast to networks with homogeneous delays are different multiple or distributed delays in the modal equations Eq. (7.40) for different eigenmodes.

7.3.4. Synchronized delay-coupled Hodgkin-Huxley neurons

Numerical results based on the eigenmode decomposition of the network are shown for the dynamics and the stability of delay-coupled Hodgkin-Huxley neurons with heterogeneous coupling delays. The Hodgkin-Huxley neuronal model is a well-known model in neurodynamics for the description of the voltage activity and the ion transport in the brain [212]. The model is similar to the system studied in [156] and the dynamics at the $i = 1, \dots, d$ nodes of the network can be described by the DDE

$$\begin{aligned}
C\dot{V}_i(t) &= I - g_{\text{Na}}m_i^3(t)h_i(t)(V_i(t) - V_{\text{Na}}) \\
&\quad - g_{\text{K}}n_i^4(t)(V_i(t) - V_{\text{K}}) \\
&\quad - g_{\text{L}}(V_i(t) - V_{\text{L}}) \\
&\quad + \frac{\kappa}{d} \sum_{j=1}^d c_{ij} (V_j(t - \tau_{ij}) - V_i(t)), \\
\dot{m}_i &= \alpha_m(V_i(t))(1 - m_i(t)) - \beta_m(V_i(t))m_i(t), \\
\dot{h}_i &= \alpha_h(V_i(t))(1 - h_i(t)) - \beta_h(V_i(t))h_i(t), \\
\dot{n}_i &= \alpha_n(V_i(t))(1 - n_i(t)) - \beta_n(V_i(t))n_i(t),
\end{aligned} \tag{7.44}$$

where the time t is measured in ms. The voltage V_i of the i -th neuron at the soma is measured in mV. The dimensionless gating variables $m_i, h_i, n_i \in [0, 1]$ characterize the "openness" of the sodium and potassium ion channels embedded in the cell membrane. The equations for m_i, h_i, n_i are based on measurements, where the nonlinear functions are defined by (cf. [213])

$$\begin{aligned}
\alpha_m(V) &= \frac{V/(10\text{mV}) + 4}{1 - e^{-(V/(10\text{mV})+4)}}, \quad \beta_m(V) = 4e^{-(V/(18\text{mV})+3.61)}, \\
\alpha_h(V) &= 0.07e^{-(V/(20\text{mV})+3.25)}, \quad \beta_h(V) = \frac{1}{1 + e^{-(V/(10\text{mV})+3.5)}}, \\
\alpha_n(V) &= \frac{V/(100\text{mV}) + 0.55}{1 - e^{-(V/(10\text{mV})+5.5)}}, \quad \beta_n(V) = 0.125e^{-(V/(80\text{mV})+0.81)}.
\end{aligned} \tag{7.45}$$

The conductances $g_{\text{Na}}, g_{\text{K}}, g_{\text{L}}$, the reference voltages $V_{\text{Na}}, V_{\text{K}}, V_{\text{L}}$, the membrane capacitance C and the driving current I are given in Table 7.2. The coupling term represents a direct electronic connection between the j -th and the i -th neuron, where κ is the conductance of the gap junction and τ_{ij} represents the time for the signal propagation from

Table 7.2.: Fixed parameters of the Hodgkin-Huxley neuronal model in Eq. (7.44)

$V_{\text{Na}} = 50 \text{ mV}$	$V_{\text{K}} = -77 \text{ mV}$	$V_{\text{L}} = -54.4 \text{ mV}$
$g_{\text{Na}} = 120 \frac{\text{mS}}{\text{cm}^2}$	$g_{\text{K}} = 36 \frac{\text{mS}}{\text{cm}^2}$	$g_{\text{L}} = 0.3 \frac{\text{mS}}{\text{cm}^2}$
$C = 1 \frac{\mu\text{F}}{\text{cm}^2}$	$I = 20 \frac{\mu\text{A}}{\text{cm}^2}$	$\kappa = 1.2 \frac{\text{mS}}{\text{cm}^2}$

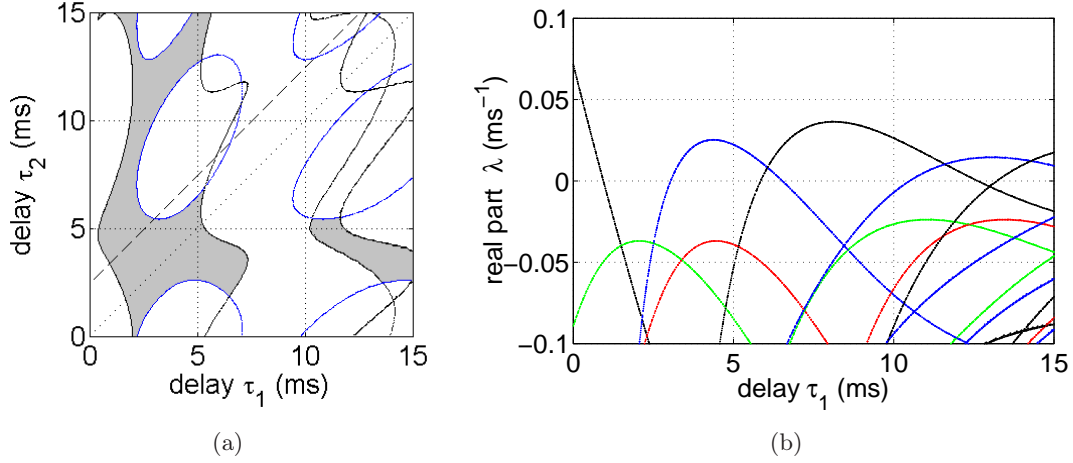


Figure 7.7.: a) Stability chart for the non-trivial equilibrium of the Hodgkin-Huxley neurons Eq. (7.44) with heterogeneous delay coupling Eq. (7.41). b) Dominant characteristic exponent λ_0 for heterogeneous delay with $\tau_2 = \tau_1 + 2.4$ (dashed line in Fig. 7.7a) for the tangential eigenmode (black) and the transversal eigenmodes with \mathcal{L}_2 (blue), \mathcal{L}_3 (red) and $\mathcal{L}_{4,5}$ (green).

the i th to the j th neuron. The conductance κ can be also interpreted as the coupling strength and is fixed to $\kappa = 1.2$ mS/cm² in this example (see Table 7.2). A network with $d = 5$ Hodgkin-Huxley neurons is considered, where the neurons are coupled with the all-to-all coupling scheme from the example in Eq. (7.41).

The system Eq. (7.44) has a non-trivial equilibrium (cf. [156]). The stability of the equilibrium in the τ_1 - τ_2 -plane is shown in Fig. 7.7a. The stability chart was calculated with the D-subdivision method described in Sec. 5.3. The D-curves corresponding to the tangential eigenmode are shown in black. The blue curves are the D-curves for the transversal eigenmode \mathcal{L}_2 in Eq. (7.42). The characteristic exponents for the modal equations associated to the other transversal eigenmodes with the operators \mathcal{L}_3 and $\mathcal{L}_{4,5}$ in Eq. (7.42) does not cross the imaginary axis in the given parameter region, and therefore, no D-curves corresponding to these eigenmodes can be found in Fig. 7.7a. This means, that these eigenmodes do not lead to an instability for time delays $\tau_1, \tau_2 \in [0, 15]$ ms. As can be seen from Fig. 7.7a for homogeneous delay coupling, i.e. the identity $\tau_1 = \tau_2$, only the tangential network eigenmode can become unstable. Thus, for the Hodgkin-Huxley neurons with only one homogeneous delay in the coupling, an unstable synchronized equilibrium typically leads to a synchronized periodic solution. Time delays corresponding to a stable synchronized equilibrium are shaded in Fig. 7.7a. Other delay combinations correspond to an unstable equilibrium. For heterogeneous delay coupling it is also possible that the transversal eigenmode $\mathbf{y}_2(t)$ leads to an instability of the equilibrium. This is illustrated in Fig. 7.7b for $\tau_2 = \tau_1 + 2.4$ ms, i.e. the dashed line in Fig. 7.7a, where the real part λ_0 of the dominant characteristic exponents of the modal equations Eq. (7.40) as a function of τ_1 is shown. In particular, the black, blue, red and green curves in Fig. 7.7b

7. Applications

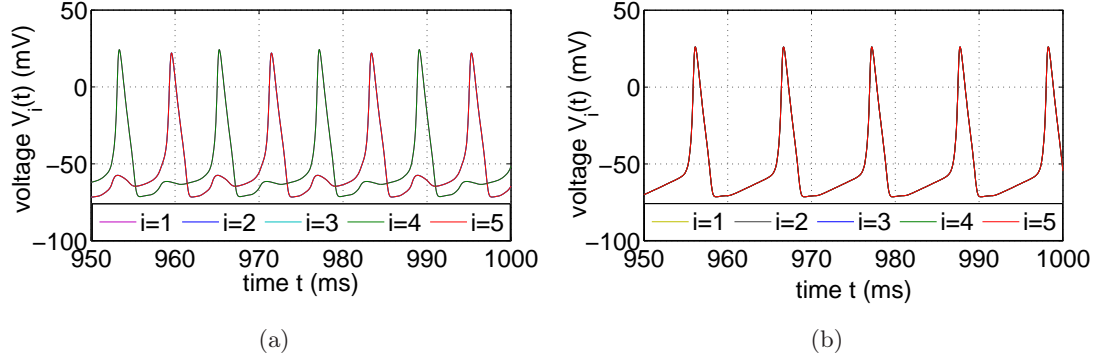


Figure 7.8.: Asymptotic solution of the Hodgkin-Huxley neurons Eq. (7.44) with heterogeneous delay coupling Eq. (7.41) for $\tau_2 = \tau_1 + 2.4$ ms. a) For $\tau_1 = 5$ ms, where the transversal eigenmode is unstable, alternating spiking of two clusters can be seen. b) For $\tau_1 = 10$ ms, where the tangential eigenmode is unstable, complete synchronized spiking appears.

correspond to the dominant exponents for the eigenmodes that are characterized by the operators $\mathcal{L}_1, \mathcal{L}_2, \mathcal{L}_3$ and $\mathcal{L}_{4,5}$ in Eq. (7.42), respectively. Consistent to Fig. 7.7a, only the tangential eigenmode (black) and the first transversal eigenmode (blue) can become unstable. Specifically, the synchronized equilibrium is stable for $\tau_1 \in [0.95, 3]$ ms. For $\tau_1 \in \{[0, 0.95], [6.05, 11.6], [14.3, 15]\}$ ms the equilibrium is unstable and the system is dominated by the unstable tangential network eigenmode. However, for $\tau_1 \in [3, 6.05]$ ms and for $\tau_1 = [11.6, 14.3]$ ms the system is unstable but dominated by an unstable transversal eigenmode, which means that in this case a desynchronized solution bifurcates from the synchronized equilibrium.

Two examples for the asymptotic solution of the network with the coupling from Eq. (7.41) are shown in Fig. 7.8 with the two delays τ_1 and $\tau_2 = \tau_1 + 2.4$, which corresponds to the dashed line in Fig. 7.7a and the dominant characteristic exponents in Fig. 7.7b. The asymptotic solution for $\tau_1 = 5$ is shown in Fig. 7.8a. In this case the synchronized equilibrium is unstable with an unstable transversal eigenmode. Indeed, in Fig. 7.8a not all nodes are synchronized but rather cluster synchronization appears, where the network dynamics is characterized by an alternating spiking of the two clusters. In contrast, for $\tau_1 = 10$ the instability of the equilibrium is due to an unstable tangential eigenmode. As a consequence, a complete synchronized period solution appears in Fig. 7.8b, where all neurons of the networks are spiking simultaneously.

The bifurcation diagrams for the network dynamics is shown for homogeneous coupling delays $\tau_1 = \tau_2$ in Fig. 7.9a and heterogeneous coupling delays $\tau_2 = \tau_1 + 2.4$ ms in Fig. 7.9b. The diagrams are taken from [205] and were calculated with DDE-Biftool [123] for the synchronized solution of the network that is described by the DDE Eq. (7.26). A stable and unstable synchronized solution is marked in Fig. 7.9 by solid red and solid green lines, respectively. In addition, the stability of the synchronized equilibria and the periodic solutions with respect to transversal perturbations was calculated by using the Hill-Floquet

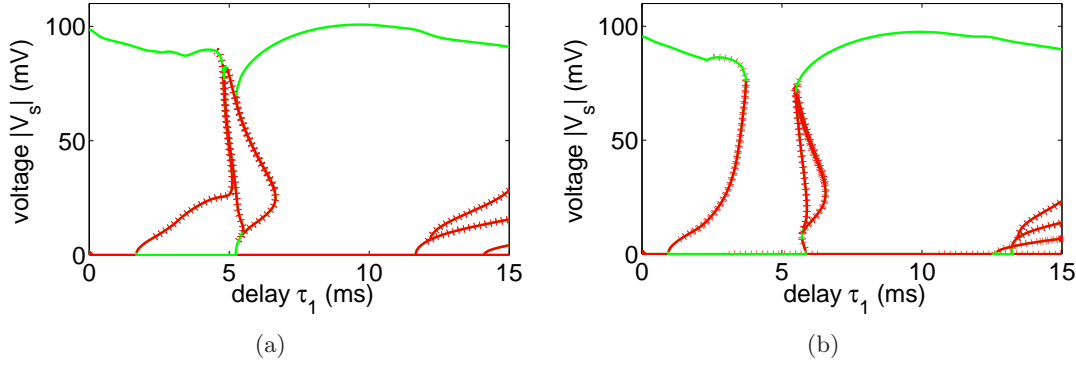


Figure 7.9.: Bifurcation diagram that shows the peak-to-peak amplitude of synchronized solutions of the Hodgkin-Huxley neurons Eq. (7.44) with the coupling scheme Eq. (7.41) as a function of the delay τ_1 . a) For homogeneous delays $\tau_1 = \tau_2$ either the synchronized equilibrium or the synchronized periodic orbit is stable (green, solid). b) For heterogeneous delays with $\tau_2 = \tau_1 + 2.4$ ms in the interval $\tau_1 \in [3.05, 5.7]$ at least one transversal eigenmode of the solution is unstable (red, dashed).

method from Chapter 6 for the calculation of the dominant Floquet exponents for the modal equations Eq. (7.40). Unstable transversal eigenmodes are marked by red dashed lines in Fig. 7.9. For $\tau_1 = \tau_2$ in Fig. 7.9a, which corresponds to the identity line in Fig. 7.7a, either the complete synchronized equilibrium or a complete synchronized periodic solution is stable. In contrast, for $\tau_2 = \tau_1 + 2.4$ ms in Fig. 7.9b, that corresponds to the dashed line in Fig. 7.7a, for $\tau_1 \in [3.05, 5.7]$ neither the synchronized equilibrium nor a synchronized periodic solution is stable. In this case, one example for the asymptotic solution of the network is the cluster synchronized state in Fig. 7.8a. As a result, one can conclude that heterogeneous delays in the coupling facilitate desynchronization in all-to-all coupled networks of Hodgkin-Huxley neurons. More results on heterogeneously delay-coupled Hodgkin Huxley neurons can be found in [205].

7.4. Summary

In this chapter specific applications were presented, where frequency domain methods are suitable for the analysis of the system. In Sec. 7.1 the stability of equilibria of single-species reaction-diffusion systems with distributed delay were studied. In particular, the focus lay on diffusion-driven instabilities because they are a source for time-invariant and time-varying spatial pattern in spatially extended systems. It was shown that classical Turing instabilities resulting in time-invariant Turing pattern are not possible in single-species reaction-diffusion systems. However, wave instabilities are possible in reaction-diffusion systems with asymmetrically distributed or time-varying delay in the reaction term. The wavenumber and frequencies of the resulting Turing-like traveling waves in

7. Applications

the Fisher-KPP equation with delay Eq. (7.8) are very close to the results of the linear stability analysis.

In Sec. 7.2 the stability of self-excited mechanical vibrations in turning processes was studied. For parallel turning processes a very simple and efficient method for the calculation of the stability chart was presented, which represents an extension of the results in [188]. This frequency domain method is based on the solution of the eigenvalue problem in Eq. (7.18), and is suitable for the analysis of the influence of different process parameters on the stability lobes. Specifically, it was shown in this thesis that the angle between the two cutting tools in parallel turning processes does not affect the stability of the process if the structural coupling between the two tools is negligible. Moreover, it is illustrated by an example that often only the regenerative effect at one tool dominates the behavior of the stability lobes, whereas the influence of the regeneration at the other tool on the stability is small. Moreover, with the example of a turning process with SSV it was shown that, according to the results from Sec. 2.2, time delay models for metal cutting processes with variable delays due to a variation of the spindle speed are equivalent to time delay systems with constant delays. For this example the stability results from the Hill-Floquet method were verified with existing results for the stability lobes from the literature.

Finally, in Sec. 7.3 the stability of synchronized solutions in networks with heterogeneous delay coupling was studied. The results from [195] for the modal decomposition of the network dynamics for synchronized equilibria was extended to the decomposition of time-dependent solutions of the network with heterogeneous delays. The decomposition is based on the adjacency lag operator \mathcal{C} , which contains the information on the topology of the network as well as the information on the time delays of the coupling. The diagonalization of the adjacency lag operator \mathcal{C} can be used to obtain the decoupled modal equations Eq. (7.40) similar to the master stability function for networks without time delays or with homogeneous delays in the coupling. Specifically, in the classical master stability function the stability is calculated as a function of a complex number, which is equivalent to the eigenvalue of the adjacency matrix, whereas in the extended version Eq. (7.40) for networks with heterogeneous delays the stability of different network eigenmodes can be determined by DDEs with different distributed delays, where the distributed delays are related to the eigenvalues of the adjacency lag operator \mathcal{C} . A specific example is shown for a network of five all-to-all coupled Hodgkin-Huxley neurons. The results show that in comparison to a network with homogeneous coupling delays, the network with heterogeneous delays is characterized by larger parameter regions with unstable transversal eigenmodes.

8. Concluding remarks

In this thesis frequency domain methods for the linear stability analysis of time delay systems are studied. The main contribution is the introduction of a general framework for the analysis of linear systems with periodic coefficients in the frequency domain, which is called Hill-Floquet method. The Hill-Floquet method transforms a non-autonomous system with periodic coefficients to a higher dimensional autonomous system with constant coefficients. The autonomous system is given by the autonomous differential equation in the time domain, which is associated with the Hill's infinite determinant as the characteristic equation. Thus, the Hill-Floquet method is a generalization of the Hill's infinite determinant method. Until now, the Hill's infinite determinant for the analysis of periodic time delay systems was only used for specific applications, for example, where a harmonic variation of the coefficients appears or where a small number of higher harmonics is sufficient for an accurate approximation. In the field of machine-tool chatter the method is known as multifrequency approach and often used for the calculation of stability charts with specific numerical tools for finding the roots of the Hill's infinite determinant. With the newly introduced Hill-Floquet method the frequency domain analysis of periodic time delay systems becomes usable for a wide area of applications because a general framework for the construction of the Hill-Floquet system and its numerical analysis was presented. In fact, many numerical tools for the analysis of autonomous time delay systems, such as the calculation of Floquet exponents with the Chebyshev collocation method as shown in Sec. 6.3, are now applicable to periodic time delay systems. In addition to the analysis of time delay systems, the method can be also used for the analysis of quantum systems with non-local potentials (cf. [76]).

In this thesis, the Hill-Floquet transformation was presented for DDEs with a constant delay distribution. A future generalization of the method to systems with a variable delay distribution may be useful because a transformation of a system with a variable delay distribution to a system with a constant delay distribution is not always possible as it was shown in Sec. 2.2. Moreover, in future work the efficiency of the Hill-Floquet method can be compared in detail to established methods for the analysis of periodic time delay systems such as the semidiscretization method [3] or the spectral element method [74], where more detailed results on the numerical effort, the convergence and the numerical error can be derived. In this thesis, the periodic coefficients and the periodic part of the solution are expanded in a Fourier series similar to the original work of Hill [77]. Nevertheless, in general, the expansion of the periodic part in an arbitrary set of basis functions is possible and an arbitrary method for the minimization of the error can be used. This opens a new field of numerical methods for the analysis of periodic systems, which are not based on the calculation of the monodromy matrix as described in Sec. 5.2.2, but rather are based on the transformation of the system to an autonomous system by a

8. Concluding remarks

series expansion for the periodic part of the solution.

In Sec. 2.2 it was shown that only systems with a time-varying or state-dependent delay distribution, which has its origin in a transport with a variable velocity over constant distances and is called variable transport delay, are equivalent to systems with a constant delay distribution. In fact, for a parameter family of discrete sinusoidally-varying delays it was shown, that, in addition to variable transport delays, a second type of so-called dissipative delays appear. For discrete delays the delay type can be identified by the dynamical properties of the retarded access map, which is defined in Eq. (2.16b). A zero Lyapunov exponent of the access map corresponds to variable transport delays, which are conjugate to constant delays, whereas a negative access map Lyapunov exponent is associated with discrete dissipative delays. At the moment, the effects of the dynamical properties of the retarded access map on the dynamics of the corresponding time delay systems are not completely clear. In [100] it is shown that the scaling of the Lyapunov spectrum of the time delay systems changes qualitatively for changing the delay type from a variable transport delay to a dissipative delay. Studying the effects of different dynamics of the retarded access map on the dynamics of the corresponding time delay system opens a new direction in the analysis of time delay systems with many open questions. For example, there is no strategy for the identification of variable transport delays from a variable delay distribution and it is not clear how the results from [100] can be extended to multiple or distributed delays.

Apart from the basic results on the equivalence of time delay systems in Chapter 2, the fundamental results on the analysis of linear DDEs in Chapter 4 and the newly introduced Hill-Floquet method in Chapter 6, new results on some specific applications with time delay effects were presented in Chapter 7. In particular, it was shown that Turing-like waves can occur already in single species reaction-diffusion systems with a distributed delay in the reaction term. More precisely, the stability of equilibria of delayed reaction-diffusion systems was studied systematically, where the well-known frequency domain methods for the analysis of autonomous systems were used. However, in general, the presented frequency domain methods are also suitable for the stability analysis of time-periodic pattern in spatially extended systems. Frequency domain methods for the stability analysis of time delay systems are often used for the analysis of machine tool vibrations in metal cutting processes. In this example, it was shown that a specific D-subdivision method for the calculation of the stability lobes is very useful for getting insight into the effects of different parameters on the stability of the system. Finally, a new method for the decomposition of synchronized solutions for networks with heterogeneous delay couplings was presented. The decomposition can be used to extend the well-known Master stability approach to networks with heterogeneous delays. Specifically, the presented approach is very useful for network design, where the node dynamics and the network topology is fixed but a desired synchronization behavior should be obtained by changing the coupling delays.

Bibliography

- [1] M.C. Mackey and L. Glass. Oscillation and chaos in physiological control systems. *Science*, 197(4300):287–289, 1977.
- [2] Y. Altintas. *Manufacturing automation: metal cutting mechanics, machine tool vibrations, and CNC design*. Cambridge University Press, New York, 2000.
- [3] T. Insperger and G. Stépán. *Semi-Discretization for Time-Delay Systems: Stability and Engineering Applications*. Springer, 2011.
- [4] S. A. Tobias. *Schwingungen an Werkzeugmaschinen*. Hanser, München, 1961.
- [5] O. Danek, M. Polacek, J. Spacek, and J. Tlustý. *Selbsterregte Schwingungen an Werkzeugmaschinen*. VEB Technik Berlin, Berlin, 1962.
- [6] E. Tziperman, L. Stone, M.A. Cane, and H. Jarosh. El niño chaos: Overlapping of resonances between the seasonal cycle and the pacific ocean-atmosphere oscillator. *Science*, 264(5155):72–74, 1994.
- [7] M. Ghil, I. Zaliapin, and S. Thompson. A delay differential model of ENSO variability: parametric instability and the distribution of extremes. *Nonlin. Proc. Geophys.*, 15:417–433, 2008.
- [8] K. Gopolsamy. *Stability and Oscillations in Delay Differential Equations of Population Dynamics*. Kluwer Academic, 1992.
- [9] Y. Kuang. *Delay Differential Equations: With Applications in Population Dynamics*. Academic Press, 1993.
- [10] H. Smith. *An Introduction to Delay Differential Equations With Applications to the Life Sciences*. Springer, 2010.
- [11] J.-P. Richard. Time-delay systems: an overview of some recent advances and open problems. *Automatica*, 39(10):1667–1694, 2003.
- [12] H. G. Schuster and E. Schöll. *Handbook of Chaos Control*. Wiley-VCH, 2007.
- [13] K. Pyragas. Continuous control of chaos by self-controlling feedback. *Phys. Lett. A*, 170(6):421–428, 1992.
- [14] F.M. Atay, J. Jost, and A. Wende. Delays, connection topology, and synchronization of coupled chaotic maps. *Phys. Rev. Lett.*, 92:144101, 2004.

Bibliography

- [15] M. Lakshmanan and D.V. Senthilkumar. *Dynamics of Nonlinear Time-Delay Systems*. Springer, 2011.
- [16] V. B. Kolmanovskij and A. Myshkis. *Introduction to the theory and applications of functional differential equations*. Kluwer Academy, Dordrecht, 1999.
- [17] S. Madrugá, S. Boccaletti, and M. A. Matias. Effect of a variable delay in delayed dynamical systems. *Int. J. Bifur. Chaos*, 11(11):2875–2880, 2001.
- [18] D. Schley, R. Shail, and S.A. Gourley. Stability criteria for differential equations with variable time delays. *Int. J. Math. Educ. Sci. Technol.*, 33(3):359–375, 2002.
- [19] H.L. Smith. Reduction of structured population models to threshold-type delay equations and functional differential equations: a case study. *Math. Bio.*, 113(1):1 – 23, 1993.
- [20] J. Bélair, M.C. Mackey, and J.M. Mahaffy. Age-structured and two-delay models for erythropoiesis. *Math. Biosci.*, 128(1–2):317 – 346, 1995.
- [21] J.M. Mahaffy, J. Bélair, and M.C. Mackey. Hematopoietic model with moving boundary condition and state dependent delay: Applications in erythropoiesis. *J. Theor. Bio.*, 190(2):135 – 146, 1998.
- [22] M. Zatarain, I. Bediaga, J. Muñoa, and R. Lizarralde. Stability of milling processes with continuous spindle speed variation: Analysis in the frequency and time domains, and experimental correlation. *CIRP Ann.*, 57(1):379 – 384, 2008.
- [23] A. Otto and G. Radons. Application of spindle speed variation for chatter suppression in turning. *CIRP J. Manuf. Sci. Technol.*, 6(2):102–109, 2013.
- [24] T. Insperger, G. Stépán, and J. Turi. State-dependent delay in regenerative turning processes. *Nonlin. Dyn.*, 47:275–283, 2007.
- [25] S.A. Voronov, A.M. Gouskov, A.S. Kvashnin, E.A. Butcher, and S.C. Sinha. Influence of torsional motion on the axial vibrations of a drilling tool. *J. Comput. Nonlinear Dynam.*, 2(1):58–64, 2007.
- [26] A. Otto and G. Radons. The influence of tangential and torsional vibrations on the stability lobes in metal cutting. *Nonlin. Dyn.*, 82:1989–2000, 2015.
- [27] A. Gjurchinovski and V. Urumov. Stabilization of unstable steady states by variable-delay feedback control. *EPL (Europhys. Lett.)*, 84(4):40013, 2008.
- [28] A. Gjurchinovski and V. Urumov. Variable-delay feedback control of unstable steady states in retarded time-delayed systems. *Phys. Rev. E*, 81:016209, 2010.
- [29] T. Jüngling and A. Gjurchinovski and V. Urumov. Experimental time-delayed feedback control with variable and distributed delays. *Phys. Rev. E*, 86:046213, 2012.

- [30] V. Pyragas and K. Pyragas. Adaptive modification of the delayed feedback control algorithm with a continuously varying time delay. *Phys. Lett. A*, 375(44):3866 – 3871, 2011.
- [31] G. Ambika and R.E. Amritkar. Anticipatory synchronization with variable time delay and reset. *Phys. Rev. E*, 79:056206, 2009.
- [32] Y. Sugitani, K. Konishi, and N. Hara. Experimental verification of amplitude death induced by a periodic time-varying delay-connection. *Nonlin. Dyn.*, 70(3): 2227–2235, 2012.
- [33] A. Gjurchinovski, A. Zakharova, and E. Schöll. Amplitude death in oscillator networks with variable-delay coupling. *Phys. Rev. E*, 89:032915, 2014.
- [34] Y. Sugitani, K. Konishi, and N. Hara. Delay- and topology-independent design for inducing amplitude death on networks with time-varying delay connections. *Phys. Rev. E*, 92:042928, 2015.
- [35] D. P. Rosin, D. Rontani, and D. J. Gauthier. Synchronization of coupled boolean phase oscillators. *Phys. Rev. E*, 89:042907, 2014.
- [36] J. Martínez-Llinàs, X. Porte, M. C. Soriano, P. Colet, and I. Fischer. Dynamical properties induced by state-dependent delays in photonic systems. *Nat. Commun.*, 6:7425, 2015.
- [37] J.M. Cushing and J.M. Cushing. *Integrodifferential equations and delay models in population dynamics*. Springer, 1977.
- [38] S. Ruan. Delay differential equations in single species dynamics. In O. Arino, M.L. Hbid, and E. Ait Dads, editors, *Delay Differential Equations and Applications*, pages 477–517. Springer, 2006.
- [39] S. A. Campbell and R. Jessop. Approximating the stability region for a differential equation with a distributed delay. *Math. Mod. Nat. Phenom.*, 4(2):1–27, 2009.
- [40] V. Sellmeier and B. Denkena. Stable islands in the stability chart of milling processes due to unequal tooth pitch. *Int. J. Mach. Tools Manuf.*, 51:152 – 164, 2011.
- [41] A. Otto and G. Radons. Frequency domain stability analysis of milling processes with variable helix tools. *Proc. 9th Int. Conf. on HSM, San Sebastian, Spain, March 7-8*, 2012.
- [42] D. Bachrathy and G. Stepan. Improved prediction of stability lobes with extended multi frequency solution. *CIRP Ann.*, 62(1):411 – 414, 2013.
- [43] J. G. Milton. Time delays and the control of biological systems: An overview. *IFAC-PapersOnLine*, 48(12):87 – 92, 2015.

Bibliography

- [44] E. Budak and A. Tekeli. Maximizing chatter free material removal rate in milling through optimal selection of axial and radial depth of cut pairs. *CIRP Ann.*, 54(1): 353 – 356, 2005.
- [45] J.J. Zulaika, F.J. Campa, and L.N. Lopez de Lacalle. An integrated process-machine approach for designing productive and lightweight milling machines. *Int. J. Mach. Tools Manuf.*, 51(7–8):591 – 604, 2011.
- [46] M. Law, Y. Altintas, and A. S. Phani. Rapid evaluation and optimization of machine tools with position-dependent stability. *Int. J. Mach. Tools Manuf.*, 68:81 – 90, 2013.
- [47] V. B. Kolmanovskij and V. R. Nosov. *Stability of functional differential equations*. Academic Press, Orlando, 1986.
- [48] S.I. Niculescu. *Delay Effects on Stability: A Robust Control Approach*. Springer London, 2003.
- [49] A.M. Lyapunov. *General Problem of the Stability Of Motion (translated by A.T. Fuller, original work from 1892)*. Taylor & Francis, 1992.
- [50] R. Bellmann and K.L. Cooke. *Differential-Difference Equations*. Academic Press, 1963.
- [51] G. Stépán. *Retarded Dynamical Systems: Stability and Characteristic Functions*. Longman Scientific & Technical, 1989.
- [52] W. Michiels and S.I. Niculescu. *Stability, Control, and Computation for Time-Delay Systems: An Eigenvalue-Based Approach, Second Edition*. Cambridge University Press, 2014.
- [53] D. Breda, S. Maset, and R. Vermiglio. *Stability of Linear Delay Differential Equations: A Numerical Approach with MATLAB*. Springer, 2014.
- [54] E. Jarlebring. *The spectrum of delay-differential equations: numerical methods, stability and perturbation*. PhD thesis, Inst. Comp. Math, TU Braunschweig, 2008.
- [55] T. Insperger, D. Lehotzky, and G. Stepan. Regenerative delay, parametric forcing and machine tool chatter: A review. *IFAC-PapersOnLine*, 48(12):322 – 327, 2015.
- [56] G. Stépán and T. Insperger. Stability of time-periodic and delayed systems — a route to act-and-wait control. *Ann. Rev. Control*, 30(2):159 – 168, 2006.
- [57] T. Insperger, P. Wahi, A. Colombo, G. Stépán, M. Di Bernardo, and S.J. Hogan. Full characterization of act-and-wait control for first-order unstable lag processes. *J. Vib. Control*, 16(7-8):1209–1233, 2010.
- [58] K. Konishi, H. Kokame, and N. Hara. Delayed feedback control based on the act-and-wait concept. *Nonlin. Dyn.*, 63(3):513–519, 2011.

- [59] T. Insperger and G. Stépán. Stability chart for the delayed Mathieu equation. *Phil. Trans. Royal Soc. A*, 458(2024):1989–1998, 2002.
- [60] N.K. Garg, B.P. Mann, N.H. Kim, and M.H. Kurdi. Stability of a time-delayed system with parametric excitation. *J. Dyn. Sys. Meas. Control*, 129:125–135, 2006.
- [61] D. Bachrathy, G. Stépán, and J. Turi. State dependent regenerative effect in milling processes. *J. Comput. Nonlinear Dynam.*, 6(4):041002, 2011.
- [62] J.K. Hale and S.M.V. Lunel. *Introduction to Functional Differential Equations*. Springer, 1993.
- [63] O. Diekmann, S. A. van Gils, S. M. Verduyn Lunel, and H. O. Walther. *Delay Equations*. Springer, New York, 1995.
- [64] E. I. Verriest. Inconsistencies in systems with time-varying delays and their resolution. *IMA J. Math. Control Inform.*, 28(2):147–162, 2011.
- [65] E. Verriest. State space for time varying delay. In R. Sipahi, T. Vyhlídal, S.-I. Niculescu, and P. Pepe, editors, *Time Delay Systems: Methods, Applications and New Trends*, pages 135–146. Springer, 2012.
- [66] F. Hartung, T. Krisztin, H.-O. Walther, and J. Wu. Functional differential equations with state-dependent delays: Theory and applications. In P. Drabek A. Canada and A. Fonda, editors, *Handbook of Differential Equations: Ordinary Differential Equations*, pages 435 – 545. North-Holland, 2006.
- [67] J. Sieber. Finding periodic orbits in state-dependent delay differential equations as roots of algebraic equations. *Discrete Contin. Dyn. Syst.*, 32(8):2607–2651, 2012.
- [68] S.G. Margolis and J.J. O’Donnell. Rigorous treatments of variable time delays. *IEEE Trans. Electron. Comput.*, 12(3):307–309, 1963.
- [69] J.P. Seddon and R.A. Johnson. The simulation of variable delay. *IEEE Trans. Comp.*, C-17:89 –94, 1968.
- [70] T.C. Tsao, M.W. McCarthy, and S.G. Kapoor. A new approach to stability analysis of variable speed machining systems. *Int. J Mach. Tools Manuf.*, 33(6):791 – 808, 1993.
- [71] K. Zenger and A.J. Niemi. Modelling and control of a class of time-varying continuous flow processes. *J Proc. Control*, 19(9):1511 – 1518, 2009.
- [72] F. Zhang and M. Yeddanapudi. Modeling and simulation of time-varying delays. In *Proc. of TMS/DEVs*, pages 34:1–34:8, San Diego, CA, USA, 2012. SCS.
- [73] E. Butcher and B. Mann. Stability analysis and control of linear periodic delayed systems using Chebyshev and temporal finite element methods. In D. E. Gilsinn, T. Kalmár-Nagy, and B. Balachandran, editors, *Delay Differential Equations*, pages 93–129. Springer, 2009.

Bibliography

- [74] F.A. Khasawneh and B.P. Mann. A spectral element approach for the stability of delay systems. *Int. J. Numer. Meth. Eng.*, 87(6):566–592, 2011.
- [75] M. Farkas. *Periodic Motions*. Springer New York, 1994.
- [76] F. L. Traversa, M. Di Ventra, and F. Bonani. Generalized Floquet theory: Application to dynamical systems with memory and Bloch’s theorem for nonlocal potentials. *Phys. Rev. Lett.*, 110:170602, 2013.
- [77] G.W. Hill. On the part of the motion of the lunar perigee which is a function of the mean motions of the sun and moon. *Acta Mathematica*, 8(1):1–36, 1886.
- [78] J. W. Rayleigh. On the maintenance of vibrations by forces of double frequency, and on the propagation of waves through a medium endowed with a periodic structure. *Phil. Mag. J. Sci.*, 24:145–159, 1887.
- [79] C. Kittel. *Introduction to solid state physics*. Wiley, 1971.
- [80] N.W. Ashcroft and N.D. Mermin. *Solid state physics*. Saunders College, 1976.
- [81] D. J. Segalman and E. A. Butcher. Suppression of regenerative chatter via impedance modulation. *J. Vibr. Control*, 6(2):243–256, 2000.
- [82] S. Jayaram, S.G. Kapoor, and R.E. DeVor. Analytical stability analysis of variable spindle speed machining. *J. Manuf. Sci. Eng.*, 122(3):391–397, 2000.
- [83] T.L. Schmitz and K.S. Smith. *Machining Dynamics: Frequency Response to Improved Productivity*. Springer, 2008.
- [84] K. Gopalan. *Introduction to Signal and System Analysis*. Cengage Learning, 2012.
- [85] E. Barsoukov and J.R. Macdonald. *Impedance Spectroscopy: Theory, Experiment, and Applications*. Wiley, 2005.
- [86] A. Altland and B. Simons. *Condensed Matter Field Theory*. Cambridge University Press, 2006.
- [87] K. Warwick. *An Introduction to Control Systems*. World Scientific, 1996.
- [88] A. Amann, E. Schöll, and W. Just. Some basic remarks on eigenmode expansions of time-delay dynamics. *Physica A*, 373:191–202, 2007.
- [89] T. J. McKetterick and L. Giuggioli. Exact dynamics of stochastic linear delayed systems: Application to spatiotemporal coordination of comoving agents. *Phys. Rev. E*, 90:042135, 2014.
- [90] J. Petit, T. Carletti, M. Asllani, and D. Fanelli. Delay-induced Turing-like waves for one-species reaction-diffusion model on a network. *EPL (Europhysics Letters)*, 111(5):58002, 2015.

- [91] C. Brecher, A. Epple, S. Neus, and M. Fey. Optimal process parameters for parallel turning operations on shared cutting surfaces. *Int. J. Mach. Tools Manuf.*, 95:13 – 19, 2015.
- [92] E. Ozturk, A. Comak, and E. Budak. Tuning of tool dynamics for increased stability of parallel (simultaneous) turning processes. *J. Sound Vibr.*, 360:17 – 30, 2016.
- [93] V. Flunkert, S. Yanchuk, T. Dahms, and E. Schöll. Synchronizing distant nodes: A universal classification of networks. *Phys. Rev. Lett.*, 105:254101, 2010.
- [94] A. Otto and G. Radons. Transformations from variable delays to constant delays with applications in engineering and biology. In T. Insperger, G. Orosz, and T. Ersal, editors, *Advances in Delays and Dynamics*. Springer, to appear.
- [95] D. Bresch-Pietri, J. Chauvin, and N. Petit. Prediction-based stabilization of linear systems subject to input-dependent input delay of integral-type. *IEEE Trans. Autom. Contr.*, 59(9):2385–2399, 2014.
- [96] D. Bresch-Pietri and N. Petit. Implicit integral equations for modeling systems with a transport delay. In E. Witrant, E. Fridman, O. Sename, and L. Dugard, editors, *Recent Results on Time-Delay Systems: Analysis and Control*, pages 3–21. Springer, 2016.
- [97] V. I. Arnold. Small denominators. I. Mapping of the circumference onto itself. In A. B. Givental *et al.*, editor, *Representations of Functions, Celestial Mechanics, and KAM Theory 1957-1965*, Vladimir I. Arnold - Collected Works, pages 152–223. Springer, 2009.
- [98] A. Katok and B. Hasselblatt. *Introduction to the Modern Theory of Dynamical Systems*. Cambridge University Press, 1997.
- [99] E. Ott. *Chaos in Dynamical Systems*. Cambridge University Press, 2002.
- [100] A. Otto, D. Müller, and G. Radons. A universal dichotomy for systems with variable delay. *in prep.*, 2016.
- [101] M. Krstic and A. Smyshlyaev. Backstepping boundary control for first-order hyperbolic pdes and application to systems with actuator and sensor delays. *Syst. Contr. Lett.*, 57(9):750 – 758, 2008.
- [102] M. Krstic. *Delay Compensation for Nonlinear, Adaptive, and PDE Systems*. Birkhäuser, 2010.
- [103] G.A. Bocharov and F.A. Rihan. Numerical modelling in biosciences using delay differential equations. *J. Comp. Appl. Math.*, 125:183–199, 2000.
- [104] B.L. Keyfitz and N. Keyfitz. The McKendrick partial differential equation and its uses in epidemiology and population study. *Math. Comp. Model.*, 26(6):1 – 9, 1997.

Bibliography

- [105] A. G. McKendrick. Applications of mathematics to medical problems. *Proc. Edin. Math. Soc.*, 44:98–130, 2 1925.
- [106] G. E. Hutchinson. Circular cause systems in ecology. *Ann. N. Y. Acad. Sci.*, 50: 221, 1948.
- [107] J.A. Sanders. On the fundamental theorem of averaging. *SIAM J. Math. Anal.*, 14 (1):1–10, 1983.
- [108] J.K. Hale. Averaging methods for differential equations with retarded arguments and a small parameter. *J. Diff. Eq.*, 2(1):57 – 73, 1966.
- [109] B. Lehman and S.P. Weibel. Fundamental theorems of averaging for functional differential equations. *J. Diff. Eq.*, 152(1):160 – 190, 1999.
- [110] W. Michiels, V. Van Assche, and S.-I. Niculescu. Stabilization of time-delay systems with a controlled time-varying delay and applications. *IEEE Trans. Autom. Control*, 50(4):493–504, 2005.
- [111] A. Otto, G. Kehl, M. Mayer, and G. Radons. Stability analysis of machining with spindle speed variation. *Adv. Mater. Res.*, 223:600 – 609, 2011.
- [112] M. Born and V. Fock. Beweis des Adiabatsatzes. *Zeitschr. f. Phys.*, 51(3):165–180, 1928.
- [113] L.F. Shampine and S. Thompson. Solving DDEs in Matlab . *Appl. Numer. Math.*, 37(4):441 – 458, 2001.
- [114] A. Bellen and M. Zennaro. *Numerical Methods for Delay Differential Equations*. Numerical Mathematics and Scientific Computation. Oxford University Press, 2013.
- [115] H. Brunner and P.J. Houwen. *The numerical solution of Volterra equations*. North-Holland, 1986.
- [116] C.T.H. Baker and N.J. Ford. Stability properties of a scheme for the approximate solution of a delay-integro-differential equation. *Appl. Num. Math.*, 9(3–5):357 – 370, 1992.
- [117] N. J. Ford and S. M. Verduyn Lunel. Characterising small solutions in delay differential equations through numerical approximations. *Appl. Math. Comp.*, 131: 253 – 270, 2002.
- [118] R. Bellman. On the computational solution of differential-difference equations. *J. Math. Anal. Appl.*, 2(1):108 – 110, 1961.
- [119] R. Bellman and K.L. Cooke. On the computational solution of a class of functional differential equations. *J Math. Anal. Appl.*, 12(3):495 – 500, 1965.
- [120] L.F. Shampine. Solving ODEs and DDEs with residual control. *Appl. Num. Math.*, 52(1):113 – 127, 2005.

- [121] N. Guglielmi. Open issues in devising software for the numerical solution of implicit delay differential equations. *J. Comp. Appl. Math.*, 185(2):261–277, 2006.
- [122] F.A. Khasawneh, D.A.W. Barton, and B.P. Mann. Periodic solutions of nonlinear delay differential equations using spectral element method. *Nonlin. Dyn.*, 67(1): 641–658, 2012.
- [123] K. Engelborghs, T. Luzyanina, and D. Roose. Numerical bifurcation analysis of delay differential equations using DDE-BIFTOOL. *ACM Trans. Math. Softw.*, 28(1):1–21, 2002.
- [124] R Szalai. Knut: A continuation and bifurcation software for delay-differential equations, 2009. URL <http://gitorious.org/knut/pages/Home>.
- [125] V. L. Kharitonov. Robust stability analysis of time delay systems: A survey. *Annu. Rev. Control*, 23:185 – 196, 1999.
- [126] E. Fridman. Tutorial on Lyapunov-based methods for time-delay systems . *Eur. J. Control*, 20(6):271 – 283, 2014.
- [127] U. Küchler and B. Mensch. Langevins stochastic differential equation extended by a time-delayed term. *Stoch. Stoch. Rep.*, 40(1-2):23–42, 1992.
- [128] A. A. Budini and M. O. Cáceres. Functional characterization of linear delay langevin equations. *Phys. Rev. E*, 70:046104, 2004.
- [129] S. Yi, A. G. Ulsoy, and P. W. Nelson. Solution of systems of linear delay differential equations via Laplace transformation. In *45th IEEE Conf. Decis. Contr.*, 2006, pages 2535–2540, 2006.
- [130] E. Jarlebring and T. Damm. The Lambert W function and the spectrum of some multidimensional time-delay systems. *Automatica*, 43(12):2124 – 2128, 2007.
- [131] R.M. Corless, D.J. Jeffrey, and D.E. Knuth. A sequence of series for the Lambert W function. In *Proc. Int. Symp. Symbol. Algebr. Comput.*, pages 197–204. ACM, 1997.
- [132] C Hwang and Y.-C. Cheng. A note on the use of the Lambert W function in the stability analysis of time-delay systems. *Automatica*, 41(11):1979 – 1985, 2005.
- [133] R. Cepeda-Gomez and W. Michiels. Special cases in using the matrix Lambert W function for the stability analysis of high-order linear systems with time delay. *IFAC-PapersOnLine*, 48(12):7 – 12, 2015.
- [134] D. Breda, S. Maset, and R. Vermiglio. TRACE-DDE: a tool for robust analysis and characteristic equations for delay differential equations. In J.-J. Loiseau, W. Michiels, S.-I. Niculescu, and R. Sipahi, editors, *Topics in Time Delay Systems*, pages 145–155. Springer, 2009.

Bibliography

- [135] J.P. Boyd. *Chebyshev and Fourier Spectral Methods*. Dover Publications, 2001.
- [136] T. Insperger and G. Stépán. Semi-discretization method for delayed systems. *Int. J. Numer. Meth. Eng.*, 55:503–518, 2002.
- [137] Y. Ding, L. Zhu, X. Zhang, and H. Ding. A full-discretization method for prediction of milling stability. *Int. J. Mach. Tools and Manuf.*, 50(5):502 – 509, 2010.
- [138] J.-Q. Sun. A method of continuous time approximation of delayed dynamical systems. *Commun. Nonlinear Sci. Numer. Simul.*, 14(4):998 – 1007, 2009.
- [139] D. Breda and E. Van Vleck. Approximating Lyapunov exponents and Sacker–Sell spectrum for retarded functional differential equations. *Numer. Math.*, 126(2):225–257, 2014.
- [140] C.P. Vyasarayani, S. Subhash, and T. Kalmár-Nagy. Spectral approximations for characteristic roots of delay differential equations. *Int. J. Dyn. Control*, 2(2):126–132, 2014.
- [141] P. Wahi and A. Chatterjee. Galerkin projections for delay differential equations. *ASME. J. Dyn. Sys., Meas., Control*, 127(1):80–87, 2004.
- [142] D. Lehotzky, T. Insperger, and G. Stepan. Extension of the spectral element method for stability analysis of time-periodic delay-differential equations with multiple and distributed delays. *Commun. Nonlinear Sci. Numer. Simulat.*, 35:177 – 189, 2016.
- [143] B.P. Mann and B.R. Patel. Stability of delay equations written as state space models. *J. Vibr. Control*, 16(7-8):1067–1085, 2010.
- [144] E.T. Whittaker and G.N. Watson. *A Course of Modern Analysis*. Cambridge University Press, 1996.
- [145] R. Denk. Convergence improvement for the infinite determinants of Hill systems. *ZAMM - J. Appl. Math. Mech.*, 75(6):463–470, 1995.
- [146] C.W. Curtis and B. Deconinck. On the convergence of Hill’s method. *AMS Math. Comput.*, 79(269):169–187, 2010.
- [147] M.A. Johnson and K. Zumbrun. Convergence of Hill’s method for nonselfadjoint operators. *SIAM J. Numer. Anal.*, 50(1):64–78, 2012.
- [148] W. Magnus and S. Winkler. *Hill’s Equation*. Courier, 2013.
- [149] B.P. Lampe and E.N. Rosenwasser. Hill method for linear periodic systems with delay. *Proc. 16th Int. Conf. MMAR*, August 22-25, Miedzyzdroje, Poland:100–106, 2011.

- [150] A. Lazarus, B. Prabel, and D. Combescure. A 3d finite element model for the vibration analysis of asymmetric rotating machines. *J. Sound Vibr.*, 329(18):3780 – 3797, 2010.
- [151] A.H. Nayfeh and D.T. Mook. *Nonlinear Oscillations*. Wiley, 2008.
- [152] B. Deconinck, N. E. Sheils, N. V. Nguyen, and R. Tian. On the spectral stability of solitary wave solutions of the vector nonlinear Schrödinger equation. *J. Phys. A: Math. Theor.*, 46(41):415202, 2013.
- [153] N. Sanford, K. Kodama, J. D. Carter, and H. Kalisch. Stability of traveling wave solutions to the Whitham equation . *Phys. Lett. A*, 378(30–31):2100 – 2107, 2014.
- [154] R. Szalai, G. Stepan, and S. J. Hogan. Continuation of bifurcations in periodic delay-differential equations using characteristic matrices. *SIAM J. Sci. Comp.*, 28(4):1301–1317, 2006.
- [155] J. Sieber and R. Szalai. Characteristic matrices for linear periodic delay differential equations. *SIAM J. Appl. Dyn. Syst.*, 10(4):129–147, 2011.
- [156] G. Orosz. Decomposing the dynamics of delayed Hodgkin-Huxley neurons. In T. Vyhldal, J.-F. Lafay, and R. Sipahi, editors, *Delay Systems: From Theory to Numerics and Applications*, pages 343–357. Springer, 2014.
- [157] N. Olgac and R. Sipahi. An exact method for the stability analysis of time-delayed linear time-invariant (LTI) systems. *IEEE Trans. Autom. Contr.*, 47(5):793–797, 2002.
- [158] R. Sipahi. *Stability Analysis of LTI Multiple Time Delay Systems: Cluster Treatment of Characteristic Roots*. VDM Publishing, 2008.
- [159] Y. Altintas, G. Stepan, D. Merdol, and Z. Dombovari. Chatter stability of milling in frequency and discrete time domain. *CIRP J. Manuf. Sci. Technol.*, 1(1):35 – 44, 2008.
- [160] A. Dabiri, M. Nazari, and E.A. Butcher. Explicit harmonic balance method for transition curve analysis of linear fractional periodic time-delayed systems. *IFAC-PapersOnLine*, 48(12):39 – 44, 2015.
- [161] D. Bachrathy and G. Stepan. Bisection method in higher dimensions and the efficiency number. *Periodica Polytechnica*, 56:81–86, 2012.
- [162] R. S. Zounes and R. H. Rand. Transition curves for the quasi-periodic Mathieu equation. *SIAM J. Appl. Math.*, 58(4):1094–1115, 1998.
- [163] G. Bennetin, L. Galgani, A. Giorgilli, and J.M. Strelcyn. Lyapunov characteristic exponents for smooth dynamical systems and for Hamiltonian systems; a method for computing all of them. Part 1: Theory. Part 2: Numerical applications. *Meccanica*, 15:9–20, 21–30, 1980.

Bibliography

- [164] J.D. Farmer. Chaotic attractors of an infinite-dimensional dynamical system. *Physica D*, 4(3):366 – 393, 1982.
- [165] D. Breda, S. Maset, and R. Vermiglio. Pseudospectral differencing methods for characteristic roots of delay differential equations. *SIAM J. Sci. Comp.*, 27(2): 482–495, 2005.
- [166] L. N. Trefethen. *Spectral Methods in MatLab*. SIAM, Philadelphia, PA, USA, 2000.
- [167] F. Ginelli, P. Poggi, A. Turchi, H. Chaté, R. Livi, and A. Politi. Characterizing dynamics with covariant Lyapunov vectors. *Phys. Rev. Lett.*, 99(130601), 2007.
- [168] H.-L. Yang, G. Radons, and H. Kantz. Covariant Lyapunov vectors from reconstructed dynamics: The geometry behind true and spurious Lyapunov exponents. *Phys. Rev. Lett.*, 109:244101, 2012.
- [169] S.C. Sinha, E.A. Butcher, and A. Dávid. Construction of dynamically equivalent time-invariant forms for time-periodic systems. *Nonlin. Dyn.*, 16(3):203–221, 1998.
- [170] A. M. Turing. The chemical basis of morphogenesis. *Phil. Trans. Royal Soc. B*, 37: 237, 1952.
- [171] A. M. Zhabotinsky, M. Dolnik, and I. R. Epstein. Pattern formation arising from wave instability in a simple reaction-diffusion system. *J. Chem. Phys.*, 103:10306, 1995.
- [172] M. Bestehorn, E. V. Grigorieva, and S. A. Kaschenko. Spatiotemporal structures in a model with delay and diffusion. *Phys. Rev. E*, 70:026202, 2004.
- [173] L. Ji and Q.S. Li. Turing pattern formation in coupled reaction-diffusion system with distributed delays. *J. Chem. Phys.*, 123:094509, 2005.
- [174] K. P. Hadeler and S. Ruan. Interaction of diffusion and delay. *Discrete Contin. Dyn. Syst. B*, 8(1):95, 2007.
- [175] S. V. Gurevich. Time-delayed feedback control of breathing localized structures in a three-component reaction–diffusion system. *Phil. Trans. Royal Soc. A*, 372(2027), 2014.
- [176] J. Hsia, W. J. Holtz, D. C. Huang, M. Arcak, and M. M. Maharbiz. A feedback quenched oscillator produces Turing patterning with one diffuser. *PLoS Comput. Biol.*, 8(1):e1002331, 2012.
- [177] A. Otto, J. Wang, and G. Radons. Turing-like waves in single-species reaction-diffusion systems with distributed delays. *in prep.*, 2016.
- [178] R. A. Fisher. The wave of advance of advantageous genes. *Ann. Eugenics*, 7(4): 355–369, 1937.

- [179] V.M. Tikhomirov. A study of the diffusion equation with increase in the amount of substance, and its application to a biological problem. In V.M. Tikhomirov, editor, *Selected Works of A. N. Kolmogorov*, volume 25 of *Math. Appl. (Soviet Series)*, pages 242–270. Springer, 1991.
- [180] T. Insperger and G. Stépán. Stability analysis of turning with periodic spindle speed modulation via semi-discretization. *J. Vib. Control*, 10(12):1835–1855, 2004.
- [181] Y. Altintas and M. Weck. Chatter stability of metal cutting and grinding. *CIRP Ann.*, 53:619 – 642, 2004.
- [182] E. Budak and E. Ozturk. Dynamics and stability of parallel turning operations. *CIRP Ann.*, 60(1):383 – 386, 2011.
- [183] N. Olgac and R. Sipahi. A unique methodology for chatter stability mapping in simultaneous machining. *ASME. J. Manuf. Sci. Eng.*, 127(4):791 – 800, 2005.
- [184] E. Shamoto, T. Mori, K. Nishimura, T. Hiramatsu, and Y. Kurata. Suppression of regenerative chatter vibration in simultaneous double-sided milling of flexible plates by speed difference. *CIRP Ann.*, 59(1):387 – 390, 2010.
- [185] C. Brecher, Y. Trofimov, and S. Bäumlér. Holistic modelling of process machine interactions in parallel milling. *CIRP Ann.*, 60(1):387 – 390, 2011.
- [186] E. Budak, A. Comak, and E. Ozturk. Stability and high performance machining conditions in simultaneous milling. *CIRP Ann.*, 62(1):403 – 406, 2013.
- [187] G. Stépán, Z. Dombovari, and J. Muñoa. Identification of cutting force characteristics based on chatter experiments. *CIRP Ann.*, 60(1):113 – 116, 2011.
- [188] A. Otto, S. Rauh, M. Kolouch, and G. Radons. Extension of Thusty’s law for the identification of chatter stability lobes in multi-dimensional cutting processes. *Int. J. Mach. Tools Manuf.*, 82–83:50 – 58, 2014.
- [189] J. Kleckner. *Ein Beitrag zur Analyse dynamischer Interaktionen bei selbsterregungs-fähigen Drehbearbeitungsprozessen*. Shaker, 2001.
- [190] T. Insperger and G. Stépán. Updated semi-discretization method for periodic delay-differential equations with discrete delay. *Int. J. Numer. Meth. Eng.*, 61:117–141, 2004.
- [191] X. Li, Y. Y. Jin, and G. Chen. Complexity and synchronization of the world trade web. *Physica A*, 328(1–2):287 – 296, 2003.
- [192] A. Pluchino, V. Latora, and A. Rapisarda. Changing opinions in a changing world: A new perspective in sociophysics. *Int. J. Mod. Phys. C*, 16(04):515–531, 2005.
- [193] M. Rohden, A. Sorge, M. Timme, and D. Witthaut. Self-organized synchronization in decentralized power grids. *Phys. Rev. Lett.*, 109:064101, 2012.

Bibliography

- [194] F. M. Atay. The consensus problem in networks with transmission delays. *Phil. Trans. Royal Soc. A*, 371(1999), 2013.
- [195] R. Szalai and G. Orosz. Decomposing the dynamics of heterogeneous delayed networks with applications to connected vehicle systems. *Phys. Rev. E*, 88:040902, 2013.
- [196] K. Schmietendorf, J. Peinke, R. Friedrich, and O. Kamps. Self-organized synchronization and voltage stability in networks of synchronous machines. *Eur. Phys. J. Spec. Top.*, 223(12), 2014.
- [197] L. Glass. Synchronization and rhythmic processes in physiology. *Nature*, 410:277–284, 2001.
- [198] E. Schöll, G. Hiller, P. Hövel, and M. A Dahlem. Time-delayed feedback in neurosystems. *Phil. Trans. Royal Soc. A*, 367(1891):1079–1096, 2009.
- [199] S. Zhu, X. Chen, X. Lu, K.S. Thornburg Jr., G. D. Vanwiggeren, and R. Roy. Synchronization of chaos in a coupled laser system. In Z. Xu, S. Xie, S.-Y. Zhu, and M. Scully, editors, *Frontiers of Laser Physics and Quantum Optics*, pages 631–634. Springer, 2000.
- [200] T. Heil, I. Fischer, W. Elsässer, J. Mulet, and C. R. Mirasso. Chaos synchronization and spontaneous symmetry-breaking in symmetrically delay-coupled semiconductor lasers. *Phys. Rev. Lett.*, 86:795–798, 2001.
- [201] V. Flunkert and E. Schöll. Chaos synchronization in networks of delay-coupled lasers: role of the coupling phases. *New J. Phys.*, 14(3):033039, 2012.
- [202] A. Pikovsky, M. Rosenblum, and J. Kurths. *Synchronization: A Universal Concept in Nonlinear Sciences*. Cambridge University Press, 2003.
- [203] A. Arenas, A. Díaz-Guilera, J. Kurths, Y. Moreno, and C. Zhou. Synchronization in complex networks. *Phys. Rep.*, 469:93–153, 2008.
- [204] L. Pecora and T. Carroll. Master stability functions for synchronized coupled systems. *Phys. Rev. Lett.*, 80:2109–2112, 1998.
- [205] A. Otto, D. Bachrathy, G. Orosz, and G. Radons. On the decomposition of networks with heterogeneous delay coupling. *in prep.*, 2016.
- [206] L. Pecora. Synchronization conditions and desynchronizing patterns in coupled limit-cycle and chaotic systems. *Phys. Rev. E*, 58:347–360, 1998.
- [207] J. Sun, E. M. Bollt, and T. Nishikawa. Master stability functions for coupled nearly identical dynamical systems. *EPL*, 85(6):60011, 2009.
- [208] F. Sorrentino and M. Porfiri. Analysis of parameter mismatches in the master stability function for network synchronization. *EPL*, 93(5):50002, 2011.

- [209] G. Orosz. Decomposition of nonlinear delayed networks around cluster states with applications to neurodynamics. *SIAM J. Appl. Dyn. Sys.*, 13(4):1353–1386, 2014.
- [210] A. Englert, S. Heilighenthal, W. Kinzel, and I. Kanter. Synchronization of chaotic networks with time-delayed couplings: An analytic study. *Phys. Rev. E*, 83:046222, 2011.
- [211] O. D’Huys, S. Zeeb, T. Jüngling, S. Heilighenthal, S. Yanchuk, and W. Kinzel. Synchronisation and scaling properties of chaotic networks with multiple delays. *EPL*, 103(1):10013, 2013.
- [212] A. L. Hodgkin and A. F. Huxley. A quantitative description of membrane current and its application to conduction and excitation in nerve. *J. Physiol.*, 117:500–544, 1952.
- [213] G. Orosz, J. Moehlis, and R. M. Murray. Controlling biological networks by time-delayed signals. *Phil. Trans. R. Soc. A*, 368(1911):439–454, 2009.

A. Appendix

A.1. Equivalent systems

Some additional remarks on systems with variable transport delays, which are presented in Chapter 2, are given in this section. In particular, in Sec. 2.2.1 a relationship between the delay distributions of the DDEs for the two equivalent representations in terms of the physical time \tilde{t} and in terms of the internal clock t is presented, which is derived in Appendix A.1.1. In Appendix A.1.2 the characteristic curves for the PDE representation of the time delay system are calculated, which are presented in Sec. 2.3.1.

A.1.1. Relation between delay kernels

Eq. (2.8) defines the memory of the standard form Eq. (2.1) in terms of the new independent variable \tilde{t} if a nonlinear time scale transformation $t = \Phi(\tilde{t})$ is applied. The relationship Eq. (2.9) between the delay distribution $\tilde{\mathbf{K}}(\tilde{t}, \tilde{\tau})$ in the new tilded variables and the delay distribution $\mathbf{K}(\tau)$ in the original variables can be derived as follows. At first, Eq. (2.5) is substituted for the retarded configurations $\mathbf{x}(t - \tau)$ in Eq. (2.2)

$$\mathbf{r}_u(t) = \int_0^{\tau_{\max}} \mathbf{K}(\tau) \tilde{\mathbf{u}}(\tilde{t} - \tilde{\tau}(\tilde{t})) d\tau, \quad (\text{A.1})$$

where the delay $\tilde{\tau}(\tilde{t})$ is defined by Eq. (2.7). A change of the integration variable from delays τ to delays $\tilde{\tau}$ yields

$$\mathbf{r}_u(t) = \int_0^{\tilde{\tau}_{\max}(\tilde{t})} \mathbf{K}(\Phi(\tilde{t}) - \Phi(\tilde{t} - \tilde{\tau})) \tilde{\mathbf{u}}(\tilde{t} - \tilde{\tau}) \frac{d\tau}{d\tilde{\tau}} d\tilde{\tau}, \quad (\text{A.2})$$

where the variable maximum delay $\tilde{\tau}_{\max}(\tilde{t})$ for the integration in the new variables can be calculated according to Eq. (2.7). In Eq. (A.2) the condition Eq. (2.6) for variable transport delays was used to express the argument τ of the delay distribution $\mathbf{K}(\tau)$ in terms of the new variable $\tilde{\tau}$. An explicit expression for the derivative $\frac{d\tau}{d\tilde{\tau}}$ can be derived from Eq. (2.6) as

$$\frac{d\tau}{d\tilde{\tau}} = \Omega(\tilde{t} - \tilde{\tau}). \quad (\text{A.3})$$

The condition Eq. (2.4) of a strictly positive velocity $\Omega(\tilde{t})$ does not only guarantee a bijective mapping between the variables t and \tilde{t} but also a bijective mapping between the two delays τ and $\tilde{\tau}$. In other words an increasing delay τ in the original systems implies

A. Appendix

an increasing delay $\tilde{\tau}$ in the transformed system. Thus, the one-to-one correspondence of the original integral in Eq. (A.1) and the integral Eq. (A.2) in the new variables is guaranteed. Putting Eq. (A.3) into Eq. (A.2) leads to

$$\mathbf{r}_{\mathbf{u}}(t) = \int_0^{\tilde{\tau}_{\max}(\tilde{t})} \mathbf{K}(\Phi(\tilde{t}) - \Phi(\tilde{t} - \tilde{\tau})) \Omega(\tilde{t} - \tilde{\tau}) \tilde{\mathbf{u}}(\tilde{t} - \tilde{\tau}) d\tilde{\tau}. \quad (\text{A.4})$$

By comparison of the memory Eq. (A.4) and the definition Eq. (2.8), the relationship between the delay distributions $\tilde{\mathbf{K}}(\tilde{t}, \tilde{\tau})$ and $\mathbf{K}(\tau)$ can be given by Eq. (2.9).

A.1.2. Characteristic curves for PDE representation

In Sec. 2.3.1 and Sec. 2.3.2 it is shown that the standard form of the time delay system Eq. (2.1) can be also described by PDEs. In general, the PDE representations can be written as

$$\frac{\partial \mathbf{v}(\tau, t)}{\partial t} + \eta(t) \frac{\partial \mathbf{v}(\tau, t)}{\partial \tau} = \mathbf{g}(\mathbf{v}(\tau, t)). \quad (\text{A.5})$$

On a suitable hypersurface, characterized by the so-called characteristic curves, the PDE Eq. (A.5) can be described by a family of ODEs. The hypersurface $\mathbf{v}(\tau(s), t(s))$ is parameterized by the scalar independent variable s . For the derivative of \mathbf{v} with respect to s we get

$$\frac{d\mathbf{v}(\tau, t)}{ds} = \frac{\partial \mathbf{v}(\tau, t)}{\partial t} \frac{dt}{ds} + \frac{\partial \mathbf{v}(\tau, t)}{\partial \tau} \frac{d\tau}{ds}. \quad (\text{A.6})$$

For $\frac{dt}{ds} = 1$ and $\frac{d\tau}{ds} = \eta(s)$ the right hand side of Eq. (A.6) is equivalent to the left hand side of the PDE Eq. (A.5). As a consequence, a set of ODEs can be used to describe the dynamics of the PDE Eq. (A.5). The complete set of ODEs can be given by

$$\frac{dt}{ds} = 1, \quad \frac{d\tau}{ds} = \eta(s), \quad \text{and} \quad \frac{d\mathbf{v}(\tau(s), t(s))}{ds} = \mathbf{g}(\mathbf{v}(\tau(s), t(s))). \quad (\text{A.7})$$

The integration of the first two ODEs in Eq. (A.7) yields the characteristic curves

$$t(s) = t(0) + s, \quad \text{and} \quad \tau(s) = \tau(0) + \int_0^s \eta(s') ds'. \quad (\text{A.8})$$

The solution along the characteristic curves can be described by the third ODE in Eq. (A.7). The characteristic curves for the first-order hyperbolic PDEs Eq. (2.19), Eq. (2.21), Eq. (2.23), and Eq. (2.25) in Sec. 2.3.1 are given in Eq. (2.27). In this case the right hand side is zero, $\mathbf{g} = \mathbf{0}$, and the solution remains constant along the characteristic curves $\mathbf{v}(\tau(s), t(s)) = \mathbf{v}(\tau(0), t(0))$. For the PDE Eq. (2.25) the specific condition $\eta(s) = 1/\Omega(\Phi^{-1}(s)) = (\Phi^{-1})'(s)$ was used. For the McKendrick Eq. (2.28) in Sec. 2.3.2 the right hand side of the PDE is linear $\mathbf{g}(\mathbf{v}(\tau, t)) = -\mu \mathbf{v}(\tau, t)$ and the third ODE in Eq. (A.7) can be solved analytically. In particular, in this case the solution along the characteristic curves can be given by

$$\mathbf{v}(\tau(s), t(s)) = e^{-\mu s} \mathbf{v}(\tau(0), t(0)). \quad (\text{A.9})$$

A.2. Analytical methods for linear DDEs

In this part of the Appendix some additional remarks on the analytical methods for time delay systems are given. A detailed derivation of the formal Laplace transform of a non-autonomous DDE, which is presented in Sec. 4.1, is given in Appendix A.2.1. The formal definition of a propagator for the time delay system from the Laplace transform Eq. (4.3) of the DDE is given in Appendix A.2.2. In Appendix A.2.3 the explicit form of the propagator from Sec. 4.2 is derived for non-autonomous DDEs with a single discrete delay by a successive application of the method of steps. The biorthonormality condition Eq. (4.35) of the eigenmode expansion for DDEs in Sec. 4.4 is derived in Appendix A.2.4.

A.2.1. Laplace transform of non-autonomous DDEs

The formal Laplace transform Eq. (4.3) of linear non-autonomous DDEs with distributed delay is derived by applying the Laplace transform as defined in Eq. (4.1) on the time delay system Eq. (3.2), which results in

$$\int_0^\infty dt (\dot{\mathbf{x}}(t) - \mathbf{A}(t)\mathbf{x}(t)) e^{-st} = \int_0^{\tau_{\max}} d\tau \int_0^\infty dt \mathbf{B}(t) \mathbf{K}(\tau) \mathbf{x}(t - \tau) e^{-st}. \quad (\text{A.10})$$

With the definition $\Psi(t) = \mathbf{x}(t)H(-t)$ for the initial function of the DDE the second integral on the right hand side of Eq. (A.10) can be split into two parts

$$\int_0^\infty dt \mathbf{B}(t) \mathbf{K}(\tau) \mathbf{x}(t - \tau) e^{-st} = \int_0^\tau dt \mathbf{B}(t) \mathbf{K}(\tau) \Psi(t - \tau) e^{-st} + \int_\tau^\infty dt \mathbf{B}(t) \mathbf{K}(\tau) \mathbf{x}(t - \tau) e^{-st}. \quad (\text{A.11})$$

The first part is a weighted Laplace transform of the initial function $\Psi(t - \tau)$ with $t - \tau \leq 0$, and the second part is a Laplace transform that contains the delayed configuration $\mathbf{x}(t - \tau)$ with $t - \tau > 0$. Substitution of Eq. (A.11) in Eq. (A.10) yields after some rearrangement

$$s\bar{\mathbf{x}}(s) - \Psi(0) - \bar{\mathbf{A}}(s) * \bar{\mathbf{x}}(s) = \int_0^{\tau_{\max}} dt \mathbf{B}(t) \mathbf{r}_\Psi(t) e^{-st} + \int_0^{\tau_{\max}} d\tau \int_\tau^\infty dt \mathbf{B}(t) \mathbf{K}(\tau) \mathbf{x}(t - \tau) e^{-st}. \quad (\text{A.12})$$

The first summand on the right hand side of Eq. (A.12) is equivalent to the definition in Eq. (4.4) and can be interpreted as the Laplace transform $\bar{\Psi}(s)$ of the initial memory $\mathbf{r}_\Psi(t)$ weighed by the matrix $\mathbf{B}(t)$. The second summand can be simplified by representing $\mathbf{B}(t)$ in terms of its Laplace transform $\bar{\mathbf{B}}(s')$ and applying the Laplace transform of the retarded configurations $\mathbf{x}(t - \tau)$ as

$$\int_0^{\tau_{\max}} d\tau \int_\tau^\infty dt \mathbf{B}(t) \mathbf{K}(\tau) \mathbf{x}(t - \tau) e^{-st} = \int_{(\Gamma)} ds' \bar{\mathbf{B}}(s') \int_0^{\tau_{\max}} d\tau \mathbf{K}(\tau) e^{-(s-s')\tau} \bar{\mathbf{x}}(s - s') \quad (\text{A.13})$$

A. Appendix

Finally, the remaining Laplace transform of the delay kernel $\mathbf{K}(\tau)$ is applied in Eq. (A.13), and the substitution of the resulting expression in Eq. (A.12) leads to

$$s\bar{\mathbf{x}}(s) - \Psi(0) - \bar{\mathbf{A}}(s) * \bar{\mathbf{x}}(s) = \bar{\Psi}(s) + \int_{(\Gamma)} ds' \bar{\mathbf{B}}(s') \bar{\mathbf{K}}(s - s') \bar{\mathbf{x}}(s - s'), \quad (\text{A.14})$$

which is equivalent to Eq. (4.3).

A.2.2. Propagator of linear DDEs

For the illustration of the structure of the Laplace transform Eq. (4.6) of the time delay system a discrete representation of the operators and functions is considered. The discrete representation in terms of matrices and vectors is only presented for the illustration of the structure and the dimension of the equations and the integrals related to the Laplace domain representation of the non-autonomous time delay system. No quantitative results are derived from the discrete analysis. It is assumed that the continuous variable s is approximated by a finite number of values s_i , with $i = 1, \dots, n$. A discrete representation of Eq. (4.6) for the Laplace transform of the non-autonomous DDE with distributed delay can be given by

$$\bar{\mathbf{T}}_n^{-1} \bar{\mathbf{x}}_n = \bar{\Psi}_{n0} + \bar{\Psi}_n, \quad (\text{A.15})$$

where the vectors for the Laplace domain representation of the configuration, the initial value and the memory are defined by

$$\bar{\mathbf{x}}_n = \begin{pmatrix} \bar{\mathbf{x}}(s_1) \\ \vdots \\ \bar{\mathbf{x}}(s_n) \end{pmatrix}, \quad \bar{\Psi}_{n0} = \begin{pmatrix} \Psi(0) \\ \vdots \\ \Psi(0) \end{pmatrix}, \quad \bar{\Psi}_n = \begin{pmatrix} \bar{\Psi}(s_1) \\ \vdots \\ \bar{\Psi}(s_n) \end{pmatrix}. \quad (\text{A.16})$$

The $N \times N$ dimensional blocks of the discrete version of the inverse $\bar{\mathbf{T}}_n^{-1}$ of the propagator is given by

$$\left\{ \bar{\mathbf{T}}_n^{-1} \right\}_{kl} = \mathbf{I} s_k \delta_{kl} - \bar{\mathbf{A}}(s_k - s_l) - \bar{\mathbf{B}}(s_k - s_l) \bar{\mathbf{K}}(s_l), \quad \text{with } k, l = 1, \dots, n. \quad (\text{A.17})$$

It is assumed that the matrix $\bar{\mathbf{T}}_n^{-1}$ is invertible. In this case, the solution of the time delay system in the discrete Laplace domain representation can be determined by

$$\bar{\mathbf{x}}_n = \bar{\mathbf{T}}_n (\bar{\Psi}_{n0} + \bar{\Psi}_n). \quad (\text{A.18})$$

For the representation of the solution and the propagator in the time domain, the matrices \mathbf{L}_n and \mathbf{L}_n^{-1} for the Laplace and the inverse Laplace transform are defined as

$$\{\mathbf{L}_n\}_{kl} = L_{kl} e^{-s_k t_l}, \quad \{\mathbf{L}_n^{-1}\}_{kl} = L_{kl}^i e^{t_k s_l}. \quad (\text{A.19})$$

In Eq. (A.19), $t_i \in [0, \infty)$, $i = 1, \dots, n$ are discrete times, and L_{kl} and L_{kl}^i are arbitrary constants originating from the integrals in the definition of the continuous Laplace

transform Eq. (4.1). With Eq. (A.19), the solution in the discrete time domain can be expressed by

$$\mathbf{x}_n = \mathbf{L}_n^{-1} \bar{\mathbf{T}}_n \mathbf{L}_n (\boldsymbol{\Psi}_{n0} + \boldsymbol{\Psi}_n) = \mathbf{T}_n (\boldsymbol{\Psi}_{n0} + \boldsymbol{\Psi}_n). \quad (\text{A.20})$$

The vectors for the configurations, the initial value and the memory in the discrete time domain are given by

$$\mathbf{x}_n = \begin{pmatrix} \mathbf{x}(t_1) \\ \vdots \\ \mathbf{x}(t_n) \end{pmatrix}, \quad \boldsymbol{\Psi}_{n0} = \begin{pmatrix} \boldsymbol{\Psi}(0) \\ 0 \\ \vdots \\ 0 \end{pmatrix}, \quad \boldsymbol{\Psi}_n = \begin{pmatrix} \mathbf{B}(t_1) \mathbf{r}_{\boldsymbol{\Psi}}(t_1) \\ \vdots \\ \mathbf{B}(t_n) \mathbf{r}_{\boldsymbol{\Psi}}(t_n) \end{pmatrix}, \quad (\text{A.21})$$

where it is assumed that $t_1 = 0$. Note that from the definition of the initial function $\boldsymbol{\Psi}(t) = \mathbf{0}$ for $t > 0$ it follows that $\mathbf{r}_{\boldsymbol{\Psi}}(t) = 0$, for $t > \tau_{\max}$.

In the original continuous representation, the following property holds between the Laplace domain representation of the propagator and its inverse,

$$\int_{(\Gamma)} \bar{\mathbf{T}}(s'', s) \bar{\mathbf{T}}^{-1}(s, s') ds = \mathbf{I} \delta(s'' - s'). \quad (\text{A.22})$$

After multiplying Eq. (4.6) with $\bar{\mathbf{T}}(s'', s)$ from the left, integrating over ds , and using the identity Eq. (A.22), the solution in the Laplace domain can be determined by Eq. (4.7). Eq. (4.7) is the continuous counterpart to Eq. (A.18). If the inverse Laplace transform is applied to Eq. (4.7), that is multiplication with $e^{s''t''}$ and integration over s'' , the solution $\mathbf{x}(t'')$ of the time delay system can be determined by

$$\mathbf{x}(t'') = \int_0^{t''} dt \int_{(\Gamma)} ds \int_{(\Gamma)} ds'' \bar{\mathbf{T}}(s'', s) e^{s''t'' - st} (\boldsymbol{\Psi}(t) \delta(t - 0) + \mathbf{B}(t) \mathbf{r}_{\boldsymbol{\Psi}}(t)). \quad (\text{A.23})$$

From Eq. (A.23) the time domain representation $\mathbf{T}(t, t')$ of the propagator of the DDE can be identified as

$$\mathbf{T}(t'', t) = \int_{(\Gamma)} ds'' \int_{(\Gamma)} ds \bar{\mathbf{T}}(s'', s) e^{s''t'' - st} \mathbf{H}(t'' - t). \quad (\text{A.24})$$

This definition of the propagator is consistent to the relationship between the discrete versions \mathbf{T}_n and $\bar{\mathbf{T}}_n$ of the propagator in Eq. (A.20). The substitution of the definition Eq. (A.24) in Eq. (A.23) leads to the general solution Eq. (4.8) of a non-autonomous DDE with distributed delay in terms of the time domain representation $\mathbf{T}(t'', t)$ of the propagator. Eq. (A.23) or Eq. (4.8), respectively, are the continuous counterparts to Eq. (A.20), where $\mathbf{r}_{\boldsymbol{\Psi}}(t) = 0$, for $t > \tau_{\max}$.

If the inverse Laplace transform Eq. (A.24) is used for the Laplace domain representation Eq. (4.9) of the propagator for the autonomous system, the time domain representation Eq. (4.10) of the propagator is obtained.

A. Appendix

A.2.3. Method of steps for DDEs with discrete delays

The recursive application of Eq. (4.13) also known as method of steps can be used to generate an explicit expression for the propagator $\mathbf{T}(t, t')$. This is shown for the solution of the non-autonomous DDE Eq. (3.2) with discrete delay τ_0 , i.e. $\mathbf{K}(\tau) = \mathbf{K}_0\delta(\tau - \tau_0)$. At first, the time scale is divided into the homogeneous intervals

$$I_j := [t_j, t_{j+1}), \quad t_j = j\tau_0. \quad (\text{A.25})$$

According to Eq. (4.13), the solution $\mathbf{x}(\theta_j)$ in the j th interval with $\theta_j \in I_j$ can be obtained from the solution $\mathbf{x}(\theta_{j-1})$ in the previous interval by

$$\mathbf{x}(\theta_j) = \mathbf{M}(\theta_j, t_j)\mathbf{x}(t_j) + \int_{t_{j-1}}^{\theta_j - \tau_0} d\theta_{j-1} \mathbf{M}(\theta_j, \theta_{j-1} + \tau_0) \mathbf{B}_K(\theta_{j-1}) \mathbf{x}(\theta_{j-1}), \quad (\text{A.26})$$

where $\mathbf{B}_K(t) = \mathbf{B}(t)\mathbf{K}_0$. From Eq. (4.8) it follows that for the specific initial function $\mathbf{x}(0) = \mathbf{\Psi}(0)$ and $\mathbf{x}(\theta_{-1}) = 0$ for $\theta_{-1} < 0$ the solution of the DDE can be written as $\mathbf{x}(t) = \mathbf{T}(t, 0)\mathbf{\Psi}(0)$. This means, that according to Eq. (A.26) the propagator $\mathbf{T}(\theta_j, 0)$ for the solution of the delay system in the interval I_j can be derived from the propagator $\mathbf{T}(\theta_{j-1}, 0)$ in the previous interval as

$$\mathbf{T}(\theta_j, 0) = \mathbf{M}(\theta_j, t_j)\mathbf{T}(t_j, 0) + \int_{t_{j-1}}^{\theta_j - \tau_0} d\theta_{j-1} \mathbf{M}(\theta_j, \theta_{j-1} + \tau_0) \mathbf{B}_K(\theta_{j-1} + \tau_0) \mathbf{T}(\theta_{j-1}, 0). \quad (\text{A.27})$$

The recursive application of Eq. (A.27) can be used to express the propagator $\mathbf{T}(\theta_j, 0)$ only in terms of the matrices \mathbf{M} and \mathbf{B}_K . In the first interval with $\theta_0 \in I_0$ the propagator is equivalent to the matrix fundamental solution of the ODE $\mathbf{T}(\theta_0, 0) = \mathbf{M}(\theta_0, 0)$. In the second interval with $\theta_1 \in I_1$ the propagator can be written as

$$\mathbf{T}(\theta_1, 0) = \mathbf{M}(\theta_1, 0) + \int_{t_0}^{\theta_1 - \tau_0} d\theta_0 \mathbf{M}(\theta_1, \theta_0 + \tau_0) \mathbf{B}_K(\theta_0 + \tau_0) \mathbf{M}(\theta_0, 0), \quad (\text{A.28})$$

and in the third interval with $\theta_2 \in I_2$

$$\begin{aligned} \mathbf{T}(\theta_2, 0) &= \mathbf{M}(\theta_2, 0) + \int_{t_0}^{\theta_2 - \tau_0} d\theta_1 \mathbf{M}(\theta_2, \theta_1 + \tau_0) \mathbf{B}_K(\theta_1 + \tau_0) \mathbf{M}(\theta_1, 0) \\ &+ \int_{t_1}^{\theta_2 - \tau_0} d\theta_1 \mathbf{M}(\theta_2, \theta_1 + \tau_0) \mathbf{B}_K(\theta_1 + \tau_0) \int_{t_0}^{\theta_1 - \tau_0} d\theta_0 \mathbf{M}(\theta_1, \theta_0 + \tau_0) \mathbf{B}_K(\theta_0 + \tau_0) \mathbf{M}(\theta_0, 0). \end{aligned} \quad (\text{A.29})$$

In the fourth interval with $\theta_3 \in I_3$ the propagator can be determined by

$$\mathbf{T}(\theta_3, 0) = \sum_{n=0}^3 \left(\prod_{j=1}^n \int_{t_{n-j}}^{\theta_{4-j}-\tau_0} d\theta_{3-j} \mathbf{M}(\theta_{4-j}, \theta_{3-j} + \tau_0) \mathbf{B}_K(\theta_{3-j} + \tau_0) \right) \mathbf{M}(\theta_{3-n}, 0) \quad (\text{A.30})$$

From Eq. (A.30) the general expression for the propagator $\mathbf{T}(t, t')$ Eq. (4.14) can be derived, which is given in Sec. 4.2.

A.2.4. Biorthonormality condition for eigenmode expansion of DDEs

The eigenmodes $\mathbf{x}_k(t)$ with the dual eigenfunctions $\mathbf{y}_k^T(t)$ satisfies the orthonormality condition Eq. (4.35). This can be shown by putting Eq. (4.32) and Eq. (4.31) in Eq. (4.35), which yields

$$\frac{\mathbf{d}_j^T}{N_j} \int_{-\tau_{\max}}^0 d\theta \left(\mathbf{I} \delta(\theta - 0) + \mathbf{B}_0 \int_0^{\tau_{\max}} d\tau \mathbf{K}(\tau) e^{-s_j(\theta+\tau)} \mathbf{H}(\theta + \tau) \right) \mathbf{q}_k e^{s_k \theta} = \delta_{jk}. \quad (\text{A.31})$$

After applying the integration in the first term, rearranging the terms and taking the Heaviside step function into the boundary of the integration over θ , the expression reads

$$\frac{\mathbf{d}_j^T}{N_j} \left(\mathbf{I} + \mathbf{B}_0 \int_0^{\tau_{\max}} d\tau \mathbf{K}(\tau) e^{-s_j \tau} \int_{-\tau}^0 d\theta e^{(s_k - s_j)\theta} \right) \mathbf{q}_k = \delta_{jk}. \quad (\text{A.32})$$

For $j \neq k$ and no degenerated roots, i.e. $s_j \neq s_k$, the evaluation of the integration over θ in Eq. (A.32) leads to

$$\frac{\mathbf{d}_j^T}{N_j} \left(\mathbf{I} + \mathbf{B}_0 \int_0^{\tau_{\max}} d\tau \mathbf{K}(\tau) \frac{e^{-s_j \tau} - e^{-s_k \tau}}{s_k - s_j} \right) \mathbf{q}_k = 0. \quad (\text{A.33})$$

With the Laplace transform $\bar{\mathbf{K}}(s)$ of the delay kernel the expression can be further simplified

$$\frac{\mathbf{d}_j^T}{N_j} \left(\mathbf{I} - \mathbf{B}_0 \frac{\bar{\mathbf{K}}(s_j) - \bar{\mathbf{K}}(s_k)}{s_j - s_k} \right) \mathbf{q}_k = 0. \quad (\text{A.34})$$

Eq. (4.23a) and Eq. (4.23b) can be used to obtain

$$\frac{\mathbf{d}_j^T}{N_j} \left(\mathbf{I} - \frac{\mathbf{I} s_j - \mathbf{A}_0 - \mathbf{I} s_k + \mathbf{A}_0}{s_j - s_k} \right) \mathbf{q}_k = 0, \quad (\text{A.35})$$

which is obviously true.

For $j = k$ the evaluation of the integral over θ in Eq. (A.32) leads to

$$\frac{\mathbf{d}_k^T}{N_k} \left(\mathbf{I} + \mathbf{B}_0 \int_0^{\tau_{\max}} d\tau \mathbf{K}(\tau) e^{-s_k \tau} \tau \right) \mathbf{q}_k = 1, \quad (\text{A.36})$$

A. Appendix

which is equivalent to

$$\frac{\mathbf{d}_k^T}{N_k} \left(\mathbf{I} - \mathbf{B}_0 \frac{d\bar{\mathbf{K}}(s)}{ds} \Big|_{s=s_k} \right) \mathbf{q}_k = 1, \quad (\text{A.37})$$

With the definition of the normalization constant N_k in Eq. (4.30) and the biorthonormality of the left and the right eigenvectors \mathbf{d}_k^T and \mathbf{q}_k it is clear that the statement Eq. (A.37) is true.

List of Figures

1.1. Machine tool vibrations	14
2.1. Illustration of variable transport delays	22
2.2. Variable transport delays vs. dissipative delays	25
2.3. Characteristic curves for advection equations	29
2.4. Approximation for fast time-varying delays	34
2.5. Approximation for slowly time-varying delays	36
6.1. Non-uniqueness of Hill-Floquet transformation	68
6.2. Convergence of Floquet exponents from the Hill-Floquet method	72
6.3. Convergence of eigenvectors from the Hill-Floquet method	74
6.4. Comparison of Hill-Floquet method and alternative method	75
6.5. Convergence of eigenvectors for alternative method	76
7.1. Stability chart for single species reaction-diffusion systems with delay . . .	86
7.2. Turing-like traveling waves in Fisher-KPP equation with distributed delay	88
7.3. Dispersion relation of traveling waves for time-varying delay	89
7.4. Parallel turning process model	91
7.5. Stability lobes for parallel turning process	93
7.6. Stability lobes for turning with spindle speed variation	96
7.7. Stability of synchronized equilibrium of Hodgkin-Huxley neuronal network	103
7.8. Asymptotic solution of Hodgkin-Huxley neuronal network	104
7.9. Bifurcation diagram for Hodgkin-Huxley neuronal network	105

List of Tables

7.1. Structural parameters for the parallel turning process	93
7.2. Fixed parameters of the Hodgkin-Huxley neuronal model	102

Selbstständigkeitserklärung nach §6 Promotionsordnung

Hiermit erkläre ich, dass ich die vorliegende Arbeit selbstständig angefertigt, nicht anderweitig zu Prüfungszwecken vorgelegt und keine anderen als die angegebenen Hilfsmittel verwendet habe. Sämtliche wissentlich verwendete Textausschnitte, Zitate oder Inhalte anderer Verfasser wurden ausdrücklich als solche gekennzeichnet.

Chemnitz, 15. August 2016

Andreas Otto

Curriculum vitae

Personal information

Name	Andreas Otto
Nationality	Germany
E-Mail	otto.a@mail.de

Education

2008-	Research Associate, Complex Systems and Nonlinear Dynamics group, Institute of Physics, Chemnitz University of Technology
2005-2008	M.Sc. Computational Science, TU Chemnitz, Germany
2002-2005	B.Sc. Computational Science, TU Chemnitz, Germany
2001-2002	Obligatory military service
2001	Abitur, Pestalozzigymnasium Greiz

Publications

Peer-reviewed journal articles

1. A. Otto and G. Radons: Stability analysis of machine-tool vibrations in the frequency domain; *J. IFACol* **48**(12), 328-333 (2015).
2. A. Otto and G. Radons: The influence of tangential and torsional vibrations on the stability lobes in metal cutting; *Nonlin. Dyn.* **82**(4), 1989-2000 (2015).
3. A. Otto, F. A. Khasawneh and G. Radons: Position-dependent stability analysis of turning with tool and workpiece compliance; *Int. J. Adv. Manuf. Technol.* **79**(9), 1453-1463 (2015).
4. A. Otto, S. Rauh, M. Kolouch and G. Radons: Extension of Tlusty's law for the identification of chatter stability lobes in multi-dimensional cutting processes; *Int. J. Mach. Tools Manuf.* **82-83**, 50-58 (2014).
5. A. Otto and G. Radons: Application of spindle speed variation for chatter suppression in turning; *CIRP J. Manuf. Sci. Technol.* **6**(2), 102-109 (2013).

6. C. Brecher, B. Sitte, R. Hermes, S. Bäumler and A. Otto: Simulationsmodell für die aktive Drehzahlvariation - Erweiterung des konventionellen Wirkungskreises der Prozessstabilität für die Drehzahlvariation; *wt Werkstattstechnik online* **101**(5), 316-320 (2011).
7. A. Otto, G. Kehl, M. Mayer and G. Radons: Stability Analysis of Machining with Spindle Speed Variation; *Adv. Mater. Res.* **223**, 600-609 (2011).

Book chapters

8. A. Otto and G. Radons: Transformations from variable delays to constant delays with applications in engineering and biology; in: *Advances in Delays and Dynamics*, T. Insperger, G. Orosz and T. Ersal (Hrsg.), Springer (accepted).
9. A. Otto: Effekte prozess-induzierter Drehzahlvariationen; in: *Realisierung effizienter Zerspanprozesse - Ergebnisbericht des BMBF Verbundprojekts ReffiZ*, C. Brecher (Hrsg.), Shaker, Aachen (2015).
10. J. Kleckner and A. Otto: Erweiterung der Bereiche stabiler Bearbeitungsprozessen durch periodische Drehzahl-Variation; in: *Virtualisierung der spanenden Bearbeitung in der Maschinenentwicklung und Prozessoptimierung (VispaB)*, C. Brecher (Hrsg.), Apprimus, Aachen (2011).
11. A. Otto: Einfachste gewöhnliche Differentialgleichung mit Gedächtnisverzögerung; in: *Materialien zum Forschungsseminar Delay Differential Equations*, G. Radons (Hrsg.), wiss. Scripten, Auerbach (2010).

Conference contributions

12. M. Diagne and N. Bekiaris-Liberis and A. Otto and M. Krstic: Control of Transport PDE/Nonlinear ODE Cascades with State-Dependent Propagation Speed (Peer-reviewed conference paper); *55th IEEE Conf. Decis. Control*, Las Vegas, NV, USA, December 12-14 (2016).
13. A. Otto and G. Radons: Analysis of systems with state-dependent delay and applications in metal cutting (Peer-reviewed conference paper); *24rd Int. Congr. of Theor. and Appl. Mech.*, Montreal, Canada, August 21-26 (2016).
14. A. Otto and G. Radons: Stability analysis of machine-tool vibrations in the frequency domain (Talk); *12th IFAC Workshop on Time Delay Systems*, Ann Arbor, MI, USA, June 28-30 (2015).
15. A. Otto, D. Müller and G. Radons: A fundamental dichotomy for dynamical systems with variable delay (Talk); *DPG Spring Meeting*, Berlin, March 15-20 (2015).
16. A. Otto, D. Müller and G. Radons: Transformation of variable delays to constant delays with application to machine tool chatter (Poster); *Dynamic Days Europe*, Bayreuth, September 8-12 (2014).

17. A. Otto, J. Wang and G. Radons: Turing instability in a one-component reaction-diffusion system with delay (Talk); *Dynamic Days Europe*, Bayreuth, September 8-12, (2014).
18. A. Otto, D. Müller and G. Radons: Transformation of variable delays to constant delays with application to machine tool chatter (Poster); *IDEAS workshop*, Budapest, July 3-5, (2014).
19. A. Otto, J. Wang and G. Radons: Turing instability in a scalar reaction-diffusion system with delay (Talk); *DPG Spring Meeting*, Dresden, March 31-April 4 (2014).
20. A. Otto, D. Müller and G. Radons: The relevance of Arnold tongues for systems with time-varying delay (Talk); *DPG Spring Meeting*, Regensburg, March 10-15 (2013).
21. A. Otto and G. Radons: The effect of runout on the stability of milling with variable helix tools (Peer-reviewed conference paper); *23rd Int. Congr. of Theor. and Appl. Mech.*, Peking, China, August 19-24 (2012).
22. A. Otto and G. Radons: Stability of metal cutting vibrations: Analysis of a system with time-varying, state-dependent and distributed delay (Talk); *Int. Conf. on Delayed Complex Systems*, Palma de Mallorca, June 04-08 (2012).
23. A. Otto and G. Radons: Applications of variable delay dynamics: Stability of regenerative chatter in machining with spindle speed variation (Poster); *DPG Spring Meeting*, Berlin, March 26-30 (2012).
24. A. Otto and G. Radons: Frequency domain stability analysis of milling processes with variable helix tools (Peer-reviewed conference paper); *9th Int. Conf. on High Speed Machining*, San Sebastian, Spain, March 7-8 (2012).
25. A. Otto, G. Kehl, M. Mayer and G. Radons: Stability Analysis of Machining with Spindle Speed Variation (Talk); *13th CIRP Conf. on Modeling of Machining Operations*, Sintra, Portugal, May 12-13 (2011).
26. A. Otto and G. Radons: Dimension of linear delay differential equations with time-varying delay (Talk); *DPG Spring Meeting*, Dresden, March 13-18 (2011).
27. A. Otto and G. Radons: Lyapunov Spectrum of Linear Delay Differential Equations with Time-Varying Delay (Peer-reviewed conference paper); *9th IFAC Workshop on Time Delay Systems*, Prague, June 7-9 (2010).
28. A. Otto and G. Radons: Lyapunov spectrum of linear delay differential equations with time-varying delay (Poster); *Int. Workshop on State-Dependent Delay Equations*, Dresden, October 12-16 (2009).
29. A. Otto and G. Radons: Lyapunov spectrum of linear delay differential equations with time-varying delay (Poster); *Int. Workshop on Delayed Complex Systems*, Dresden, October 5-9 (2009).

30. A. Otto and G. Radons: Lyapunov spectrum of linear delay differential equations with time-varying delay (Poster); *DPG Spring Meeting*, Dresden, March 22-27 (2009).